MATHEMATICAL MODELING AND SIMULATION OF PHOTOSYNTHETIC GROWTH IN CONTINUOUS CULTURE UNDER BICARBONATE AND LIGHT LIMITED CONDITIONS

by

CRAIG E. CURLESS

B. S., Kansas State University, 1985

A MASTER'S THESIS

submitted in partial fulfillment of the

requirements for the degree

MASTER OF SCIENCE

College of Engineering
Department of Chemical Engineering

KANSAS STATE UNIVERSITY
Manhattan, Kansas

1986

Approved by:

Larry E. Erickson, Major Professor

Table of Contents

ACKNOWLEDGMENTS

I wouid iike to thank Professor Larry E. Erickson for his direction and guidance throughout the duration of this project. My thanks aiso go to Professors L. T. Fan and L. C. Davis.

The Nationai Science Foundation receives my appreciation for their financiai support during this work.

I wish to express my gratitude to Dr. H. Y. Lee, whose data proved to be invaiuabie.

I send a speciai thanks to my father, Wiiiiam T. Curiess for his advice and assistance. Finaiiy, I wouid iike to thank my wife Kathleen whose heip and support made it aii possibie.

Introduction

Algae have many commercial uses including human food, animal food and waste treatment. Thus, it would be desirable to grow algae continuosly and have the ability to predict the production level. To accomplish this goal a mathematical model that describes the growth rate of algae should be developed. To model the growth of any living organism, one must know which factors are limiting. Here, both light and carbon are considered to be such factors.

In Chapter 1, the literature discussing three topics is reviewed. First, a survey of the literature dealing with the carbon species assimilated by aqueous, photosynthetic growth is presented. Next, attempts at modeling carbon-limited, aqueous, photosynthetic growth are discussed. Last, investigations of simultaneous light and bicarbonate limited algae growth are examined.

Chapter 2 presents a Monod-type model based on bicarbonate for describing algal growth. This model is combined with the kinetics of aqueous, inorganic carbon chemistry in the form of material balances for each carbon species present in a gas-and-liquid-fed chemostat. Simulations are performed for a bicarbonate-limited chemostat where all carbon is introduced as bubbled CO_2.

In Chapter 3, kinetic models are developed to describe the growth of algae in a continuous-flow, stirred tank under both bicarbonate and light limitations. Two types of models are considered. The first type is the product of two Monod-type models based on bicarbonate and light, respectively. The other model assumes that either light or bicarbonate

limitations prevail. Thus, because of self-shading, it is possible that part of a tank could follow light-limited kinetics while a different section follows bicarbonate-limited kinetics. Each model is applied to situations where light is introduced from one side and light is introduced from two, opposing sides, respectively.

Chapters 2 and 3 are organized in the manner typical for formal journal articles, with two exceptions. All figures and tables are located at the end of their respective chapters. Also, Chapter 4 contains an Appendix where simulation predictions for cases not included in the results section can be found. Those simulations were not placed in the formal report because all unique trends are illustrated by the figures already mentioned in the Results section.

Chapter 1

LITERATURE REVIEW

Introduction

In this chapter, literature pertinent to the modeling of carbon and light limited aquatic photosynthetic growth is surveyed.[1-40] There has been much debate over which inorganic carbon source (CO_2, HCO_3^-, $CO_3^=$ or H_2CO_3) is actually assimilated by aquatic, photosynthetic organisms. The question is of importance because only the carbon source assimilated is directly related to the specific growth rate of algae. Consequently, the literature which is devoted to answering this question has been reviewed. It is also worthwhile to develop a familarity with experimental studies of strictly carbon-limited aquatic, photosynthetic growth in order to appreciate what progress has been made. Therefore, a review of carbon-limited algal growth literature is also included. A review of the literature which addresses the effects of simultaneous carbon and light limitation on the specific growth rate of algae is presented; however, the topic of simultaneous carbon/light limitation has not been well-studied. Consequently, the literature pertaining to the more general case of light/nutrient limitation has been included. The conclusions that can be drawn from the literature survey on these three topics are then presented.

Inorganic Carbon Species Assimilated by Aqueous Photosynthetic Growth

Any attempt at modeling the growth of microbial cultures requires knowledge of the limiting substrate. Photosynthetic organisms are known to consume inorganic carbon as substrate, but the particular form of carbon assimilated is a debated topic. The kinetics of aqueous inorganic carbon chemistry can be described by the following reactions:[33]

1) $CO_2(aq) + H_2O \leftrightarrows H_2CO_3$

2) $CO_2(aq) + OH^- \leftrightarrows HCO_3^-$

3) $HCO_3^- + H^+ \leftrightarrows H_2CO_3$

4) $HCO_3^- + OH^- \leftrightarrows CO_3^{-2} + H_2O$.

Reactions (3) and (4) are virtually instantaneous, whereas reactions (1) and (2) are relatively slow. Consequently, any experimental attempt to determine which of the species (CO_2, HCO_3^-, CO_3^{-2} or H_2CO_3) serves as substrate must allow for the reactions listed above.

Three experimental methods have commonly been employed to determine the particular form of inorganic carbon used as substrate. The first method entails measuring the rate of photosynthesis in the culture being studied. The measurement is in terms of moles of carbon assimilated per unit volume per unit time. The photosynthetic rate is then compared to the rate of conversion of HCO_3^- to CO_2. If the rate of carbon fixation in photosynthesis is greater than the rate of conversion of HCO_3^- to CO_2 then one can conclude that the organism is able to assimilate bicarbonate.

In the second method, the culture being investigated is grown in a solution at equilibrium with respect to inorganic carbon. Data is obtained so that the half-saturation constant of photosynthesis (K_m) can be calculated based on both $[CO_2]$ and $[HCO_3^-]$, respectively. Values of K_m on each basis are obtained at several different values of pH. The carbon

species whose values of K_m change the least with pH is assumed to be the one assimilated by the organism.

The final method is described by Lehman.[24] Here, the carbon source is either ^{14}C - labelled gaseous CO_2 or liquid-phase $NaH^{14}CO_3$. After a short time (short enough that little conversion between CO_2 and HCO_3^- occurs) the cells are collected and analyzed for radioactive ^{14}C content. In the gaseous $^{14}CO_2$-fed experiment, high levels of cellular radioactivity are indicative of CO_2-consumption. Conversely, in the $NaH^{14}CO_3$ - fed experiment the presence of cellular radioactivity indicates consumption of bicarbonate.

A review of some recent investigations into the carbon species assimilated by aquatic, photosynthetic growth is presented. For a review of publications between 1920 and 1956, the reader is referred to Nielsen.[31] Publications from the 1950's and the 1960's have been reviewed by Goldman.[17]

The carbon species assimilated by Chlamydomonas reinhardtii was investigated by Lehman using the method involving radioactive carbon.[24] He found that CO_2 serves as the primary carbon substrate, but the presence of HCO_3^- enhances the rate of carbon fixation. This enhancement indicates that HCO_3^- either speeds up the cellular transport mechanism for CO_2 or that HCO_3^- can also be assimilated. A similar study by Findenegg confirmed that C. reinhardtii can use bicarbonate directly.[9] More recently, Imamura used ^{14}C-studies to show that C. reinhardtii which are adapted to an environment with

a low CO_2-content can assimilate HCO_3^-.[18] However, when adapted to 5% CO_2-enriched air the organism will not use HCO_3^-.

The cyanobacteria Synechococcus also have the ability to assimilate bicarbonate. Badger carried out his studies with radioactive carbon and also investigated the effect of pH on values of K_m.[1] The study of K_m values indicated that HCO_3^- was the preferred carbon aource whereaa the radioisotope experiment showed that both CO_2 and HCO_3^- can be assimilated. Chemostat studies with Synechococcus leopolienais by Miller showed that the rate of conversion of HCO_3^- to CO_2 is too slow to account for the observed rate of photosynthesis by the organism.[29] Miller also showed that Coccochloris peniocystis can fix carbon at a rate 50 times the maximum rate of conversion of HCO_3^- to CO_2 under alkaline conditions.[30]

Richmond studied the competition between Chlorella vulgaris and Spirulina platensis in a chemostat.[37] He found that S. platensis grows better on HCO_3^- than on CO_2. Earlier, Kaplan had shown that S. platensis adapted to low levels of CO_2 uses bicarbonate for carbon.[19] The effect of pH on both K_m ($[CO_2]$) and K_m ($[HCO_3^-]$) lead Kaplan to this conclusion.

Apparently, the blue-green alga Anabaena variabilis has an active bicarbonate pump. This conclusion is based on the obaervation that the organism can concentrate inorganic carbon at a pH where HCO_3^- is the dominant

carbon species in the solution.[20] However, Keenan showed that in photosynthetic rate studies, Anabaena flos-aquae responds to pH, not the carbon species present.[21]

The red alga Porphyridium cruentum has also demonstrated the ability to assimilate bicarbonate directly.[5] The photosynthetic rate of this alga exceeds the rate of conversion of HCO_3^- to CO_2 over the pH range 7.5-9.0.

The carbon source preferred by Scenedesmus obliquus has been thoroughly studied by Findenegg.[10-11] S. obliquus has the ability to fix carbon at a rate greater than HCO_3^- can be converted to CO_2 under both basic and acidic conditions. Radioactive carbon-labelling experiments indicate that only after S. obliquus is adapted to low levels of CO_2 is it able to assimilate bicarbonate.[9] However, even at pH 5.7 these organisms are able to assimilate nearly all of the bicarbonate present in solution.

Chlorella sp. seem to be less facultative with respect to bicarbonate. Studies of the variability of K_m ($[CO_2]$) and K_m($[HCO_3^-]$) with pH indicate that Chlorella pyrenoidosa uses carbon dioxide.[38] Indirect evidence that Chlorella vulgaris has a low affinity for HCO_3^- was obtained by growing the organism in competition with Spriulina platensis.[37] C. vulgaris dominated when only gaseous CO_2 was supplied, but was nearly washed out when pure $NaHCO_3^-$ was the only carbon source. On the other hand, Birmingham showed

that the rate of dehydration of HCO_3^- is not sufficient to account for the rate of photosynthesis in C. vulgaris.[3] Radioactive tracer studies verified that low-CO_2 adapted C. vulgaris can assimilate bicarbonate.[9]

Aqueous Photosynthetic Growth Under Carbon Limited Conditions

One of the earliest studies of carbon-limited aquatic growth was performed by Pipes.[34] He investigated the green-alga Chlorella pyrenoidosa - known to consume CO_2. The carbon source introduced to the chemostat was bubbled CO_2. Pipes found that the cell density in the culture was directly proportional to the inverse of the dilution rate.

Goldman did extensive work with both Selenastrum capricornutum and Scenedesmus quadricauda under carbon-limited conditions.[15] Cultures were grown in chemostats at three different pH ranges: 7.05 - 7.23, 7.25 - 7.39, and 7.43 - 7.61. The carbon-yield-to-biomass for each organism was constant at each pH. Monod type models based on total inorganic carbon (C_{TOT}) were fit to each set of growth data. The value of μ_{max} did not vary with pH. However, the parameter K_s was found to increase with increasing pH. King used Goldman's data to show that the value of K_s ($[CO_2]$) varies less with pH than K_s ($[C_{TOT}]$) does.[22] Therefore, King concluded that the algae respond to aqueous CO_2 ratber than to the total carbon pool.

Goldman successfully rebutted King's argument by first showing that $K_s([CO_2])$ was not constant over the pH range studied.[16] In fact, King's plot of K_s ($[CO_2]$) versus pH was done with such a small ordinate scale that the dependence of K_s ($[CO_2]$) on pH was not visible. In addition, Goldman pointed out that as long as inorganic carbon equilibrium is maintained in the culture, the carbon species chosen to define K_s is immaterial. This is because tbe value of K_s can be converted to any carbon basis using equilibrium constants.

Brune et al. studied the growth of Chlorella vulgaris, Scenedesmus quadricauda and Cblorella salina under carbon-limited conditions in both batch and continuous cultures.[4] The analysis assumed equilibrium between carbon species in the cultures - a reasonable assumption according to Goldman.[16] The data showed that the Monod model defined in terms of either $[C_{TOT}]$ or $[HCO_3^-]$ was not valid for S. quadricauda. A good Monod fit based on $[CO_2]$ was obtained for C. vulgaris. A problem with the above analysis is that the pH changed considerably in the experimental cultures. Consequently the effect of pH on K_s was not eliminated when collecting the kinetic data.

Goldman et al. worked with cultures of Chlorella vulgaris and Scenedesmus obliquus in carbon-limited chemostats.[13] The carbon source introduced to the chemostat was an aqueous, equilibrium solution of sodium bicarbonate. The internal cellular ratios of carbon/biomass, carbon/nitrogen and carbon/chlorophyll were each found to be constant and

independent of specific growth rate. Monod models based on $[C_{TOT}]$ were fit to the growth data of each organism. It was found that for S. obliquus, a first-order/zero-order model may be more appropriate than the Monod model.

A second carbon-limited growth study of C. vulgaris and S. obliquus was carried out by Goldman.[14] Three different sources of inorganic carbon were used as feed: aqueous $NaHCO_3^-$, small gas bubbles, and large gas bubbles, respectively. Botb air and 1% CO_2-enriched air were used. Results with S. obliquus indicated that algal productivity increases linearly as the gas flow rate increases for cultures fed either bubbled air or 1% CO_2-enriched air. Also, small bubbles promote a higher mass-transfer efficiency than do large bubbles. With 100% CO_2 in the gas phase, there was no growth and the cells died.

For algae grown with bubbled CO_2 as the carbon cource, the rate of transfer of CO_2 from gas to liquid is an important consideration. Lee and Pirt looked at the effect of pH on the overall gas/liquid mass transfer coefficient (K_La).[23] It was found that as the pH increased from 6.5 to 7.5 the value of K_La increased by 80%. The authors attributed this increase to changes in bubble size, diffusivity of CO_2, and the kinetics of CO_2 in the gas and liquid boundary layers. However, the effect of pH on the rate of carbon metabolism of the algal culture was overlooked.

De Le Noue studied the effect of agitation form on batch growth of Oocystis sp. with gaseous CO_2 as the carbon source.[7] Two agitation situations were examined:

1. Gaseous CO_2 is bubbled into the culture
2. Gaseous CO_2 exists over the liquid surface and the culture is mechanically agitated.

It was found that much higher biomass concentrations could be reached if air was bubbled into the culture. As the bubbling rate increased, the biomass concentration increased as well. However, the rate of mechanical agitation did not affect the biomass concentration in situation #2. If 5% CO_2-enriched air was used, the same biomass concentration was achieved with mechanical agitation as with bubbled gas. Pure gaseous CO_2 killed the algae.

Miller performed a two-fold study of the cyanobacteria Synechococcus leopoliensis.[29] In the first part of the study, it was found that this alga prefers bicarbonate as a carbon source. The second part involved obtaining carbon-limited growth data of S. leopoliensis in a chemostat. The data were successfully fit to a Monod model based on the total inorganic carbon pool (i.e. $[C_{TOT}]$).

Work with carbon-limited cultures of S. leopoliensis has been continued by Turpin.[39] He attempted to predict the carbon-limited growth kinetics of this alga from its photosynthetic kinetics. The photosynthetic kinetics were of the Monod form based on $[C_{TOT}]$, but two different Monod fits were found to apply. One fit was for specific growth rates (μ) less than 1.7

day^{-1}, and the other was for $\mu > 1.7\ day^{-1}$. The discontinuity at $\mu = 1.7\ day^{-1}$ was attributed to a change from high-affinity photosynthetic kinetics to low-affinity photosynthetic kinetics.

Aqueous Photosynthetic Growth Under Nutrient/Light Limitations

There is little literature addressing the subject of simultaneous carbon and light limited photosynthetic growth. However, Markl conducted such a study with Chlorella vulgaris in a chemostat.[27] Bubbled CO_2 was supplied as the carbon source. Data obtained were rate of CO_2 uptake versus entering partial pressure of CO_2 for 4 different incident light intensities.

A model of the form

$$P = \text{rate of photosynthesis} = f_1([CO_2]) \int_{\text{reactor}} f_2(I)dV$$

has been proposed by Markl, where f_1 is a function of carbon concentration, and f_2 represents the spatial distribution of light intensity in the reactor.[27] Hence, the model is multiplicative with respect to carbon and light. The term f_1 is assumed to be of the Monod form and the rate of mass transfer from gas to liquid and from liquid to cell are modeled as resistances in series. A single, lumped transfer parameter is derived to account for the resistances.

The values of the Monod parameter K_s and the lumped transfer parameter were determined experimentally.[27] It was found that both K_s and the lumped

transfer parameter were needed to achieve a good fit of the data. Also, the mass transfer resistance at the gas/liquid interface was more important than that at the liquid/cell interface.

Frischknecht et al. studied the effects of mixing, temperature, light intensity, CO_2 concentration, culture density and pH on the growth of Anacystis nidulans.[12] They found that the curve of CO_2-uptake-rate versus incident light intensity is strongly dependent on culture density. This dependence is presumably due to self-shading by the culture.

Growth data for Skeletonema costatum and Dunnaliella tertiolecra were collected by McAllister.[28] The rate of carbon uptake was determined as a function of light intensity for different ratios of nitrogen to phosphorus. All curves had shapes that suggested Monod models would be appropriate. However, different parameter values for each level of nitrogen to phosphorus would be required.

Experiments exploring the three variables just mentioned were performed with Nitzschia closterium and Tetraselmis sp. Data for each alga were collected by Maddux at 4 light intensities and 2 levels of phosphorus and nitrogen.[26] The doubling rate of each algae showed maxima at different light intensities. For high levels of nitrogen and phosphorus, the maxima appeared at higher light intensities. No modeling attempts were made.

Bates looked at the effect of ammonium and light intensity on the rate of nitrogen uptake by Skeletonema costotum.[2] The plots of nitrate uptake rate versus light intensity had hyperbolic shapes for each level of ammonium. If ammonium was absent, the hyperbola had a much higher maximum

value, indicating that if NH_4^+ is present, less nitrate is needed by the cell.

MacIsaac et al. studied the effect of light intensity on the rate of nitrate uptake by algae at various ocean depths (and consequently, nutrient levels).[25] Michaelis-Menton kinetics were found to prevail at each ocean depth. However, the values of v_{max} and K_m varied with ocean depth.

Rhee et al. explored the effect of nitrate limitation on the growth of Scenedesmus sp. at three light intensities.[35] The nitrogen cell quota (i.e. the internal nitrogen content per cell) increased with both specific growth rate and light intensity. At light intensities below saturation, fewer cells were present in the chemostat. However, the cells present were of normal composition. The cell-quota of carbon was found to be constant and independent of both specific growth rate and light intensity. Maintenance cell-quotas of nitrate increased as light energy decreased, indicating that multiplicative models in which only μ_{max} changes are in error. Instead, an either/or threshold model would be more appropriate for describing simultaneous light and nitrate limited growth of Scenedesmus.

Chemostat studies of the cyanobacterium Oscillatoria argardhii under simultaneous light and nitrate limitations were carried out by Zevenboom et al.[40] At high light intensities, the nitrogen cell-quota was a linear function of the average light intensity. The saturating nitrogen cell-quota is dependent on specific growth rate according to the equation

$$Q_s = \frac{\mu_{max} \, k_{QS}}{\mu_{max} - \mu}$$

where

Q_S = saturating nitrogen cell quota

μ_{max} = maximum specific growth rate

μ = specific growth rate

k_{QS} = nitrogen cell quota required for maintenance.

Falkowski has developed a mathematical model to describe simultaneous light and nitrogen limited growth of phytoplankton.[8] The model assumes that nitrate uptake can be described by the reaction sequence

Light + Nitrate + Cell → LNC* → CN.

For steady-state accumulation of nitrate, this set of reactions yields a half-saturation constant that accounts for the combined effects of light and nitrate on the rate of nitrate uptake. The model is

$$v = \frac{v_{max} LN}{K_{LN}+NK_L+LK_N+LN}$$

where

v = velocity of nitrate uptake

v_{max} = maximum possible velocity of nitrate uptake

K_L = half-saturation constant for strictly light-limited growth

K_N = half-saturation constant for strictly nitrate-limited growth

K_{LN} = half-saturation constant that accounts for the combined effects of light (L) and nitrate (N) on nitrate uptake.

Note that if $K_{LN} = K_L \cdot K_N$ then the model reduces to

$$v = \frac{v_{max}\, L}{K_L + L} \cdot \frac{N}{K_N + N} .$$

The effects of silicate and light limitation on a marine phytoplankton were also investigated. The organism Skeletonema costatum was studied in continuous culture by Davis.[6] Silicate was maintained at a limiting level in all experiments. The level of light ranged from saturating to 1% of the saturating intensity. Washout occurred at intensities lower than 20% of saturation. The light-saturated cultures behaved exactly like silicate-limited cultures. However, cultures experiencing 30% of light saturation did not respond to added silicate by growing faster. Instead, the cells present just increased in size. It was concluded that a sharp transition between light-limitation and light-saturation exists for S. costatum.

Nyholm developed a general model to describe growth of algae in a natural pond.[32] Variables considered included temperature, diurnal lighting, light intensity, phosphorus concentration and nitrogen concentration. The light intensity was modeled using the Lambert-Beer Law. The kinetics of both phosphorus and nitrogen uptake were described using complex Monod-type models similar to resistance-in-series models.

Conclusions

Some general conclusions can be drawn from the literature review. First, it is the prevalent view that all algae can assimilate carbon dioxide directly under some circumstances. Nearly all algae (with the exception of Chlorella sp. perhaps) can also consume bicarbonate under certain conditions. Some organisms which are adapted to low levels of CO_2 tend to

prefer HCO_3^- as a carbon source. A Monod model describes adequately carbon-limited algal growth. If an equilibrium exists between the inorganic carbon algal species, then growth data can be fit equally well using any carbon species. Monod-type product models have been used to model light/nutrient-limited growth with some success. Threshold models have been suggested for modeling some light/nutrient limited cultures.

References

1. Badger, M. R., et al., Plant Physiology, 70:517-523 (1982).

2. 8ates, S. S., et al., Limnology and Oceanography, 21(2):212-218 (1976).

3. Birmingham, B. C., et al., Plant Physiology, 64:892-895 (1979).

4. 8rune, D. E., et al., J. Appl. Micro. and Biotech., 13:71-76 (1981).

5. Colman, B., et al., J. Phycology, 19:218-219 (1983).

8. Davis, C. O., J. Phycology, 12:291-300 (1976).

7. DeLe Noue, J., et al., Biomass, 4:43-58 (1984).

8. Falkowski, P. G., J. Theor. 8iol., 64:375-379 (1977).

9. Findenegg, G. R., Plant Science Letters, 18:289-297 (1980).

10. Findenegg, G. R., Transmembrane Ionic Exchanges in Plants, Colloque Internat. CNRS Nr. 258, Paris, 275-281 (1977).

11. Findenegg, G. R., Z. Pflanzenphysiol., 79:428-437 (1976).

12. Frischknecht, K., et al., Arch. of Micro., 120:215-221 (1979).

13. Goldman, J. C., et al., Appl. and Envir. Micro., 41(1):80-70 (1981a).

14. Goldman, J. C., et al., 8iotech. and 8ioeng., 23:995-1014 (1981b).

15. Goldman, J. C., J. of Water Poll. Contr. Fed., 46:554-574 (1974a).

18. Goldman, J. C., J. of Water Poll. Contr. Fed., 46:2785-2787 (1974b).

17. Goldman, J. C., et al., Water Research, 6:637-879 (1972).

18. Imamura, M., et al., Plant and Cell Physiol., 24(3):533-540 (1983).

19. Kaplan, A., J. of Expt. 8ot., 32(129):669-677 (1981).

20. Kaplan, A., et al., Planta, 149:219-226 (1980).

21. Keenan, J. D., Physiol. Plant., 34:157-161 (1975).

22. King, D. L., et al., J. of Water Poll. Contr. Fed., 48:1812-1818 (1974).

23. Lee, Y. K., et al., J. Chem. Tech. and 8iotechn., 348:28-32 (1984).

24. Lehman, J. T., J. Phycol., 14:33-42 (1978).

25. MacIsaac, J. J., et al., Deep Sea Research, 19:209-232 (1972).

26. Maddux, W. S., et al., Limnology and Oceanography, 9:79-86 (1964).

27. Markl, L., Biotechn. and Bioeng., 19:1851-1862 (1977).

28. McAllister, C. D., J. Fish. Res. Bd. Can., 31:159-181 (1964).

29. Miller, A. G., et al., Plant Physiol., 75:1064-1070 (1984).

30. Miller, A. G., et al., Plant Physiol., 65:397-402 (1980).

31. Nielsen, E. S., Encycl. of Plant Physiol., Springer-Verlag, Berlin, 70-84 (1960).

32. Nyholm, N., Mitt. Internat. Verein Limnol., 21:193-206 (1978).

33. Palmer, D. A., et al., Chemical Reviews, 83:651-731 (1983).

34. Pipes, W. O., Appl. Micro., 10:281-289 (1962).

35. Rhee, G. Y., et al., Limnology and Oceanography, 26(4):649-659 (1981).

38. Rhee, G. Y., Adv. in Aquat. Micro., Academic Press, 2:151-203 (1979).

37. Richmond, A., et al., Plant and Cell Physiology, 23(8):1411-1417 (1982).

38. Shelp, B. J., et al., Plant Physiol., 65:774-779 (1980).

39. Turpin, D. H., J. Phycol., 21:409-418 (1985).

40. Zevenboom, W., et al., Arch. Micro., 125:59-65 (1980).

Chapter 2

MODELING AND SIMULATION OF BICARBONATE-LIMITED PHOTOSYNTHETIC GROWTH

Introduction

Algae can be used commercially for human food, waste treatment, and animal food. Continuous cultivation provides one method for producing these products. From the standpoint of process optimization, it is desirable to have the ability to predict the production level of the system under a given set of operating conditions. A computer simulation program can be created to accomplish such a task.

Simulations can also be used to analyze experimental data. For example, unknown system parameters can be guessed repeatedly until simulation results match the experimental data. The validity of the model used in the simulation can also be established using experimental data. In this case, all system parameters must be known in advance.

The most important step in creating a simulation program is developing a mathematical model for the system. For carbon-limited photosynthetic growth, Monod models based on various carbon sources have been formulated and experimentally validated.[1-4] Carbon dioxide, bicarbonate ion, and total dissolved inorganic carbon (DIC), have been selected as the carbon source for these Monod models. It has been shown that under most conditions encountered, equilibrium between carbon species in solution exists, and thus the carbon source used in the model is immaterial.[5] This is because under equilibrium conditions, model parameters based on one carbon species can easily be converted to those based on another carbon source.

Which carbon source do algae actually consume is a debated question.[6] Nevertheless, considerable evidence exists that many species

of algae can assimilate HCO_3^-.[7-9] Examples include Scenedesmus, Spirulina and Chlamydomonas. Studies indicate that some of these algal have an active bicarbonate pump and may prefer HCO_3^- as a substrate.[10] In these cases, it would be more appropriate to model carbon-limited growth using the bicarbonate concentration. In this chapter, a model describing bicarbonate-limited photosynthetic growth in a chemostat will be presented. The model is the first one to take the kinetics of aqueous inorganic chemistry into account. This model has been incorporated into a computer simulation program which is applied to two systems, one containing Scenedesmus obliquus and the other Spirulina platensis.

Theory

The system being modeled consists of a chemostat (perfectly mixed) with both liquid and gas feed streams. Growth of the algal culture in the tank is presumed to be bicarbonate-limited. The temperature and pH within the tank are maintained at fixed levels by controlling devices. Light is assumed to be present at the saturation level throughout the tank. This last assumption is a good one for either dilute cultures or optically thin fermentors.

The kinetics of aqueous carbon chemistry can be completely described by the reactions in Figure 2-1.[11] At this point, it is worthwhile to compare the magnitudes of the rate constants of reactions 1,2,3 and 4 (presented in Figure 2-1) at 25°C and pH 7:

$k_1[H_2O]$ = 0.039 sec^{-1}

k_{-1} = 23.7 sec^{-1}

$k_2[OH^-]$ = 0.00080 sec^{-1}

k_{-2} = 0.00025 sec^{-1}

$k_3[H^+]$ = 4700 sec^{-1}

k_{-3} = 1.3×10^7 sec^{-1}

$k_4[OH^-]$ = 680 sec^{-1} (20°C)

$k_{-4}[H_2O]$ = 1.44×10^6 sec^{-1} (20°C)

It is apparent that reactions 1 and 2 are relatively slow, whereas reactions 3 and 4 are virtually instantaneous. The temperature dependence of the rate constants k_1, k_{-1} and k_2 are also given in Figure 2-1. Because reactions 3 and 4 are so fast, the rate constants for these reactions are available only at a single temperature. To estimate these rate constants at higher temperatures, the value of one constant in each reaction is raised so that the value of the equilibrium constant is correct at this temperature.

The liquid feed is assumed to be at equilibrium with a known total inorganic carbon content at a given temperature and pH. For reaction 1, the equilibrium constant is estimated from values of k_1 and k_{-1}. All other equilibrium constants have been obtained from the text by Stumm and Morgan.[12] Values are given from 0°C to 50°C at 5°C increments.

The simulation program will do a linear interpolation of log K_{eq} vs 1/T to estimate equilibrium constants at temperatures in this range not evenly divisible by 5. The effect of ionic strength on equilibrium constants is neglected.

CO_2 - transfer from the gas phase to the liquid phase is modeled using a mass-transfer coefficient term defined as

$$R_{CO_2} = k_L a([CO_2^*] - [CO_2])V_L$$

where

R_{CO_2} = rate of transfer of CO_2 from gas to liquid (mol/sec)

$k_L a$ = volumetric mass transfer coefficient (sec^{-1})

V_L = volume of liquid in the tank (m^3)

$[CO_2]$ = bulk concentration of aqueous CO_2 in the tank (mol/m^3)

$[CO_2^*]$ = concentration of aqueous CO_2 that would be in equilibrium with the exiting gas phase CO_2 (mol/m^3)

The value of $k_L a$ is somewhat system specific. However, an expression given by Joshi et al. is used as a first estimate: [13]

$$k_L a = P_G^{0.58} V_G^{0.75} D_T/1000 \cdot V_L$$

where

P_G = gas power (W)

V_G = superficial gas velocity (m/s)

D_T = tank diameter (m).

The gas stream is assumed to be perfectly mixed within the chemostat and the entering molar flow rate is set equal to that flowing out. This last stipulation is reasonable for bubbled air because little CO_2 is present to dissolve (0.036%) and oxygen is generated during photosynthesis.

The specific growth rate of the algae is described by a Monod model (denoted as Model 1) based on bicarbonate:

$$\mu_{AVG} = \frac{\mu_{max}[HCO_3^-]}{K_s + [HCO_3^-]}$$

where

μ_{AVG} = average specific growth rate (hr^{-1})

μ_{max} = maximum specific growth rate (hr^{-1})

K_s = half-saturation constant (mol/m^3)

$[HCO_3^-]$ = concentration of bicarbonate in the tank (mol/m^3)

The rate of consumption of bicarbonate is given by $\mu_{AVG}X/Y_c$ where X is the biomass concentration and Y_c is the carbon yield to biomass. The value of Y_c is assumed to be 1 mol of carbon in biomass per mol of bicarbonate consumed. It has been shown that the fraction of carbon in algae on a dry weight basis is constant and near 0.479. [14] Thus, if one knows the amount of carbon consumed by the algal, the corresponding increase in biomass can be estimated.

Now that all of the assumptions made in the modeling procedure have been described, material balances for each form of carbon in the chemostat can be constructed (Figure 2-2). Under the assumptions presented in this section, for a fixed dilution rate and gas flow rate, Figure 2-2 shows 6 equations with the following 6 unknowns: $[CO_2]$, $[HCO_3^-]$, $[H_2CO_3]$, $[CO_3^=]$, $p^{out}_{CO_2}$ and X. The equations can be solved explicitly for X by using a series of substitutions. However, the resulting equation is rather unwieldy. Consequently, the equation is incorporated into a computer program so that repeated calculations can be performed easily.

Results

It has been shown that S. obliquus has the ability to assimilate bicarbonate, hence this green alga is a reasonable candidate on which to test the simulation. [15-16] The Monod kinetic parameters for S. obliquus have been presented by Goldman et al. : μ_{max} = 1.59 day^{-1} and K_s = 0.16 mg carbon/liter. [3] These parameters were determined using data obtained with a chemostat at 20°C and pH 7.1 - 7.2 using a liquid feed with 1 mM total carbon. Simulations at these conditions indicated that the four carbon species in solution were essentially at equilibrium in the chemostat. Values of $2 \cdot \mu_{max}$, $\mu_{max}/2$ and $5 \cdot K_s$, $K_s/5$ were also simulated to verify that carbon equilibrium would be closely approximated even if the kinetic parameters were significantly different.

The Monod parameters based on bicarbonate were used in a simulation at the conditions employed in a different experiment by Goldman et al. (Figure 2-3). [17] These experimental conditions can be found in Table 2-1. No carbon was present in the liquid feed; therefore, bubbled air served as the carbon source. The mass transfer coefficients presented by Goldman are defined on a different basis than those used in the simulation. Consequently, it was necessary to vary $k_L a$ in the simulation until a value was found that fit the data well. The simulation used a Henry's Law constant of 0.0389 M atm^{-1} at 20°C. [12]

Figure 2-3 shows a comparison of model productions for various values of $k_L a$ and the results obtained by Goldman. [17] A value of 0.4 min^{-1} seems to fit the data best (Figure 2-4). Figure 2-5 presents plots of four ratios, each having the dilution rate as the independent variable. The dotted line is the fraction of total dissolved and suspended carbon that is present as biomass (F_c). The dot-dashed curve shows the fraction of the carbon in the entering gas that does not dissolve ($p^{out}_{CO_2} / p^{in}_{CO_2}$). The solid curve is the ratio of bicarbonate concentration present in the tank to the concentration of bicarbonate that would be in equilibrium with the dissolved CO_2 concentration ($[HCO_3^-]/[HCO_3^-*]$). The other dashed line depicts the ratio of aqueous CO_2 to the concentration of dissolved CO_2 that would be in equilibrium with tbe exiting gas ($[CO_2]/[CO_2*]$). Carbonate and carbonic acid

concentrations were predicted to be at equilibrium with respect to bicarbonate in the chemostat.

The blue-green bacterium S. platensis has been shown to prefer bicarbonate as a carbon source.[9] Extensive kinetic studies of this organism have been performed by Lee.[4] Optimal growth conditions have been found to be 33°C and pH 9.2. Average carbon-limited Monod parameters based on $[HCO_3^-]$ are $\mu_{max} = 0.09 hr^{-1}$ and $K_s = 1.39 \times 10^{-5} M$. In Lee's work, the liquid feed contained 0.02 g carbon/liter and the chemostat had a volume of 13.5 liter; no gas feed was used. Figure 2-6 compares simulation predictions of exiting biomass concentration under the given conditions (See Table 2-1) with results obtained by Lee. The three sets of data points in Figure 2-6 correspond to the three incident light intensities investigated by Lee.

Figures 2-7 to 2-11 show simulation predictions for growth of S. platensis with bubbled air as the only carbon source (pH 9.2 and 33°C). Other simulation conditions can be found in Table 2-1. Mass-transfer coefficient is considered as a parameter because its value is seldom known precisely, a priori. Figure 2-7 shows exiting biomass concentration as a function of the dilution rate. Figure 2-8 depicts conversion of transferred carbon to biomass. This plot is useful for seeing where washout occurs. Figures 2-9 and 2-10 show how close to equilibrium the concentrations of HCO_3^- and dissolved CO_2 are. The fraction of carbon dissolved is depicted in Figure 2-11. Finally, for

all values of $k_L a$ and D, both carbonate and carbonic acid concentrations are predicted to be at equilibrium with respect to bicarbonate.

Discussion

There is good agreement in Figure 2-4 between simulation predictions for $k_L a = 0.4\ min^{-1}$ and the growth results for S. obliquus given by Goldman.[17] From the $p^{out}_{CO_2}/p^{in}_{CO_2}$ curve in Figure 2-5 one can see that for D=0.5 day^{-1}, 13% of the entering carbon is used. This is in close agreement with the 14% transfer efficiency obtained by Goldman. As expected, the concentration of aqueous CO_2 is far from equilibrium with respect to the gas phase. However, at higher values of dilution rate, $[CO_2]$ approaches this equilibrium value because little biomass is present to draw CO_2 away from the solution.

Figure 2-5 implies that if S. obliquus consumes only bicarbonate under the operating conditions, then aqueous carbon equilibrium is not established. Using radioactive $H^{14}CO_3^-$, Findenegg has found that S. obliquus adapted to air consumes the same proportion of bicarbonate ion present in the total carbon pool at pH 5.7. The rest of the carbon uptake is in the form of dissolved CO_2. The simulation predicts that no more than 65% of the total inorganic carbon pool in the chemostat exists as bicarbonate. Thus, it is possible that S. obliquus obtains 35% or more of its carbon in the form of CO_2. This situation would indicate

that the Monod model based solely on the concentration of bicarbonate (Model 1) was not appropriate. Rather, a model based on both dissolved CO_2 and HCO_3^- would be in order. However, at high pH, bicarbonate is present almost to the exclusion of CO_2. Consequently, at high pH it is more likely that Model 1 would be appropriate for describing the photoautotrophic growth of bicarbonate-consuming algae.

The results for Lee's liquid-fed cultures of S. platensis (Figure 2-6) indicate that generally more biomass is present in the chemostat than predicted by tbe simulation. This occurs because the nitrogen source used in the experimental work was urea - a compound containing carbon. The feed stream contained 0.14 g $NaHCO_3$/liter and 2.5 g urea/liter. Allowance for normal utilization of urea in the carbon balances predicts no more than an 8% increase in biomass concentration. At a dilution rate of 0.03 hr^{-1}, the simulation prediction is in error by well over 8%. Thus, the bacterium is not only using urea for nitrogen, but also as a second source of carbon. Considering this extra carbon source was present, the simulation curve is in good agreement with the experimental data. The simulation predicts washout before 0.09 hr^{-1} because of the low bicarbonate concentration in the feed.

Figure 2-7 illustrates a steep drop-off of biomass concentration with dilution rate for gas-fed S. platensis cultures. One can see that the mass-transfer coefficient affects strongly the biomass concentration achieved. The plots of conversion versus dilution rate (Figure 2-8) can be used to estimate the washout dilution rate. As expected, the washout

dilution rate increases with the mass transfer coefficient (and the corresponding increase in dissolved carbon).

Figure 2-9 shows that bicarbonate and aqueous CO_2 are not predicted to be at equilibrium with each other. However, as the dilution rate increases, equilibrium is approached. Presumably this effect is due to the lower biomass concentration at a higher dilution rate. With a high biomass concentration, the algae serve as a significant bicarbonate sink, drawing HCO_3^- from solution faster than CO_2 can dissolve and be hydrated.

Figure 2-10 indicates that as the dilution rate is increased, the concentration of dissolved CO_2 moves towards equilibrium with the gas phase until the onset of washout. After washout, the shorter residence time moves CO_2 farther from gas/liquid equilibrium. Finally, Figure 2-11 shows that the fraction of carbon which does not dissolve increases gradually as the dilution rate is increased for each mass transfer coefficient. However, at a higher dilution rate, mass transfer efficiency decreased sharply for a higher mass transfer coefficient. This decrease can be attributed to the sharp downward trend in the biomass curve (Figure 2-7) near washout.

Conclusions

First, if the reactor is liquid-fed, all four inorganic carbon species exist at or near chemical equilibrium. This conclusion is in agreement with Goldman's analysis.[5] If the culture is air-fed, then

HCO_3^-, CO_3^{-2}, and H_2CO_3 levels are maintained at or near equilibrium. However, under air-fed conditions, both the rate of transfer of CO_2 from gas to liquid and the rate of conversion of CO_2 to HCO_3^- limit the growth rate. The limiting rate of gas/liquid mass transfer has been experimentally validated for S. obliquus.[17] Nevertheless, the prediction of a bottleneck in the rate of conversion of CO_2 to HCO_3^- is a unique finding.

NOMENCLATURE

D = Dilution rate

F_c = Fraction of suspended and dissolved carbon present as biomass

K_S = Half-saturation constant for HCO_3^-

K_j = Equilibrium constant for aqueous carbon reaction "j"

k_j = Rate constant for aqueous carbon reaction "j"

k_La = Mass-transfer coefficient

$p_{CO_2}^{in}$ = Partial pressure of CO_2 in gas entering tank

$p_{CO_2}^{out}$ = Partial pressure of CO_2 in gas exiting tank

pH = pH in the tank

pH_{feed} = pH of the liquid feed

Q_{in} = Volumetric flow rate of gas entering tank

Q_{out} = Volumetric flow rate of gas exiting tank

R = Ideal gas constant

T_{feed}^{liq} = Temperature of the liquid feed

T_{in}^{gas} = Temperature of gas entering tank

T_{out}^{gas} = Temperature of gas exiting tank

V_L = Volume of liquid in tank

Y_c = Carbon yield to biomass

$[CO_2^*]$ = Concentration of aqueous CO_2 that would be in equilibrium with the exiting gas stream

$[HCO_3^-{}^*]$ = Concentration of aqueous HCO_3^- that would be in equilibrium with the exiting aqueous CO_2 concentration

["i"] = Aqueous concentration within the tank (and therefore exiting the tank); $[CO_2]$ = dissolved CO_2, $[HCO_3^-]$ = dissolved HCO_3^-, $[CO_3^=]$ = dissolved $CO_3^=$, $[H_2CO_3]$ = dissolved H_2CO_3

$["i"]_{in}$ = Aqueous concentration of species "i" in the liquid feed; see definitions immediately above

μ_{max} = Maximum specific growth rate of biomass

REFERENCES

1. Brune, D. E., et al., Eur. J. of Appl. Biotech., 13:71-76, (1981).

2. Goldman, J. C., et al., J. Water Pollut. Contr. Fed., 46:554-574, (1974).

3. Goldman, J. C., et al., Appl. and Env. Micro., 41(1): 60-70, (1981).

4. Lee, H.Y. and Erickson, L. E., Biotech.and Bioeng. Symp., Vol. 17, In Press (1988).

5. Goldman, J. C., et al., J. Water Pollut. Contr. Fed., 46:2785-2787, (1974).

6. Raven, J. A., Energetics and Transport in Aquatic Plants: MBL Lectures in Biology, Vol. 4, Alan R. Liss, Inc., New York, (1984).

7. Raven, J. A., Biological Reviews, 45:167-221, (1970).

8. Findenegg, G. R., Plant Sci. Letters, 18:289-297, (1980).

9. Kaplan, A., J. of Expt. Botany, 32(129):669-877, (1981).

10. Berry, J., et al., Yrbk Carnegie Instn., 77:251-261, (1976).

11. Palmer, D. A., et al., Chem. Rev., 83:651-731, (1983).

12. Stumm, W. and Morgan, J. J., Aquatic Chemistry: An Introduction Emphasizing Chemical Equilibria in Natural Waters, Wiley-Interscience, New York, (1970).

13. Joshi, J. B., et al., Chem. Eng. Sci., 37:813-844, (1982).

14. Lee, H. Y. and Erickson, L. E., Biotech. and Bioeng., 26:758-763, (1984).

15. Findenegg, G. R., Z. Pflanzenphysiol., 79:428-437, (1976).

18. Findenegg, G. R., Exchanges Ioniques Transmembranaires Chez Les Vegetaur, Colloque de C.N.R.S., Paris, 275-281, (1976).

17. Goldman, J. C., Biotech. and Bioeng., 23:995-1014, (1981).

18. Pinsent, B. R., et al., Trans. Faraday Soc., 47:263-289, (1951).

19. Eigen, M., Angew. Chem., 75:489-498, (1963).

Table 2-1. Parameter Values Used in the Simulations Depicted in Figures 2-3 to 2-11.

Parameter	Values Used in Figures 3 to 5	Values Used in Figure 6	Values Used in Figures 7 to 11
pH_{feed}	--	9.2	--
T_{feed}^{liq}	--	25°C	--
$[CO_2]_{in}$	0	2.20×10^{-6} mol/liter	0
$[H_2CO_3]_{in}$	0	5.64×10^{-9} mol/liter	0
$[HCO_3^-]_{in}$	0	1.55×10^{-3} mol/liter	0
$[CO_3^{-2}]_{in}$	0	1.15×10^{-4} mol/liter	0
$[H_2O]$	55.56 mol/liter	55.56 mol/liter	55.56 mol/liter
pH	6.65	9.2	9.2
T	20°C	33°C	33°C
V_L	0.5 liter	13.5 liter	13.5 liter
Q_{in}	0.63 liter/min	0	13.5 liter/min
Q_{out}	0.63 liter/min	0	13.5 liter/min
$p_{CO_2}^{in}$	0.00036 atm	--	0.000316 atm
T_{in}^{gas}	20°C	--	33°C
T_{out}^{gas}	20°C	--	33°C
Y_C	26.67 g biomass/mol C	25.67 g biomass/mol C	25.67 g biomass/mol C
K_S	0.813 mg HCO_3^-/liter	11.693 mg HCO_3^-/liter	11.693 mg HCO_3^-/liter
μ_{max}	0.06625 hr^{-1}	0.09 hr^{-1}	0.09 hr^{-1}

Figure 2-1. Aqueous Inorganic Carbon Chemistry

Reactions	Equilibrium Constants
1. $CO_2 + H_2O \underset{k_{-1}}{\overset{k_1}{\rightleftharpoons}} H_2CO_3$	$K_1 = k_1/k_{-1}$
2. $CO_2 + OH^- \underset{k_{-2}}{\overset{k_2}{\rightleftharpoons}} HCO_3^-$	$K_2 = k_2/k_{-2}$
3. $HCO_3^- + H^+ \underset{k_{-3}}{\overset{k_3}{\rightleftharpoons}} H_2CO_3$	$K_3 = k_3/k_{-3}$
4. $HCO_3^- + OH^- \underset{k_{-4}}{\overset{k_4}{\rightleftharpoons}} CO_3^{-2} + H_2O$	$K_4 = k_4/k_{-4}$

Temperature Dependence of Rate Constants*

$k_1 [H_2O] = 2.165 \times 10^{10} \exp(-8056.7/T)\ (sec^{-1})\ (T[=]K)^{11}$

$k_{-1} = 1.035 \times 10^{12} \exp(-7300.9/T)\ (sec^{-1})\ (T[=]K)^{11}$

$k_2 = 4.3152 \times 10^{13} \exp(2895.0/T)\ (sec^{-1})\ (T[=]K)^{18}$

$k_{-2} = k_2/K_2\ sec^{-1}$

$k_3 = 4.7 \times 10^{10}\ M^{-1}sec^{-1}$ at 25°C [19]

$k_{-3} = k_3/K_3\ sec^{-1}$

$k_4 = K_4 \cdot k_{-4}\ M^{-1}sec^{-1}$

$k_{-4} = 2.6 \times 10^{4}\ M^{-1}sec^{-1}$ at 20°C [19]

* Dependence of rate constants on ionic strength was not considered.

Figure 2-2. Material Balances*

Liquid Phase CO_2 Balance

$$\frac{d[CO_2]}{dt} = 0 = k_L a([CO_2^*]-[CO_2])+D([CO_2]_{in}-[CO_2])+k_{-1}[H_2CO_3]$$
$$-k_1[H_2O][CO_2]+k_{-2}[HCO_3^-]-k_2[OH^-][CO_2]$$

Gas Phase CO_2 Balance

$$\frac{V_g}{RT}\frac{dp_{CO_2}}{dt} = 0 = \frac{Q_{in}\, p_{CO_2}^{in}}{RT_{in}^{gas}} - \frac{Q_{out}\, p_{CO_2}^{out}}{RT_{out}^{gas}} - k_L a([CO_2^*]-[CO_2])V_L$$

$CO_3^=$ Balance

$$\frac{d[CO_3^=]}{dt} = 0 = D([CO_3^=]_{in}-[CO_3^=])+k_4[OH^-][HCO_3^-]-k_{-4}[H_2O][CO_3^=]$$

H_2CO_3 Balance

$$\frac{d[H_2CO_3]}{dt} = 0 = D([H_2CO_3]_{in}-[H_2CO_3])+k_1[H_2O][CO_2]-k_{-1}[H_2CO_3]$$
$$+k_3[H^+][HCO_3^-]-k_{-3}[H_2CO_3]$$

Biomass Balance

$$\frac{dX}{dt} = 0 = -DX + X\mu_{AVG}$$

HCO_3^- Balance

$$\frac{d[HCO_3^-]}{dt} = 0 = D([HCO_3^-]_{in}-[HCO_3^-])+k_2[OH^-][CO_2]-k_{-2}[HCO_3^-]$$
$$+k_{-3}[H_2CO_3]-k_3[H^+][HCO_3^-]+k_{-4}[H_2O][CO_3^=]$$
$$-k_4[OH^-][HCO_3^-]-\frac{X\mu_{AVG}}{Y_c}$$

*See Nomenclature for a description of the symbols.

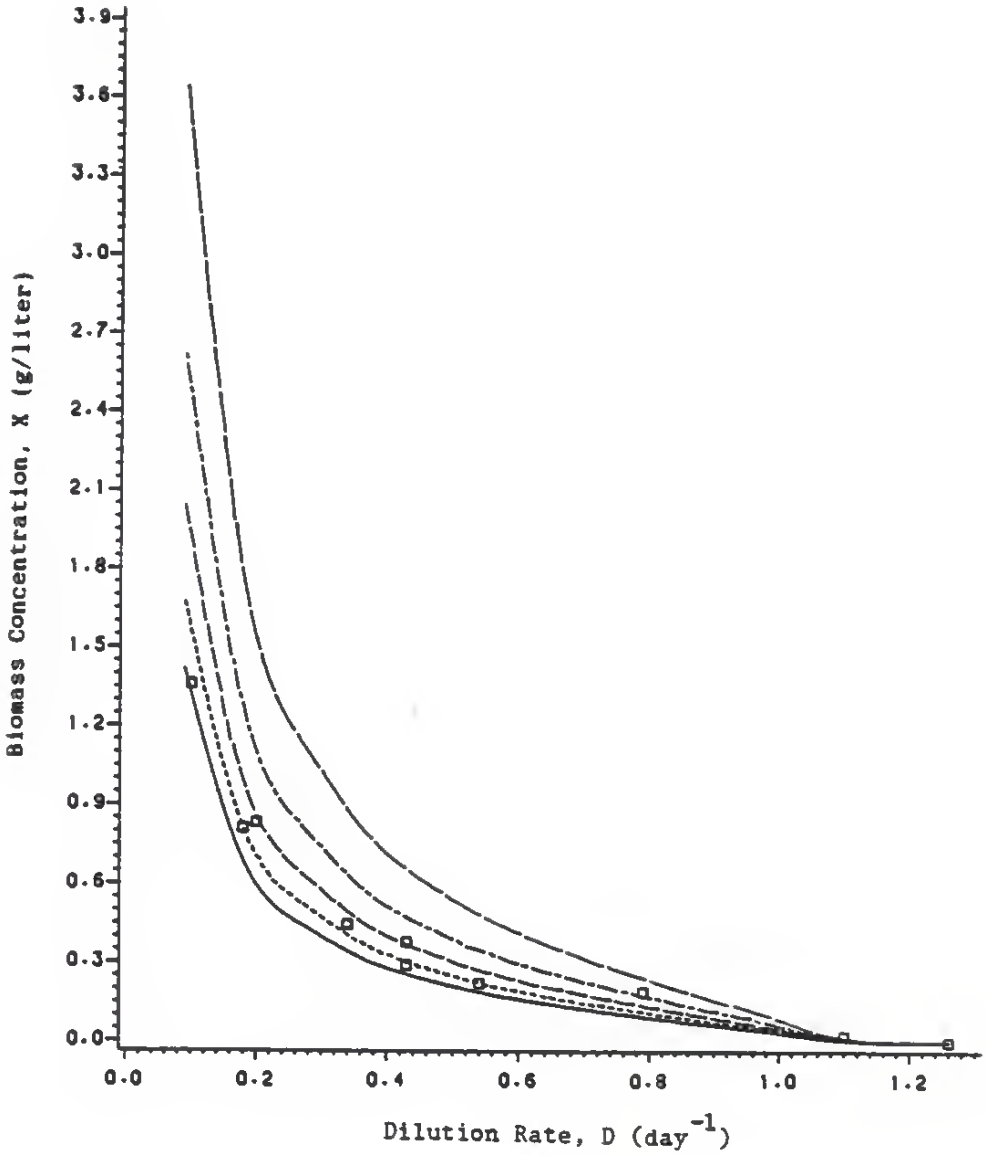

Figure 2-3. Comparison between experimental growth data for S. obliquus and predicted results; mass transfer coefficient is the parameter. Values of $k_L a$ in min^{-1} are ——— 0.32, - - - - - 0.4, — — — 0.533, — - — - 0.8, ——— 1.6 and ▫ ▫ ▫ data from Goldman.

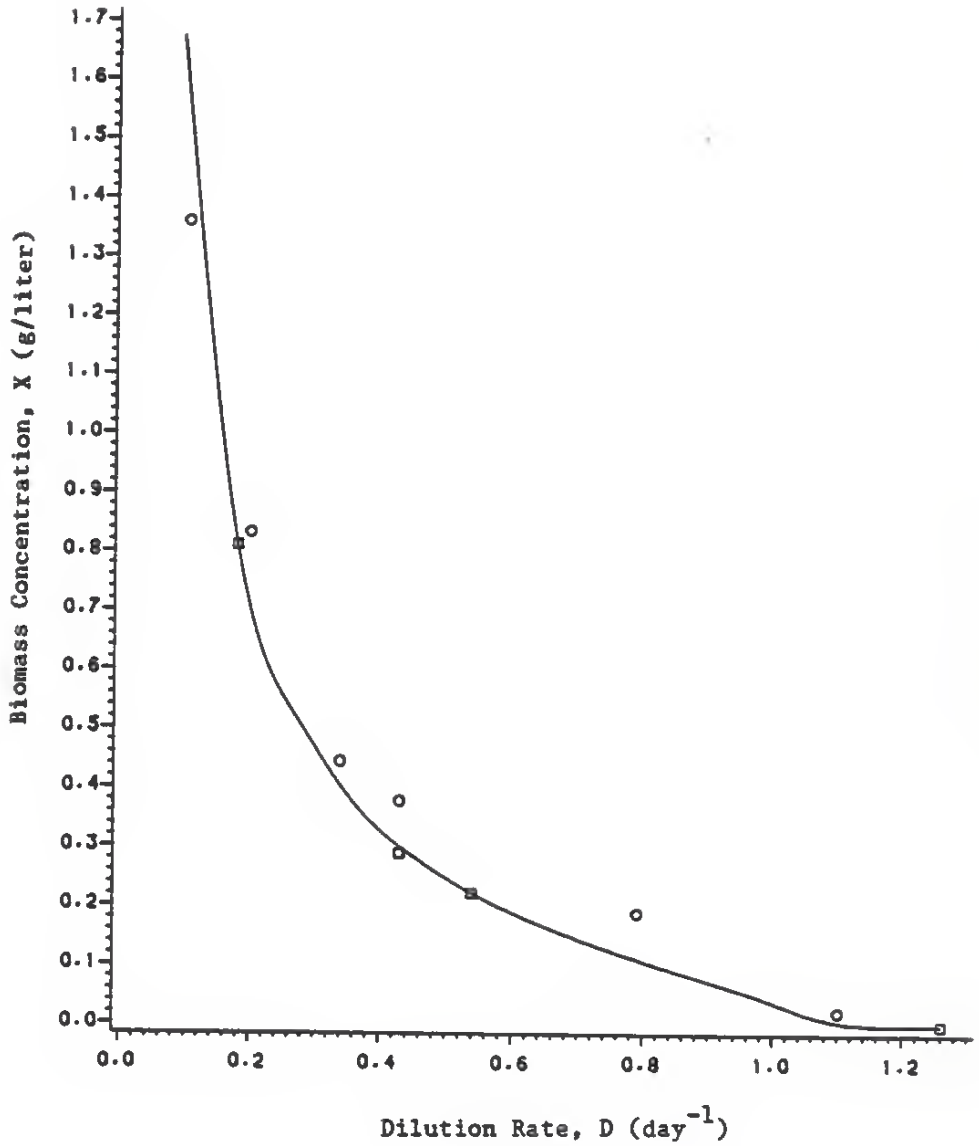

Figure 2-4. Comparison of experimental data for S. obliquus and simulation prediction for $k_L a$ = 0.4 /min. ——— simulation prediction, o o o data from Goldman.

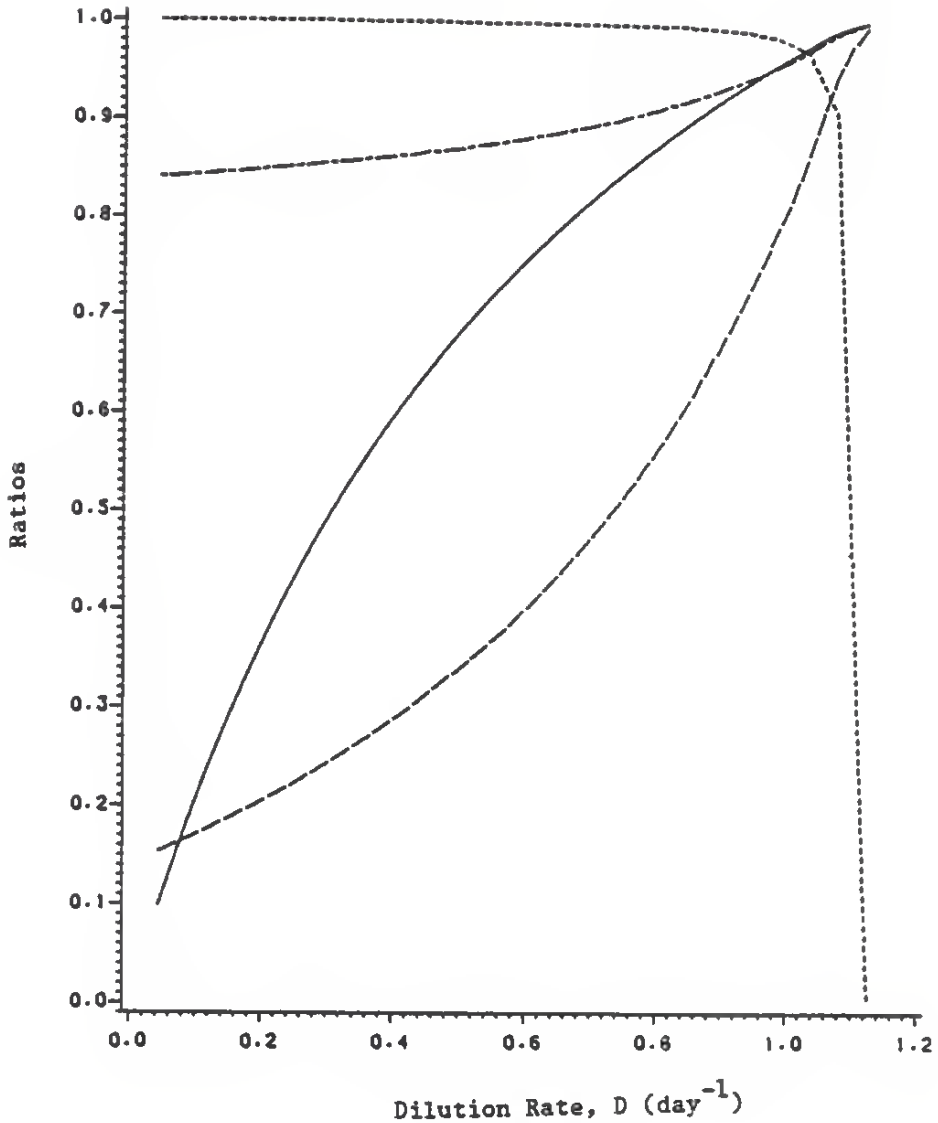

Figure 2-5. Variation of several ratios with dilution rate for S. obliquus. The value of $k_L a$ is 0.4 /min. ---- F_c, ----- $p^{out}_{CO_2}/p^{in}_{CO_2}$, — — $[CO_2]/[CO_2^*]$, ——— $[HCO_3^-]/[HCO_3^{-*}]$. See Nomenclature for a description of variables.

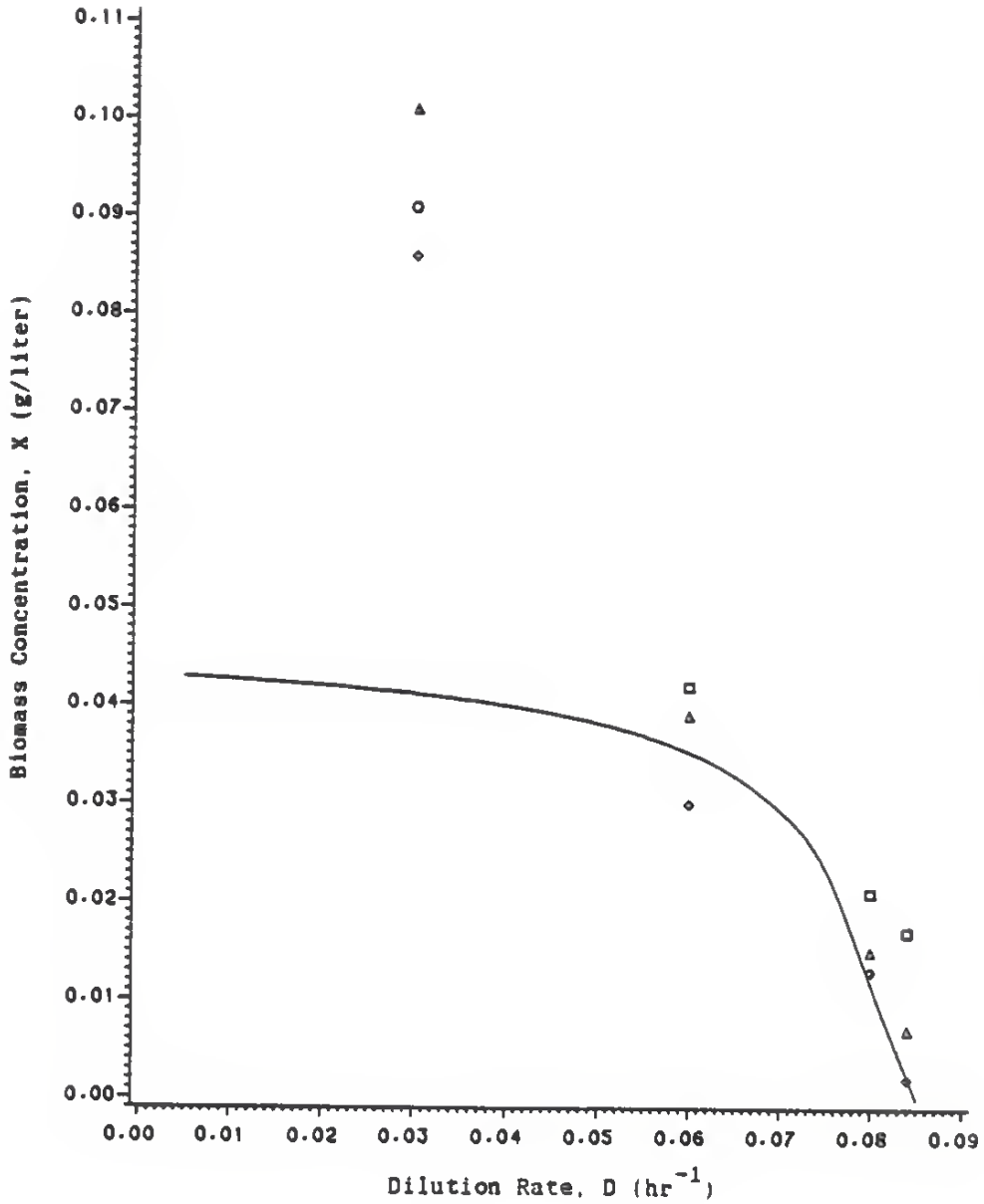

Figure 2-6. Comparison of simulation prediction with Lee's carbon-limited growth data for S. platensis. Variation in biomass concentration with dilution rate is shown. Symbols are ——— simulation prediction; o o o Incident light intensity = 14.4 W/m^2; ▲ ▲ ▲ I_o = 29.2 W/m^2 and ◆ ◆ ◆ I_o = 51.4 W/m^2.

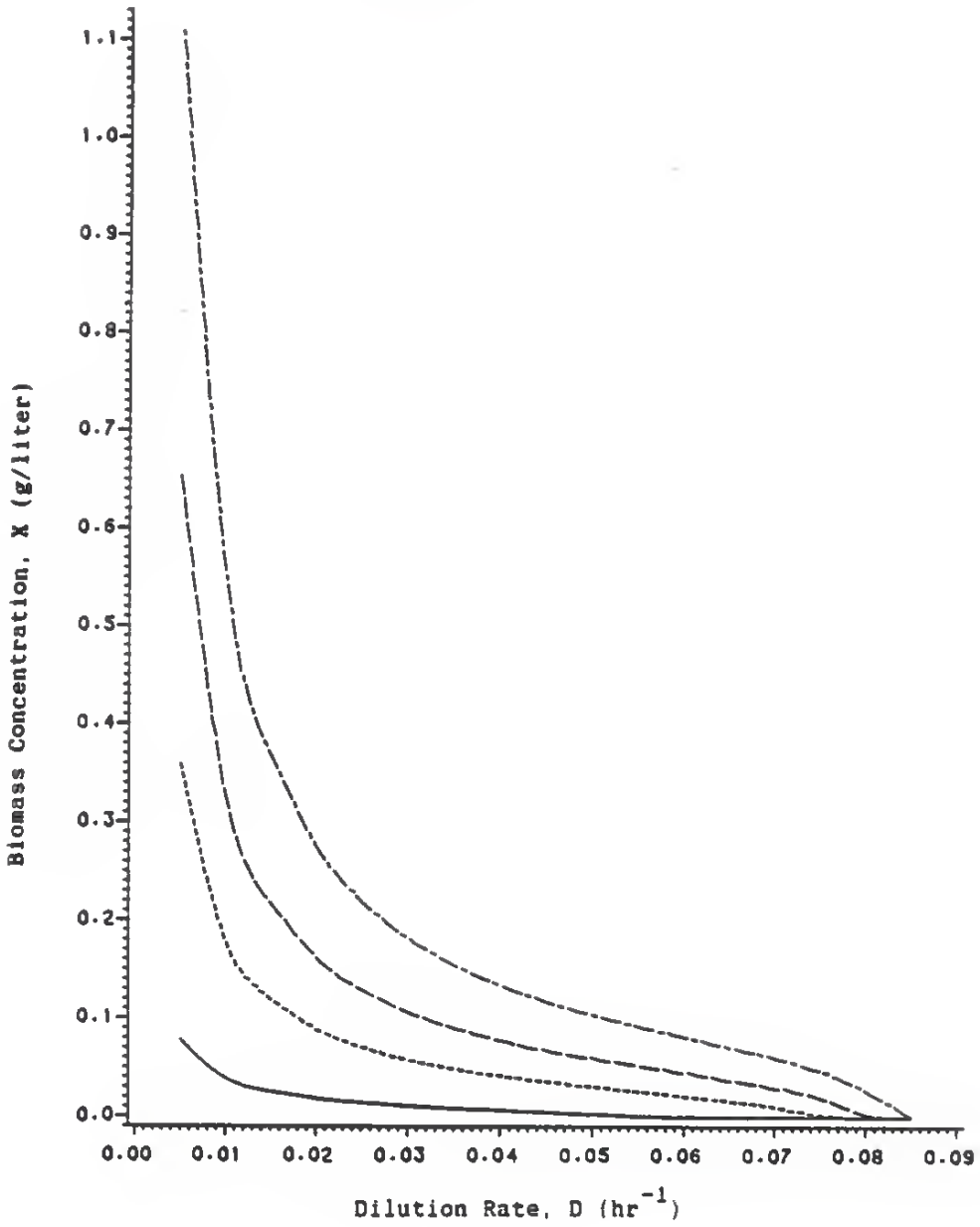

Figure 2-7. Variation of biomass concentration with dilution rate for S. platensis; mass-transfer coefficient is the parameter. Values of $k_L a$ in hr^{-1} are ——— 1.775, - - - - - 8.874, — — — 17.75, and - - - - 35.5.

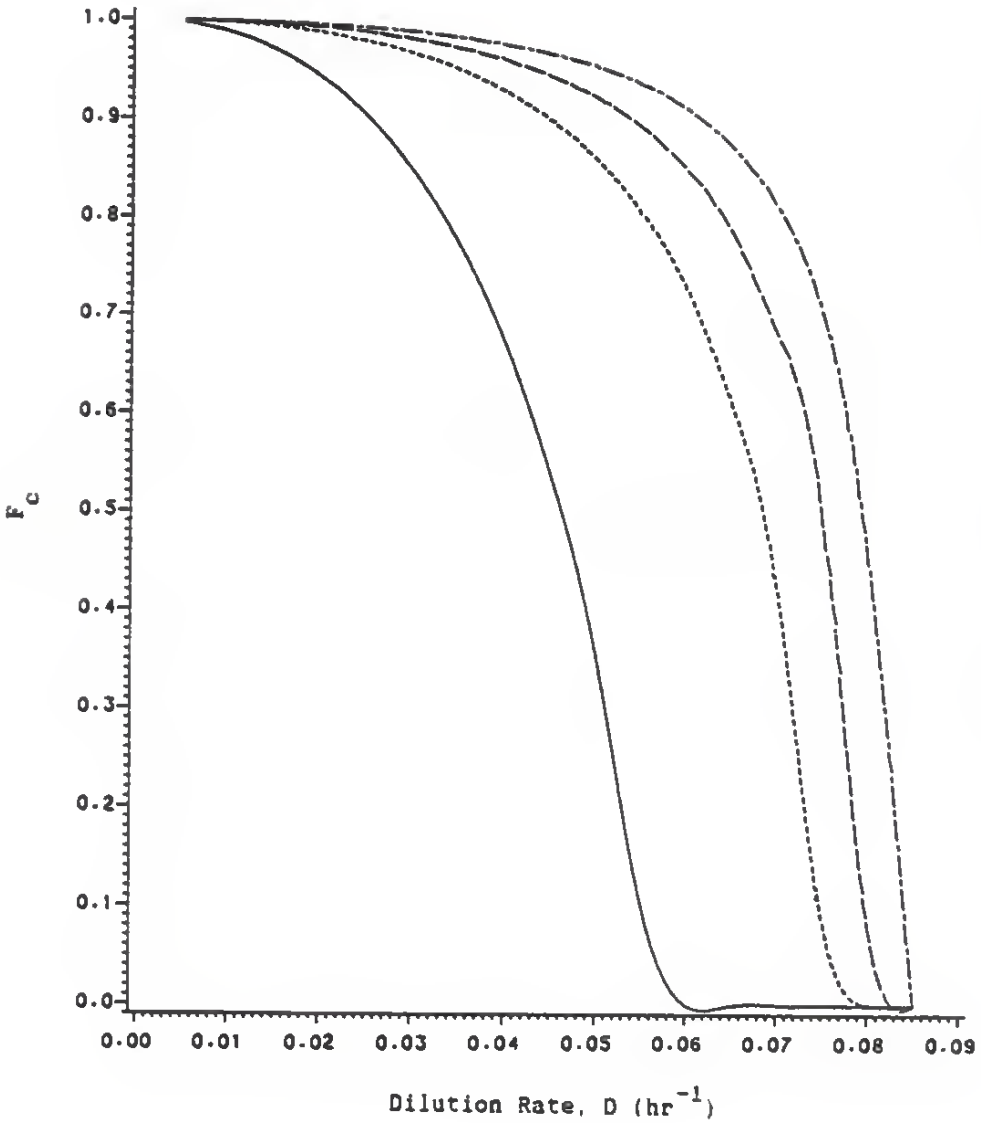

Figure 2-8. Variation in fraction of dissolved and suspended carbon converted to biomass with dilution rate; mass-transfer coefficient is the parameter. Symbols are as defined in Figure 2-7.

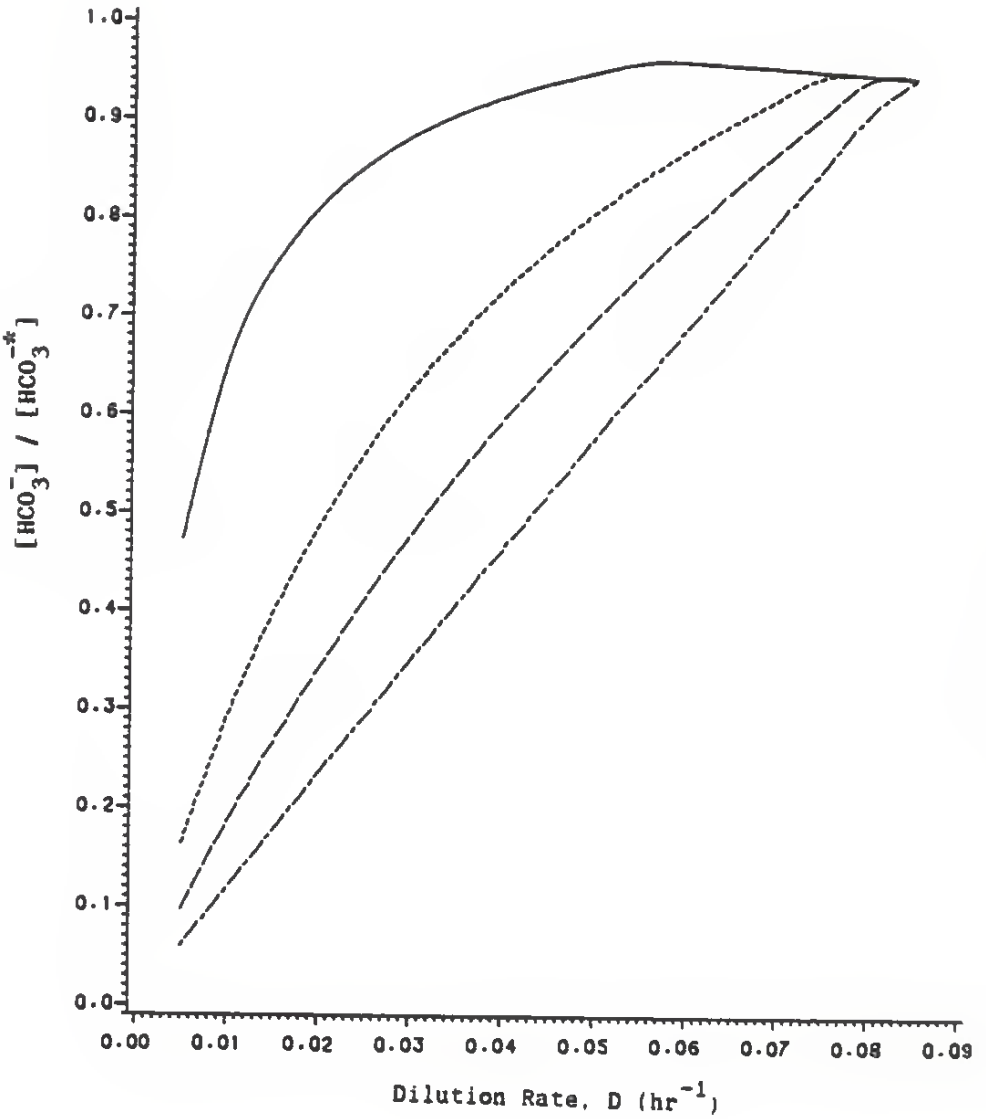

Figure 2-9. Variation in the degree of equilibrium between bicarbonate and dissolved carbon dioxide with dilution rate; mass-transfer coefficient is the parameter. Symbols are as defined in Figure 2-7.

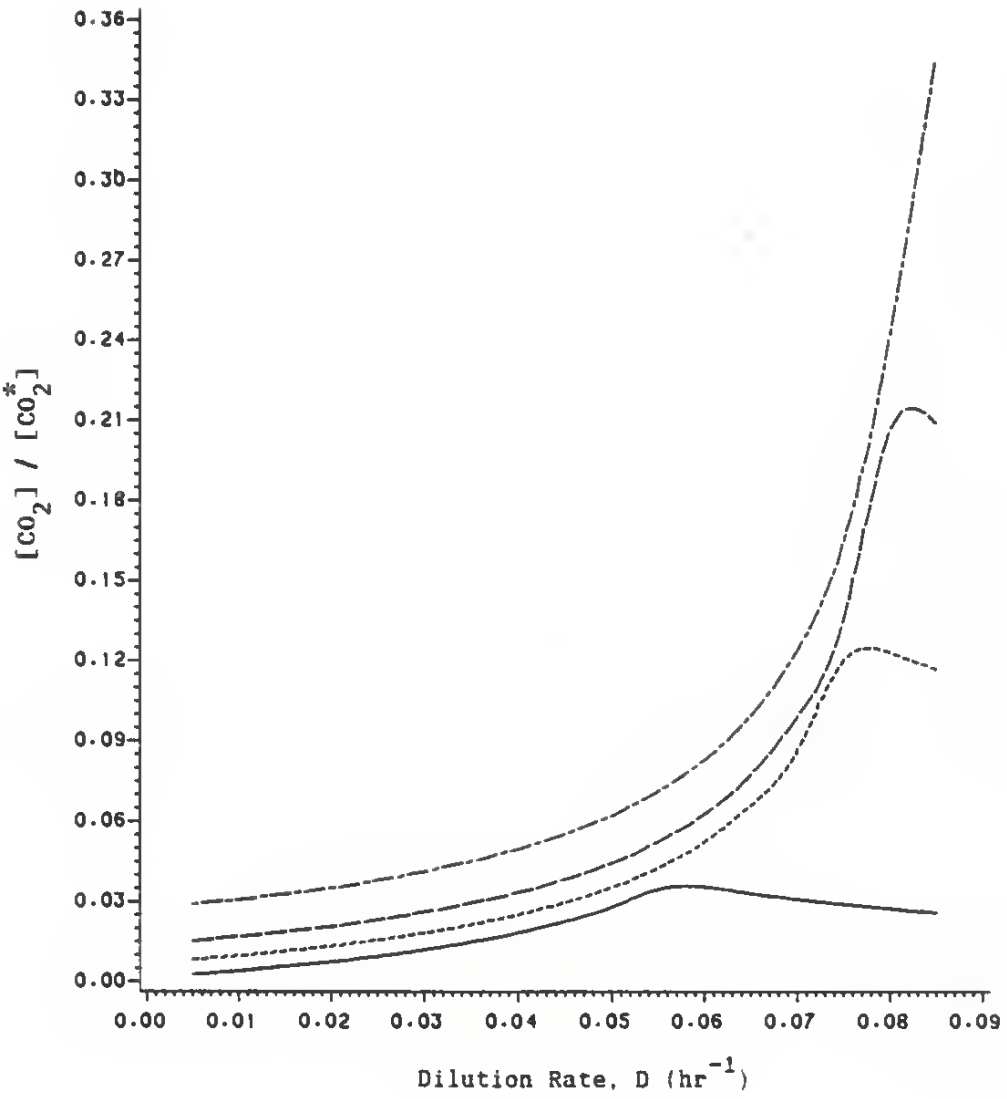

Figure 2-10. Variation in the degree of equilibrium between dissolved CO_2 and CO_2 in the exiting gas with dilution rate; mass-transfer coefficient is the parameter. Symbols are as defined in Figure 2-7.

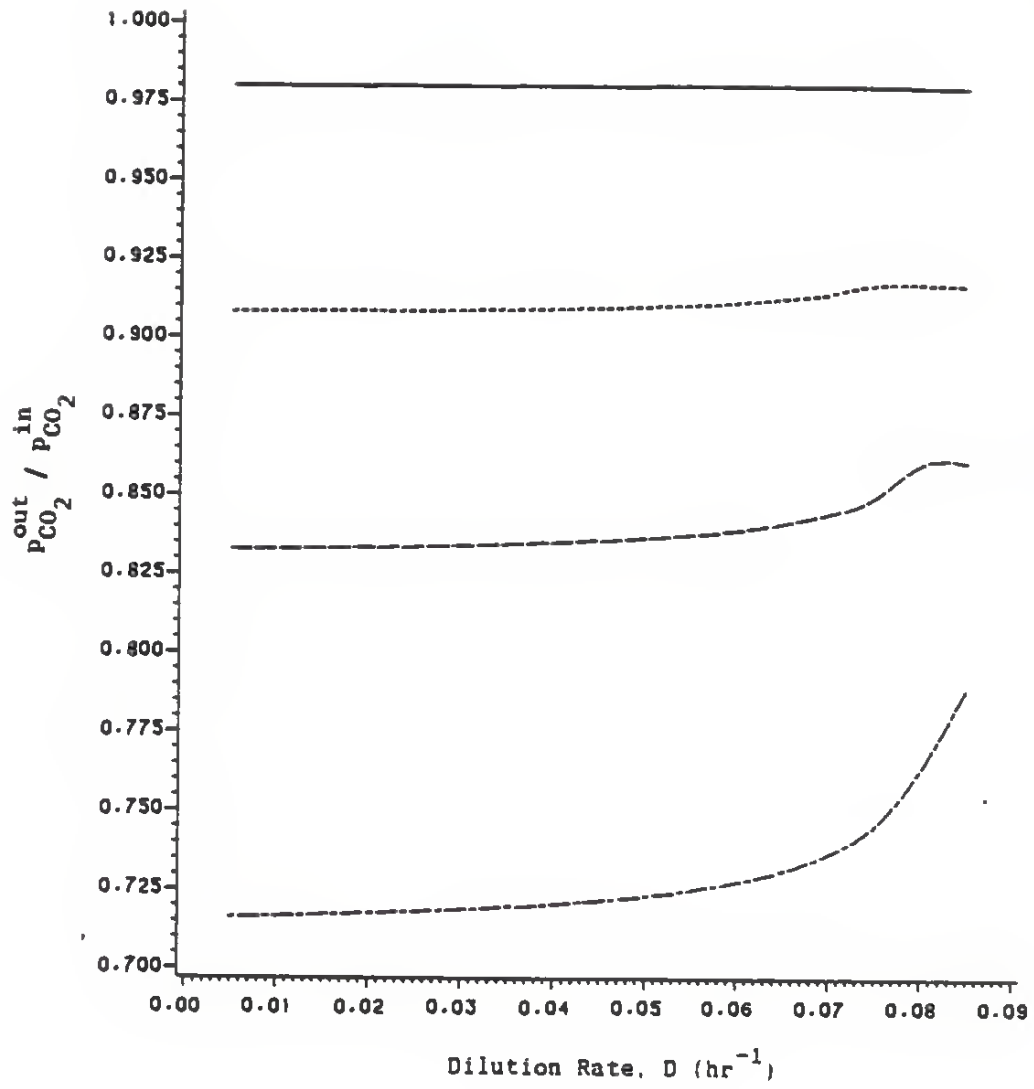

Figure 2-11. Variation in the fraction of carbon in the entering gas that does not dissolve with dilution rate; mass-transfer coefficient is the parameter. Symbols are as defined in Figure 2-7.

Chapter 3

MODELING AND SIMULATION OF LIGHT AND BICARBONATE LIMITED PHOTOSYNTHETIC GROWTH

Introduction

Studies of algal growth are often conducted in chemostats where only a single nutrient is limiting. [1-3] Typical nutrients include phosphorus, nitrogen and carbon. Although it is not a nutrient, light is often a factor limiting the growth rate of algal. Michaelis-Menton kinetics are commonly used to relate the growth rate to the external nutrient concentration or light intensity. [1-3]

Modeling of aquatic, photosynthetic growth under carbon limited conditiona is complicated by two factors. First, one must know which carbon species the organism of interest assimilates. Some algal prefer dissolved CO_2 whereas others choose bicarbonate. [4-7] Second, dissolved CO_2 undergoes a series of aquatic reactions which interconvert the various carbon species, CO_2, HCO_3^-, $CO_3^=$, and H_2CO_3. If aqueous inorganic carbon equilibrium exists in the tank, any carbon species can be used in a modeling attempt with equal validity. This is because kinetic growth parameters baaed on one carbon species can be converted to another carbon basis using equlibrium chemistry. [8]

It can usually be assumed that all dissolved chemical species exist in uniform concentrations throughout a stirred fermentation tank. However, modeling light-limited algal growth can be complicated by self-shading of the culture. Self-shading causes a variation of light intensity with position inside the tank.

Some studies of algal growth have been carried out so that light and a single nutrient simultaneously limit growth. [9-11] Rhee has found that a sharp transition between nitrogen limitation and light limitation occurs for Scenedesmus sp. [12] Markl has suggested that a product model of the form

$$P = f_1([CO_2]) \cdot f_2(I)$$

would be appropriate for modeling the simultaneous carbon and light limited growth of Chlorella vulgaris. [13] Here, P is the rate of photosynthesis, f_1 is a function of dissolved CO_2 concentration, and f_2 is a function of light intensity. The variation of light intensity with position is taken into account.

In a pond, sunlight can enter from only one direction. However, in experimental studies, one possible reactor geometry consists of a rectangular tank with light shining in from two, opposing faces. [14] The models presented here are the first to consider the latter case. In this chapter, both cases of incident light will be considered.

Theory

The system being modeled consists of a perfectly mixed rectangular tank with both gas and liquid feed streams as well as exiting gas and liquid streams. Two different cases of incident light are considered: light shining from only one side and light shining from two, opposing faces. The aqueous inorganic carbon reactions of kinetic importance are listed in Figure 3-1. Material balances for each form of carbon present

in the tank are listed in Figure 3-2. A description of the balances and assumptions involved in their construction can be found in Chapter 2. Equations (3-1) through (3-5) are linear with the six unknowns, X, $p_{CO_2}^{out}$, $[CO_2]$, $[H_2CO_3]$, $[HCO_3^-]$, and $[CO_3^=]$. Consequently, a series of substitutions can be used to eliminate $p_{CO_2}^{out}$, $[CO_2]$, $[H_2CO_3]$, and $[CO_3^=]$ from Equation (3-5), thereby yielding

$$[HCO_3^-] = C_1X + C_2 \qquad (3\text{-}7)$$

where C_1 and C_2 are constants. Because the dilution rate is known, and the form of μ_{AVG} is assumed to be a function of only light intensity $[HCO_3^-]$ and X, Equations (3-6) and (3-7) comprise two equations with two unknowns. However, Equation (3-6) can depend nonlinearily on the expression chosen for the specific growth rate (μ).

Two types of models are presented for μ. The first is a product model:

$$\mu(Z) = \frac{\mu_{max}\ [HCO_3^-]}{K_s + [HCO_3^-]} \cdot \frac{I(Z)}{K_I + I(Z)} \ . \qquad (3\text{-}8)$$

All chemical species are assumed to be well-mixed and thus, independent of position (Z). The second model assumes that the tank can consist of two portions. One portion obeys light-limited kinetics:

$$\mu_I(Z) = \frac{\mu_{maxI}\ I(Z)}{K_I + I(Z)} \ . \qquad (3\text{-}9)$$

The other portion obeys carbon-limited kinetics:

$$\mu_c = \frac{\mu_{maxc}\ [HCO_3^-]}{K_s + [HCO_3^-]} \quad . \qquad (3\text{-}10)$$

The equation used for modeling the specific growth rate is determined by which expression (3-9 or 3-10) gives the lowest value of μ at that particular position in the tank. Thus the portion(s) closest to the light can be carbon-limited and modeled with Equation (3-10) while positions farther away from the light source(s) follow Equation (3-9). At the geometric position Z=M, the changeover from carbon to light limitation occurs; thus,

$$\frac{\mu_{maxc}\ [HCO_3^-]}{K_s + [HCO_3^-]} = \frac{\mu_{maxI}\ I(M)}{K_I + I(M)} \quad . \qquad (3\text{-}11)$$

The relationship between light intensity and position depends on whether light is introduced from one side or two opposing sides. In either case, the Beer Law is assumed to prevail. Thus, for light entering from only one side:

$$I_1(Z) = I_o \exp(-\alpha \times Z) \qquad (3\text{-}12)$$

where α is the absorption coefficient, I_o is the incident light intensity and $I_1(Z)$ is the light intensity at position Z. If light enters from two opposing faces:

$$I_2(Z) = I_o \exp(-\alpha \times Z) + I_o \exp[-\alpha \times (L-Z)] \qquad (3\text{-}13)$$

where L is the length of the reactor and $I_2(Z)$ is the total light intensity at position Z.

Expressions for each case will be developed. The expression denoted as Model 1 is presented in Chapter 2. Model 1 is a Monod model based on bicarbonate as the only limiting nutrient.

Model 2: Product Model, Light Enters from One Side

Equation (3-8) may be rewritten in the form:

$$\mu(Z) = \frac{\mu_{max}\,[HCO_3^-]}{K_s + [HCO_3^-]} \cdot \frac{I_o \exp(-\alpha XZ)}{K_I + I_o \exp(-\alpha XZ)} \qquad (3\text{-}14)$$

The volume-average specific growth rate (μ_{AVG}) is obtained as

$$\mu_{AVG} = \frac{\int_0^L \mu(Z)dZ}{\int_0^L dZ} . \qquad (3\text{-}15)$$

Recalling from Equation (3-6) that $D = \mu_{AVG}$, Equation (3-15), in conjunction with Equation (3-14), yields

$$\mu_{AVG} = D = \frac{\mu_{max}\,[HCO_3^-]}{(K_s + [HCO_3^-])L\alpha X} \ln\left[\frac{K_I + I_o \exp(-\alpha XL)}{K_I + I_o}\right] . \qquad (3\text{-}16)$$

Equation (3-7) can be substituted into the above equation to yield an equation which is a function of a single variable X. This equation can be solved explicitly for D, or implicitly for X using a trial-and-error method.

Model 3: Threshold Model, Light Enters from One Side

$$\mu_{AVG} = \frac{M}{L} \frac{\int_0^M \frac{\mu_{maxc} [HCO_3^-]dZ}{K_s + [HCO_3^-]}}{\int_0^M dZ}$$

$$+ \frac{L-M}{L} \frac{\int_M^L \frac{\mu_{maxI} I_o \exp(-\alpha XZ)dZ}{K_I + I_o \exp(-\alpha XZ)}}{\int_M^L dZ} . \qquad (3\text{-}17)$$

This expression can be integrated and combined with Equation (3-6) to give

$$\mu_{AVG} = D = \frac{M}{L} \frac{\mu_{maxc} [HCO_3^-]}{K_s + [HCO_3^-]} + \frac{\mu_{maxI}}{\alpha XL} \ln \left[\frac{K_I + I_o \exp(-\alpha XL)}{K_I + I_o \exp(-\alpha XM)} \right] . \qquad (3\text{-}18)$$

At the point (Z=M) where the cause of growth limitation changes from carbon to light:

$$\frac{\mu_{maxc} [HCO_3^-]}{K_s + [HCO_3^-]} = \frac{\mu_{maxI} I_o \exp(-\alpha XM)}{K_I + I_o \exp(-\alpha XM)} . \qquad (3\text{-}19)$$

Solving this equation for M:

$$M = -\frac{1}{\alpha X} \ln \left[\frac{\mu_{maxc} K_I [HCO_3^-]}{\{(K_s + [HCO_3^-])\mu_{maxI} - \mu_{maxc}[HCO_3^-]\} I_o} \right] . \qquad (3\text{-}20)$$

Equation (3-7) can be used to substitute for $[HCO_3^-]$ in Equations (3-18) and (3-20). Then Equation (3-20) can be inserted into Equation (3-18) for M. This leaves a single, nonlinear equation with the unknown X. This final equation can be solved using trial-and-error.

For the case where light enters the tank from opposing faces, the dependence of light intensity on position is given in Equation (3-13). To arrive at an expression for μ_{AVG}, it will be necessary to evaluate the integral

$$\int \frac{I_2(Z)dZ}{K_I + I_2(Z)} \tag{3-21}$$

where $I_2(Z)$ is given by Equation (3-13). Letting $a = -\alpha X$, $b = \exp(-\alpha XL)$, $m_1 = \exp(-\alpha XZ)$, $m_2 = \exp(\alpha XZ)$ and $q = 4I_o^2\, b - K_I^2$, two solutions are possible. First, for $q > 0$,

$$\int \frac{I_2(Z)dZ}{K_I + I_2(Z)} = \frac{1}{2a} \ln \frac{(I_o b + K_I m_1 + I_o m_1^2)}{(I_o + K_I m_2 + I_o b m_2^2)} + \frac{K_I}{a\, q} \left[\tan^{-1} \frac{2I_o b m_2 + K_I}{q} - \tan^{-1} \frac{2I_o m_1 + K_I}{q}\right] . \tag{3-22}$$

Second, for $q < 0$,

$$\int \frac{I_2(Z)dZ}{K_I + I_2(Z)} = \frac{1}{2a} \ln \frac{(I_o b + K_I m_1 + I_o m_1^2)}{(I_o + K_I m_2 + I_o b m_2^2)} + \frac{K_I}{2a\ -q} \ln \left[\frac{(2I_o m_1 + K_I\ + -q)\ (2I_o b m_2 + K_I\ -\ -q)}{(2I_o m_1 + K_I\ -\ -q)\ (2I_o b m_2 + K_I\ +\ -q)} \right] \tag{3-23}$$

Note that Equations (3-22) and (3-23) are both functions of onIy X. Now the final two models will be developed.

Model 4: Product Model with Light Entering from Two Opposing Sides.

$$\mu_{AVG} = \frac{\int_0^L \frac{\mu_{max}[HCO_3^-]}{K_s + [HCO_3^-]} \frac{I_2(Z)dZ}{K_I + I_2(Z)}}{\int_0^L dZ}$$

$$= \frac{\mu_{max}[HCO_3^-]}{(K_s + [HCO_3^-])L} \int_0^L \frac{I_2(Z)\, dZ}{K_I + I_2(Z)} \qquad (3\text{-}24)$$

From Equation (3-6), $D = \mu_{AVG}$ and from Equation (3-7), $[HCO_3^-] = f(X)$. By substituting these two values into Equation (3-24) and using Equations (3-22) and (3-23), one is left with an equation with X as the only unknown. A trial-and-error procedure can be used to solve for X.

Model 5: Threshold Model with Light Entering from Two Opposing Sides

$$\mu_{AVG} = \frac{2M}{L} \frac{\int_0^M \frac{\mu_{maxc}[HCO_3^-]dZ}{K_s + [HCO_3^-]}}{\int_0^M dZ} + \frac{L-2M}{L} \frac{\int_M^{L-M} \frac{\mu_{maxI} I_2(Z)dZ}{K_I + I_2(Z)}}{\int_M^{L-M} dZ}$$

$$= \frac{2M}{L} \frac{\mu_{maxc}[HCO_3^-]}{(K_s + [HCO_3^-])} + \frac{\mu_{maxI}}{L} \int_M^{L-M} \frac{I_2(Z)\, dZ}{K_I + I_2(Z)} \qquad (3\text{-}25)$$

At the point (M) where the source of growth limitation changes from bicarbonate to light:

$$\frac{\mu_{maxc}[HCO_3^-]}{(K_s + [HCO_3^-])} = \frac{\mu_{maxI}\{I_o \exp(-\alpha XM) + I_o \exp[-\alpha X(L-M)]\}}{K_I + I_o \exp(-\alpha XM) + I_o \exp[-\alpha X(L-M)]} \qquad (3\text{-}26)$$

Solving for M:

$$M = \frac{-1}{\alpha X} \ln \left\{ \frac{K_I \mu_c}{2I_o(\mu_{maxI} - \mu_c)} \pm \left[\left[\frac{K_I \mu_c}{2I_o(\mu_{maxI} - \mu_c)} \right]^2 - \exp(-\alpha XL) \right]^{1/2} \right\} \tag{3-27}$$

where $\mu_c = \mu_{maxc} [HCO_3^-]/(K_s + [HCO_3^-])$ and the positive case is found to be the correct one. As before, Equations (3-6), (3-7), (3-22), (3-23), and (3-27) can each be substituted into Equation (3-25) to give one equation containing the single unknown X.

These four models are incorporated into a single computer program that solves the material balances for $[HCO_3^-]$, $[CO_2]$, $[CO_3^=]$, $[H_2CO_3]$, $p_{CO_2}^{out}$ and X. Once the biomass concentration in the tank is known, other quantities of interest can be calculated. One such quantity is the biomass energetic yield, given by

$$\eta = \frac{DXV_L \sigma_b \gamma_b Q_o}{12 I_a A} . \tag{3-28}$$

The biomass energetic yield is the fraction of light energy absorbed which is converted to biomass energy. The average light intensity in the tank when light shines from both sides can be estimated using the equation from Lee: [14]

$$I_{AVG} = \frac{I_{in} + I_{out} + 2I_{center}}{2} . \tag{3-29}$$

Results

All results presented are for the bacterium Spirulina plantensis. Kinetic parameters for this organism were obtained by Lee. [14]

Conditions used in all the simulations can be found in Tables 3-1 and 3-2. Values of parameters not listed in these tables are either shown in each figure or mentioned below.

The first set of results (Figures 3-3 to 3-6) show comparisons of model predictions and data obtained under carbon-limited growth conditions by Lee. Light was introduced from opposing faces and the liquid feed contained 1.67 mmol C/liter. No gas feed was used. For Model 5, the simulations predicted that growth was carbon-limited for all conditions except I_o = 14.4 W/m^2 and D>0.07 hr^{-1}.

Figures 3-7 to 3-8 compare model predictions with light-limited growth data obtained by Lee. Light was introduced from both sides and the liquid feed contained 5.016 mmol C/liter. No gas feed was used. Model 5 indicated that conditions were light-limited over the whole range of biomass concentration and light intensity explored.

Statistical analyses using the results shown in Figures 3-3 to 3-8 were performed to determine which model fit the experimental data better (See Table 3-3). Based on the mean square of residuals, Model 5 fit the data better than did Model 4. However, each F-test revealed that Model 5 was not significantly better than Model 4.

Figures 3-9 through 3-15 show the effect of three parameters on the predicted steady-state biomass concentration exiting the tank. Two feed situations are considered in these figures: carbon is in the liquid feed with no gas feed and carbon is in the gas feed, but no carbon is in the liquid feed (See Table 3-2). Parameters considered are the total dissolved carbon in the liquid feed ($[C_{TOT}]_{in}$), the gas-to-liquid mass

transfer coefficient ($k_L a$), and the incident light intensity (I_o). Parameter values are selected so that biomass concentration is in a range typically encountered. Incident light intensity is kept below 75 W/m^2 to ensure that no photoinhibited conditions are encountered. Enough figures are included so that one can compare the differences between model-types and also see the effects of each parameter on a single model (Model 4). Nominal values of the parameters are I_o = 25 W/m^2, $[C_{TOT}]_{in}$ = 0.025 mol/liter, and $k_L a$ = 17.7 hr^{-1}.

Figures 3-16 through 3-20 show the effect of the same parameters on the biomass energetic yield. Again, model 4 is shown because it illustrates the same trends found with each model. Figure 3-20 is included so that one can see the differences between the biomass energetic yields predicted by the threshold model and those predicted by the product model.

A direct comparison of the dependence of η and I_{AVG} on the dilution rate is illustrated in Figure 3-21. This comparison is made for model 5 under completely light-limited conditions.

Finally, Figures 3-22 and 3-23 show the local light intensity and specific growth rate for each model at every position in the tank. The dilution rate used in the simulations is 0.05 hr^{-1} and only a liquid feed stream is included. The biomass concentrations predicted by each model under these conditions are as follows:

Model 2: 0.0633 g/liter

Model 3: 0.0641 g/liter

Model 4: 0.146 g/liter

Model 5: 0.148 g/liter.

Discussion

Figures 3-3 and 3-4 demonstrate that neither Model 4 nor Model 5 fits Lee's data well for D = 0.03 hr^{-1}. This can be attributed to the fact that urea was used as a nitrogen source; carbon contained in urea served as a second source of carbon for the algal (see Discussion, Chapter 2). The role of urea would be especially important at a low dilution rate because the chemostat would be operating under bicarbonate-depleted conditions. Thus the models should predict a low biomass concentration for each dilution rate. This holds true for Model 5, which fits the data rather well for D > 0.05 hr^{-1}. However, Model 4 does not fit the data as well as Model 5 for any dilution rate.

Figures 3-5 and 3-6 show comparisons of biomass energetic yields obtained by Lee and those predicted by each model. Each model predicts the correct trend of increasing η with dilution rate until a maximum is reached near washout. Both models also correctly predict a decrease in η with increasing light intensity. Again Model 5 fits the data much better than Model 4 does. Neither model closely matches the data points for D = 0.03 hr^{-1}. This discrepency can be attributed to the presence of urea as a second carbon source.

Figure 3-7 shows that Model 5 fits all of the data for X = 0.05 g/liter quite well. This result is expected because the kinetic parameters used in Model 5 under these conditions were obtained using

the same set of data. Model 4 also fits the data nearly as well as Model 5 for the same reason. The fact that each model shows nearly the same results for X = 0.04 g/liter and X = 0.05 g/liter indicates that little self-shading of the culture is occurring. However, the data for X = 0.04 g/liter are higher than those predicted by either model. Perhaps this is due to the more uniform light intensity at 0.04 g/liter.

Figure 3-8 shows that both models predict biomass energetic yields in agreement with Lee's data for 0.05 g/liter. For 0.04 g/liter each model predicts a bioenergetic yield that is too low. This result is a reflection of the erroneously low specific growth rates shown in Figure 3-7.

Figure 3-9 shows simulation predictions for Model 2 with varying amounts of carbon in the liquid feed. For the lowest level of carbon, the results indicate that growth takes place under carbon-limited conditions at every dilution rate. This is evidenced by the concave downward shape of the curve. For higher carbon inputs the tank is carbon-limited only at lower values of dilution rate. At higher values of dilution rate, the curves converge to form a single curve that is concave upward, indicating that growth is light-limited. Figure 3-11 shows that the same trends exist for Model 4. For Model 3 (see Figure 3-10) one difference exists. There is a more distinct and abrupt transition from carbon-limited to light-limited kinetics. Model 5 (see Figure 3-12) predictions differ from those for Model 3 in that at D > 0.08 hr^{-1} there is a sharp turn downwards in the curve. This turn

occurs near washout because the kinetics revert back to a carbon-limited basis ($\mu_{maxI} > \mu_{maxc}$).

Figure 3-13 shows the effect of incident light intensity on effluent biomass concentration from a liquid-fed tank. At the lowest values of dilution rate, carbon-limitation occurs. As the dilution rate increases, the simulations predict light-limited growth. As the incident light intensity increases, biomass concentration also goes up and the degree of concavity upward decreases. This change in concavity illustrates the increasing role of carbon limitation as light intensity increases.

Figures 3-14 and 3-15 illustrate the shapes of X versus D in gas-fed chemostats. In this mode of operation, the shape of curve produced by light-limited conditions is indistinguishable from that produced by carbon-limited conditions.

To analyze the dependence of biomass energetic yield on the dilution rate, the limiting cases should be discussed. For strictly carbon-limited conditions, the biomass energetic yield will increase with the dilution rate until a maximum is reached. This maximum roughly corresponds to the maximum in productivity (X·D). However, for light-limited conditions the biomass energetic yield is highest at low values of dilution rate and then drops off as the dilution rate increases. This drop corresponds to an increase in the light intensity caused by a reduction in the biomass concentration.

Figures 3-16 to 3-20 illustrate these limiting conditions; they show the transition from one case to another as parameter values change.

The transition region exhibits a shift in the dilution rate where the maximum in η occurs. This shift is due to the opposing forces of a decreasing η with D for light-limited conditions and an increasing η with D for carbon-limited conditions. Figures 3-16 and 3-17 can be compared to see the differences in predictions between the threshold model and the product model. The threshold model undergoes a more abrupt transition from carbon-limited behavior to light-limited behavior of η versus D. Also, the curves for Model 5 all converge to a single curve of η versus D.

Figure 3-21 is for completely light-limited conditions; it shows a direct comparison of the relationship between η and I_{AVG}. The decrease in η with D can be attributed to the increase in I_{AVG} with D. Figures 3-22 and 3-23 show that when light is shining from only one side, very little of the incident light reaches the back of the tank. For light shined from opposing faces, symmetry is observed. However, only a fraction of the incident light reaches the center. An analogous dependence of μ on position is apparent from Figure 3-23.

Conclusions

The Monod model based on bicarbonate combined with the Beer Law predicts that the biomass energetic yield increases with dilution rate until a maximum near washout is reached. The light-based Monod model combined with the Beer Law predicts that η will decrease with increasing dilution rate; a unique finding. For simultaneous carbon and light

limited growth, a maximum in η versus D occurs at a dilution rate dependent on the contribution of each type of limitation.

Only two differences between product and threshold models were observed. First, the threshold model predicts a more abrupt transition from carbon-limitation to light limitation and vice versa. Second, there is a greater difference between the two types of models under carbon-limited conditions, because the value of $\mu_{maxc} < \mu_{max}$, whereas $\mu_{maxI} = \mu_{max}$. This investigation is the first one that directly compares predictions by each type of model.

NOMENCLATURE

A = Area of one side through which light passes

D = Dilution rate

I_a = $I_{in} - I_{out}$ = Actual amount of light absorbed by cell culture

I_{AVG} = Average light intensity as defined in equation (29)

I_{center} = Light intensity directionally measured at the center with shining from both sides

I_{in} = Light intensity measured at the front with shining from one side

I_{out} = Light intensity measured at the back when light is shining from one side

K_I = Half-saturation constant for light

K_j = Equilibrium constant for aqueous carbon reaction "j"

K_s = Half-saturation constant for $[HCO_3^-]$

k_j = Rate constant for aqueous carbon reaction "j"

k_La = Mass transfer coefficient

L = Distance across tank that light travels

M = Position in the tank where a change from carbon to light limitation occurs

$p_{CO_2}^{in}$ = Partial pressure of CO_2 entering tank

$p_{CO_2}^{out}$ = Partial presure of CO_2 exiting tank

pH = pH in the tank

pH_{feed} = pH of the liquid feed

Q_{in} = Volumetric flow rate of gas entering tank

Q_o = Energy content of blue-green algal per equivalent of available electrons.

Q_{out} = Volumetric flow rate of gas exiting tank

R = Ideal gas constant

T_{feed}^{liq} = Temperature of the liquid feed

T_{in}^{gas} = Temperature of gas entering tank

T_{out}^{gas} = Temperature of gas exiting tank

V_L = Volume of liquid in tank

Y_c = Carbon yield to biomass

Z = Position in the tank

$[CO_2^*]$ = Concentration of aqueous CO_2 that would be in equilibrium with the exiting gas stream

$[C_{TOT}]_{in}$ = Aqueous concentration of total dissolved carbon in the liquid feed

["i"] = Aqueous concentration within the tank (and therefore exiting the tank); $[CO_2]$ = dissolved CO_2, $[HCO_3^-]$ = dissolved HCO_3^-, $[CO_3^=]$ = dissolved $CO_3^=$, $[H_2CO_3]$ = dissolved H_2CO_3, $[H_2O]$ = water conc., [OH-] = dissolved OH^-, $[H^+]$ = dissolved H^+.

$["i"]_{in}$ = Aqueous concentration in the liquid feed; see definitions immediately above.

α = Absorption coefficient

γ_b = Reductance degree of biomass

μ_{AVG} = Average specific growth rate

μ_{max} = Maximum specific growth rate of biomass

μ_{maxc} = Bicarbonate limited maximum specific growth rate of biomass

μ_{maxI} = Light-limited maximum specific growth rate of biomass

σ_b = Weight fraction carbon in biomass

References

1. 8rune, D. E., et al., Eur. J. of Apl. 8iotech., 13:71-76 (1981).

2. Goldman, J. C., et al., J. of Water Pollut. Contr. Fed., 46:554-574 (1974).

3. Goldman, J. C., et al., Appl. and Env. Micro., 41(1):60-70 (1981).

4. Badger, M. R., et al., Plant Physiology, 70:517-523 (1982).

5. Findenegg, G. R., Transmembrane Ionic Exchanges in Plants, Colloque Internat. CNRS Nr. 258, Paris, 275-281 (1977).

6. Kaplan, A., J. of Expt. 8ot., 32(129):689-877 (1981).

7. Miller, A. G., et al., Plant Physiology, 75:1084-1070 (1984).

8. Goldman, J. C., et al., J. Water Pollut. Contr. Fed., 46:2785-2787 (1974).

9. Davis, C. O., J. Phycology, 12:291-300 (1978).

10. McAllister, C. D., J. Fish. Res. 8d. Can., 31(1):159-181 (1984).

11. MacIsaac, J. J., et al., Deep Sea Research, 19:209-232 (1972).

12. Rhee, G. Y., et al., Limnology and Ocean., 28(4):649-659 (1981).

13. Markl, L., 8iotech. and Bioeng., 19:1851-1862 (1977).

14. Lee, H. Y., 8ioenergetics and Kinetics of Photosynthetic Single Cell Protein Production Processes, PhD Dissertation, Kansas State Univ. (1988).

15. Palmer, D. A., et al., Chem. Rev., 83:851-731 (1983).

18. Pinsent, 8. R., et al., Trans. Faraday Soc., 47:263-269 (1951).

17. Eigen, M., Angew. Chem., 75:489-498 (1963).

Table 3-1. Parameter values used in all simulations.

Parameter	Value
pH_{feed}	9.2
T_{feed}^{liq}	25°C
pH	9.2
T	33°C
V_L	13.5 liter
Y_c	25.18 g biomass/mol C
σ_b	0.4766
γ_b	4.402 equiv. of avail. elec./g atom C
Q_o	26.95 kcal/equiv. of avail. elec.
A	0.07 m^2
L	0.18 m
μ_{max}	0.1199 hr^{-1}
μ_{maxI}	0.1199 hr^{-1}
μ_{maxC}	0.090 hr^{-1}
K_I	12.7388 W/m^2
K_S	11.643 mg HCO_3^-/liter

Table 3-2. Parameter values used in gas-fed simulations.

Total Pressure is 1 atm.

Parameter	Value
Q_{in}	13.5 liter/min
Q_{out}	13.5 liter/min
$p^{in}_{CO_2}$	0.000316 atm
T^{gas}_{in}	33°C
T^{gas}_{out}	33°C

Table 3-3. Statistical Comparison of Models 4 and 5.

Source of Data	Model	Degrees of Freedom	Sum of Squares of Residuals	Mean Square of Residuals	F
Figure 3-3*	4	5	1.50×10^{-3}	3.00×10^{-4}	2.459
Figure 3-4*	5	4	4.89×10^{-4}	1.22×10^{-4}	
Figure 3-5	4	8	3.60×10^{-2}	4.50×10^{-3}	1.275
Figure 3-6	5	7	2.47×10^{-2}	3.53×10^{-3}	
Figure 3-7	4	18	4.95×10^{-3}	3.09×10^{-4}	1.251
	5	15	3.71×10^{-3}	2.47×10^{-4}	
Figure 3-8	4	16	3.82×10^{-2}	2.39×10^{-3}	1.101
	5	15	3.26×10^{-2}	2.17×10^{-3}	

*The point at D = 0.03 hr^{-1} was an outlier, so it was neglected.

Figure 3-1. Aqueous Inorganic Carbon Chemistry

Reactions	Equilibrium Constants
1. $CO_2 + H_2O \underset{k_{-1}}{\overset{k_1}{\rightleftharpoons}} H_2CO_3$	$K_1 = k_1/k_{-1}$
2. $CO_2 + OH^- \underset{k_{-2}}{\overset{k_2}{\rightleftharpoons}} HCO_3^-$	$K_2 = k_2/k_{-2}$
3. $HCO_3^- + H^+ \underset{k_{-3}}{\overset{k_3}{\rightleftharpoons}} H_2CO_3$	$K_3 = k_3/k_{-3}$
4. $HCO_3^- + OH^- \underset{k_{-4}}{\overset{k_4}{\rightleftharpoons}} CO_3^{-2} + H_2O$	$K_4 = k_4/k_{-4}$

Temperature Dependence of Rate Constants*

$$k_1 [H_2O] = 2.165 \times 10^{10} \exp(-8058.7/T) \ (sec^{-1}) \ (T[=]K)^{1.5}$$

$$k_{-1} = 1.035 \times 10^{12} \exp(-7300.9/T) \ (sec^{-1}) \ (T[=]K)^{1.5}$$

$$k_2 = 4.3152 \times 10^{13} \exp(2895.0/T) \ (sec^{-1}) \ (T[=]K)^{1.6}$$

$$k_{-2} = k_2/K_2 \ sec^{-1}$$

$$k_3 = 4.7 \times 10^{10} \ M^{-1} sec^{-1} \text{ at } 25°C \ [17]$$

$$k_{-3} = k_3/K_3 \ sec^{-1}$$

$$k_4 = K_4 \cdot k_{-4} \ M^{-1} sec^{-1}$$

$$k_{-4} = 2.6 \times 10^4 \ M^{-1} sec^{-1} \text{ at } 20°C \ [17]$$

* Dependence of rate constants on ionic strength was not considered.

Figure 3-2. Material Balances*

Liquid Phase CO_2 Balance

$$\frac{d[CO_2]}{dt} = 0 = k_L a([CO_2^*]-[CO_2])+D([CO_2]_{in}-[CO_2])+k_{-1}[H_2CO_3] \\ -k_1[H_2O][CO_2]+k_{-2}[HCO_3^-]-k_2[OH^-][CO_2] \quad (3\text{-}1)$$

Gas Phase CO_2 Balance

$$\frac{V_g}{RT}\frac{dP_{CO_2}}{dt} = 0 = \frac{Q_{in}\,P_{CO_2}^{in}}{RT_{in}^{gas}} - \frac{Q_{out}\,P_{CO_2}^{out}}{RT_{out}^{gas}} - k_L a([CO_2^*]-[CO_2])V_L \quad (3\text{-}2)$$

$CO_3^=$ Balance

$$\frac{d[CO_3^=]}{dt} = 0 = D([CO_3^=]_{in}-[CO_3^=])+k_4[OH^-][HCO_3^-]-k_{-4}[H_2O][CO_3^=] \quad (3\text{-}3)$$

H_2CO_3 Balance

$$\frac{d[H_2CO_3]}{dt} = 0 = D([H_2CO_3]_{in}-[H_2CO_3])+k_1[H_2O][CO_2]-k_{-1}[H_2CO_3] \\ +k_3[H^+][HCO_3^-]-k_{-3}[H_2CO_3] \quad (3\text{-}4)$$

HCO_3^- Balance

$$\frac{d[HCO_3^-]}{dt} = 0 = D([HCO_3^-]_{in}-[HCO_3^-])+k_2[OH^-][CO_2]-k_{-2}[HCO_3^-] \\ +k_{-3}[H_2CO_3]-k_3[H^+][HCO_3^-]+k_{-4}[H_2O][CO_3^=] \\ -k_4[OH^-][HCO_3^-]-\frac{X\,\mu_{AVG}}{Y_c} \quad (3\text{-}5)$$

Biomass Balance

$$\frac{dX}{dt} = 0 = -DX + X\,\mu_{AVG} \quad (3\text{-}6)$$

*See Nomenclature for a description of the symbols.

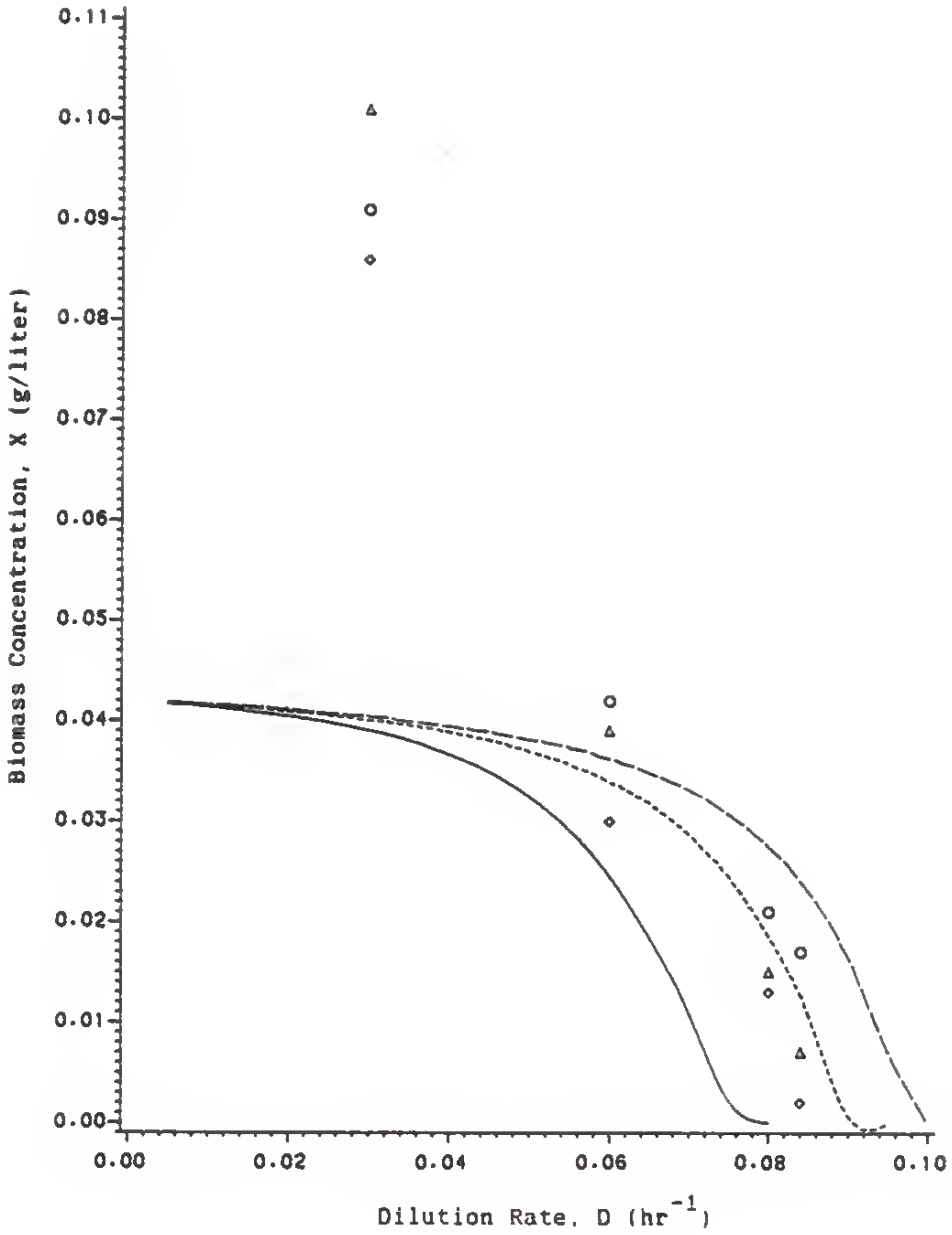

Figure 3-3. Comparison of Model 4 predictions and Lee's carbon-limited growth data for S. platensis. Variation in biomass concentration with dilution rate with incident light intensity as a parameter is shown. Values of I_o in W/m^2 are ⊙ 14.4, △ 29.2, and ⊡ 51.4.

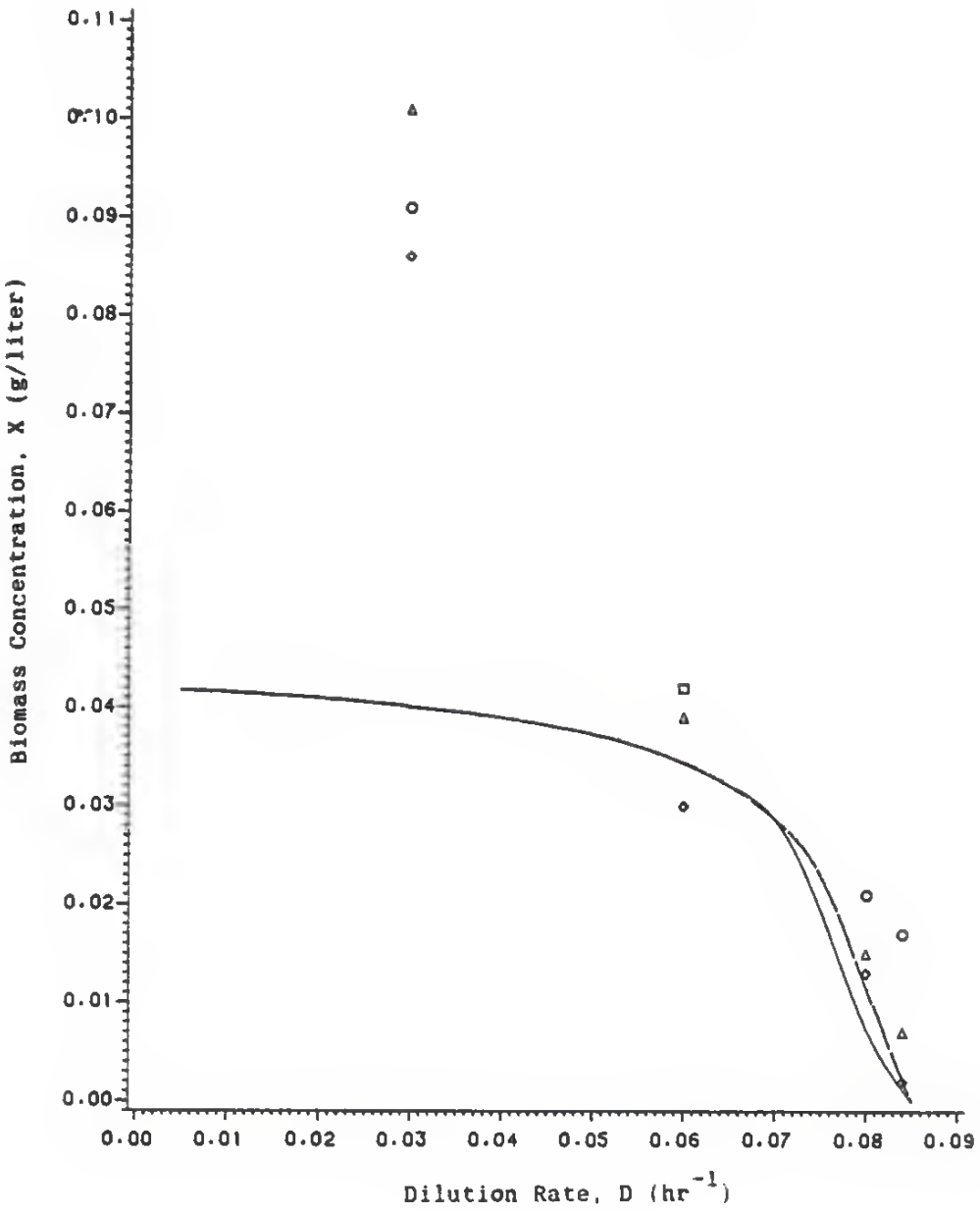

Figure 3-4. Comparison of Model 5 predictions and Lee's carbon-limited growth data for S. platensis. Variation in biomass concentration with dilution rate with incident light intensity as a parameter is shown. Symbols are as defined in Figure 3-3.

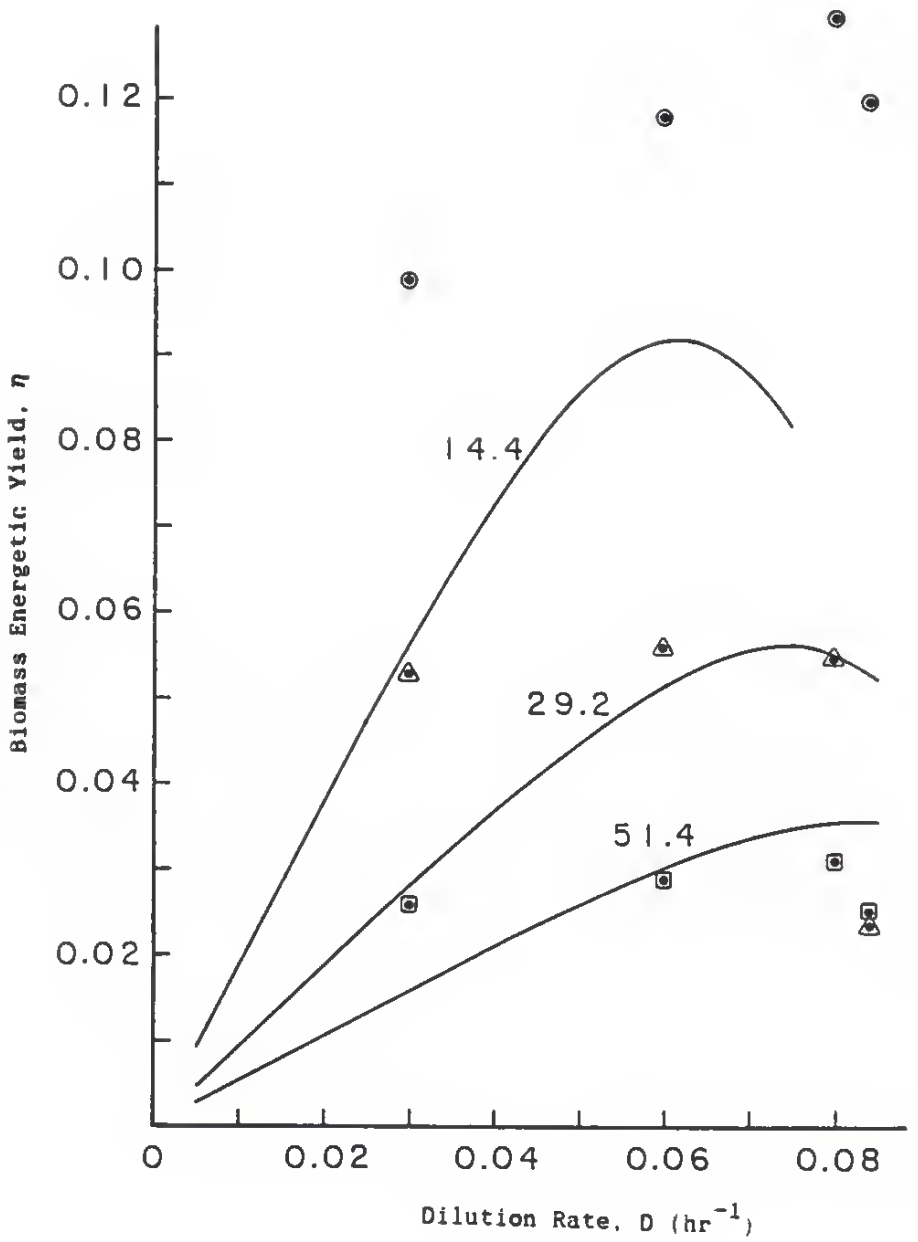

Figure 3-5. Comparison of Model 4 predictions and Lee's carbon-limited growth data for S. platensis. Variation in biomass energetic yield with dilution rate with incident light intensity as a parameter is shown. Respective values of I_o in W/m^2 are listed with each curve. Symbols are as defined in Figure 3-3.

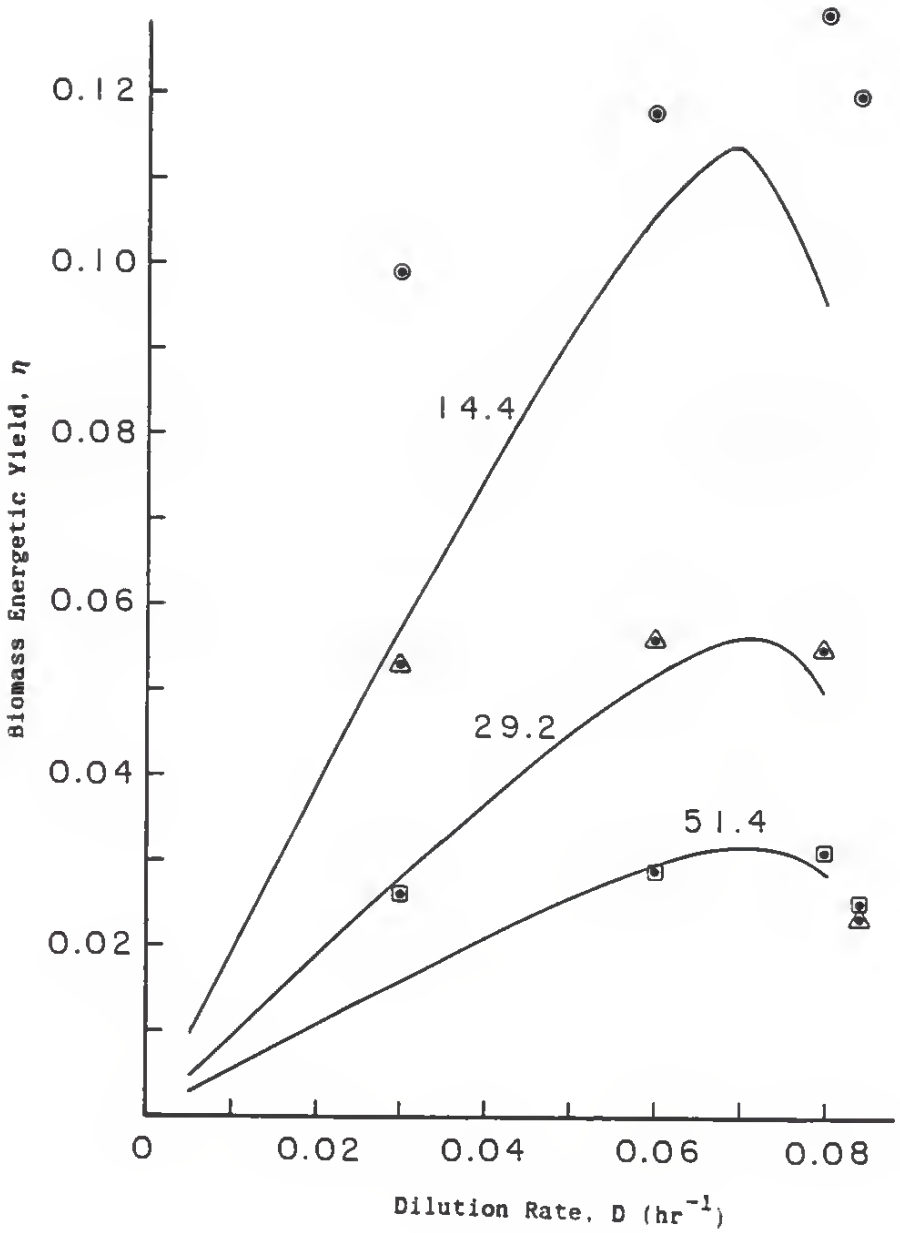

Figure 3-6. Comparison of Model 5 predictions and Lee's carbon-limited growth data for S. platensis. Variation in biomass energetic yield with dilution rate with incident light intensity as a parameter is shown. Respective values of I_o in W/m^2 are listed with each curve. Symbols are as defined in Figure 3-3.

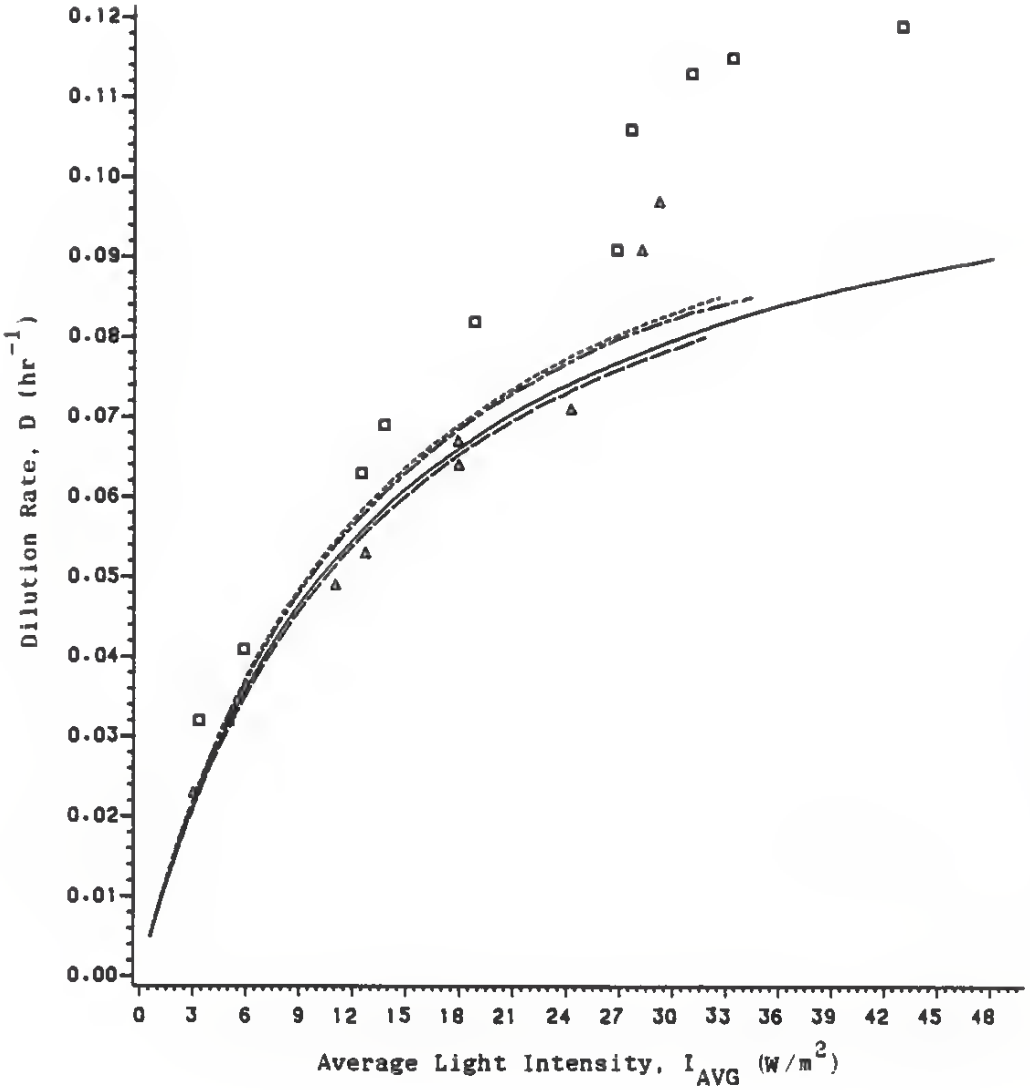

Figure 3-7. Comparison of Model 4 and 5 predictions with Lee's light-limited kinetic data for S. platensis. Variation in dilution rate with average light intensity for X = 0.04 g/liter and X = 0.05 g/liter is shown. Symbols used for X = 0.04 g/liter are ——— model 4, - - - - model 5, □ □ Lee's data. For X = 0.05 g/liter, — — model 4, — — - — model 5, △ △ Lee's data.

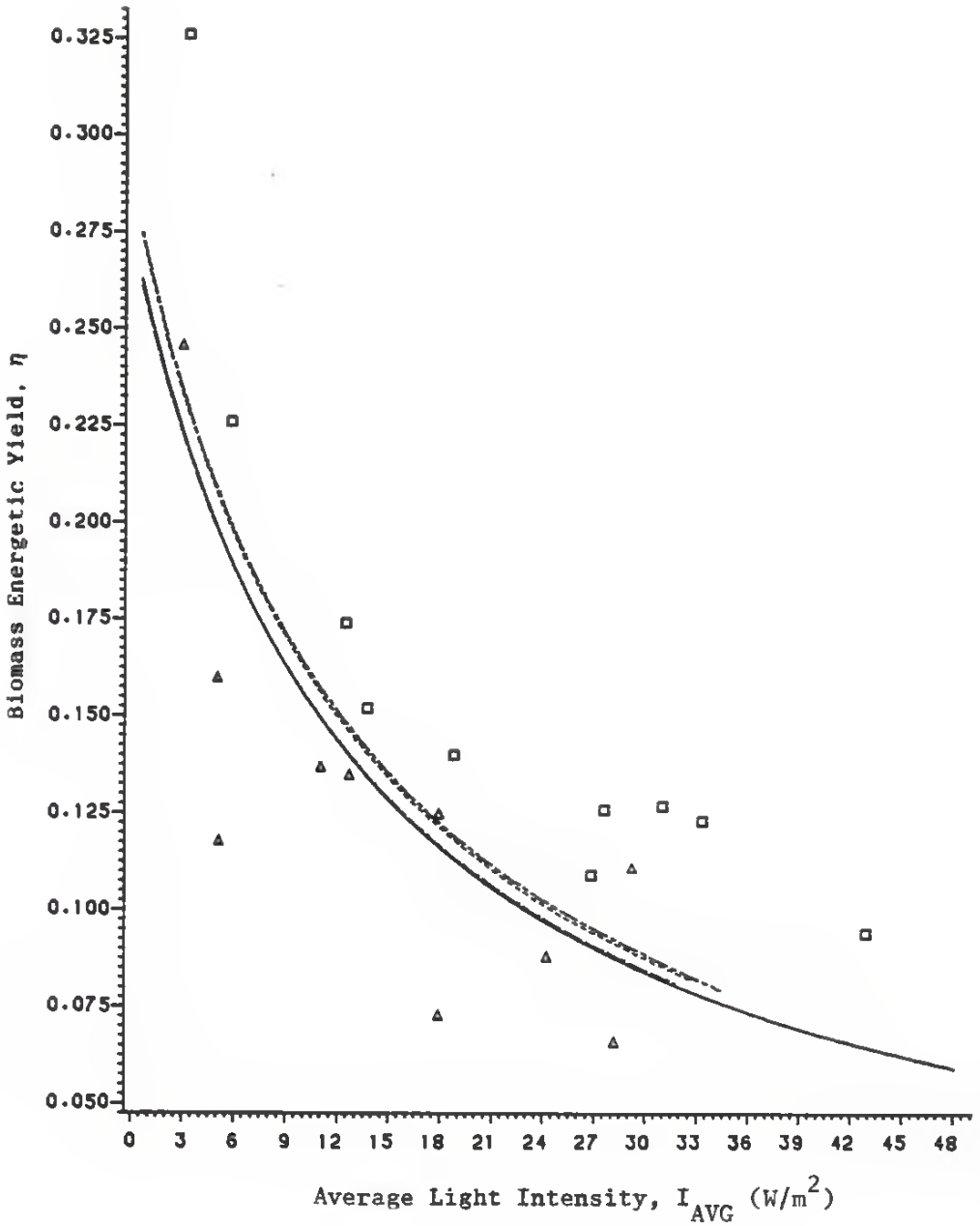

Figure 3-8. Comparison of Model 4 and 5 predictions with Lee's light-limited kinetic data for S. platensis. Variation in biomass energetic yield with average light intensity for X = 0.04 g/liter and X = 0.05 g/liter is shown. Symbols are as defined in Figure 3-7.

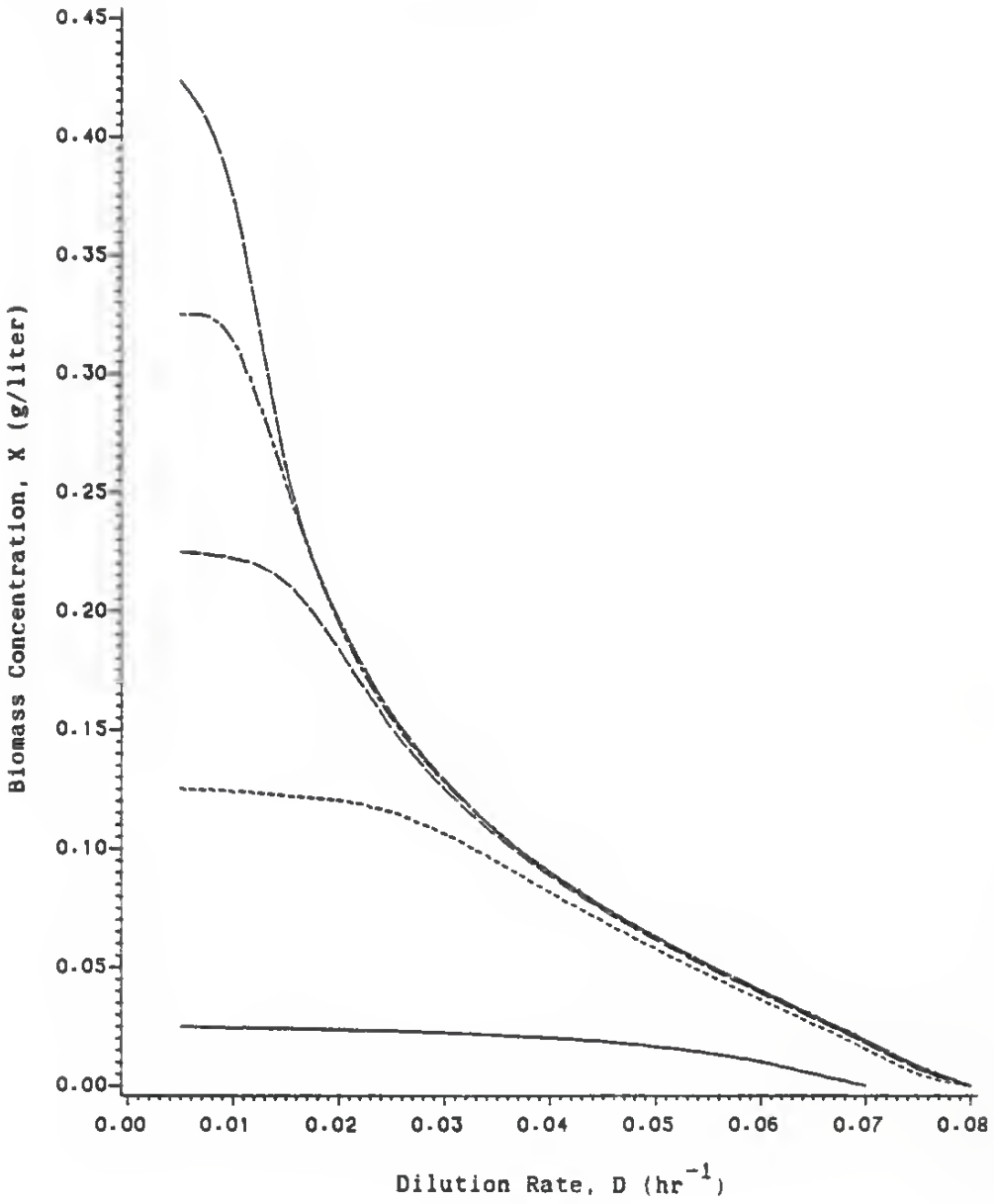

Figure 3-9. Model 2 predictions of the variation in biomass concentration with dilution rate with influent total carbon concentration as parameter. Values of $[C_{TOT}]_{in}$ in mmol/liter are ——— 1, - - - - - 5, — — — 9, - — - — 13, — — — 17.

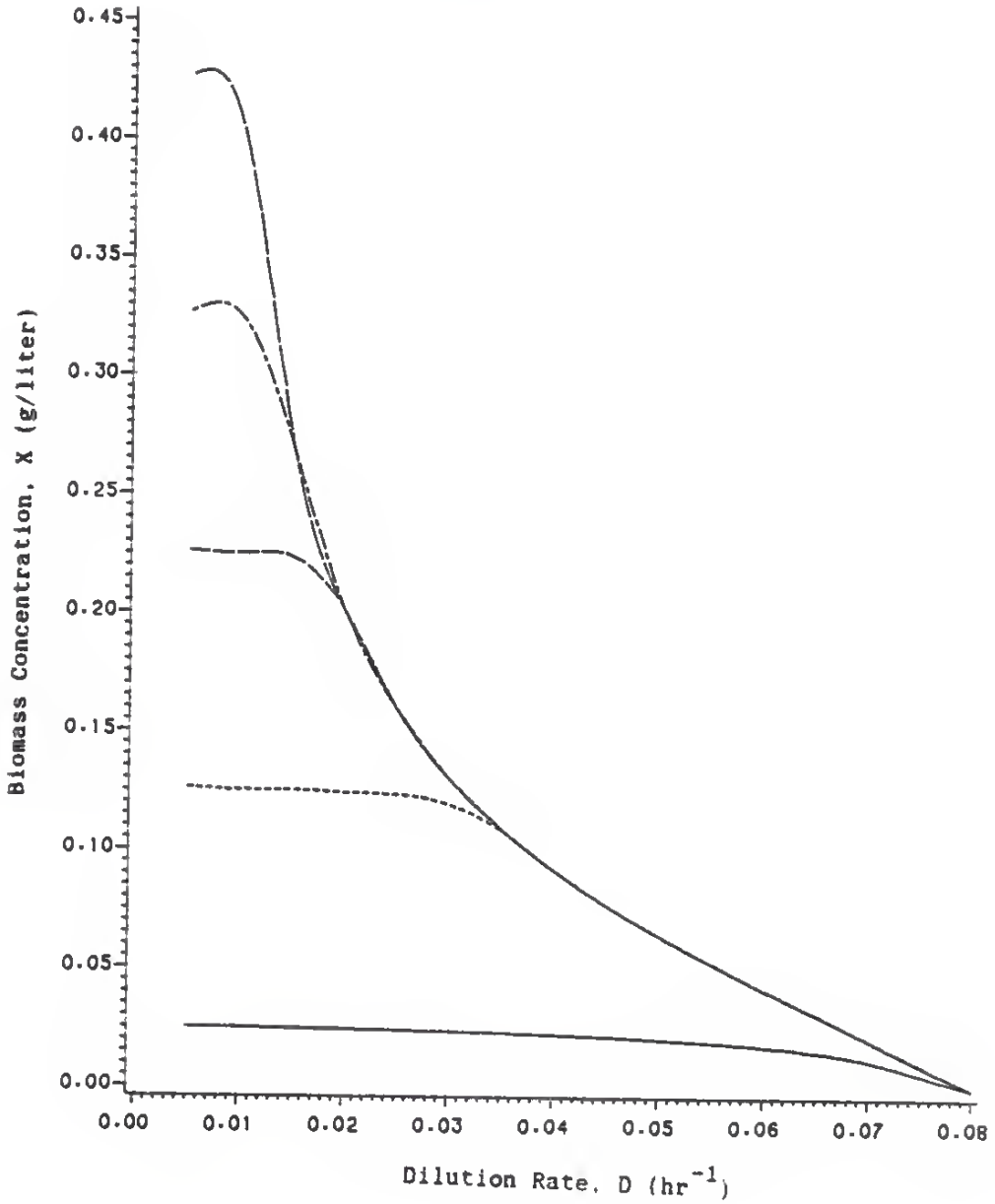

Figure 3-10. Model 3 predictions of the variation in biomass concentration with dilution rate with influent total carbon concentration as parameter. Symbols are as defined in Figure 3-9.

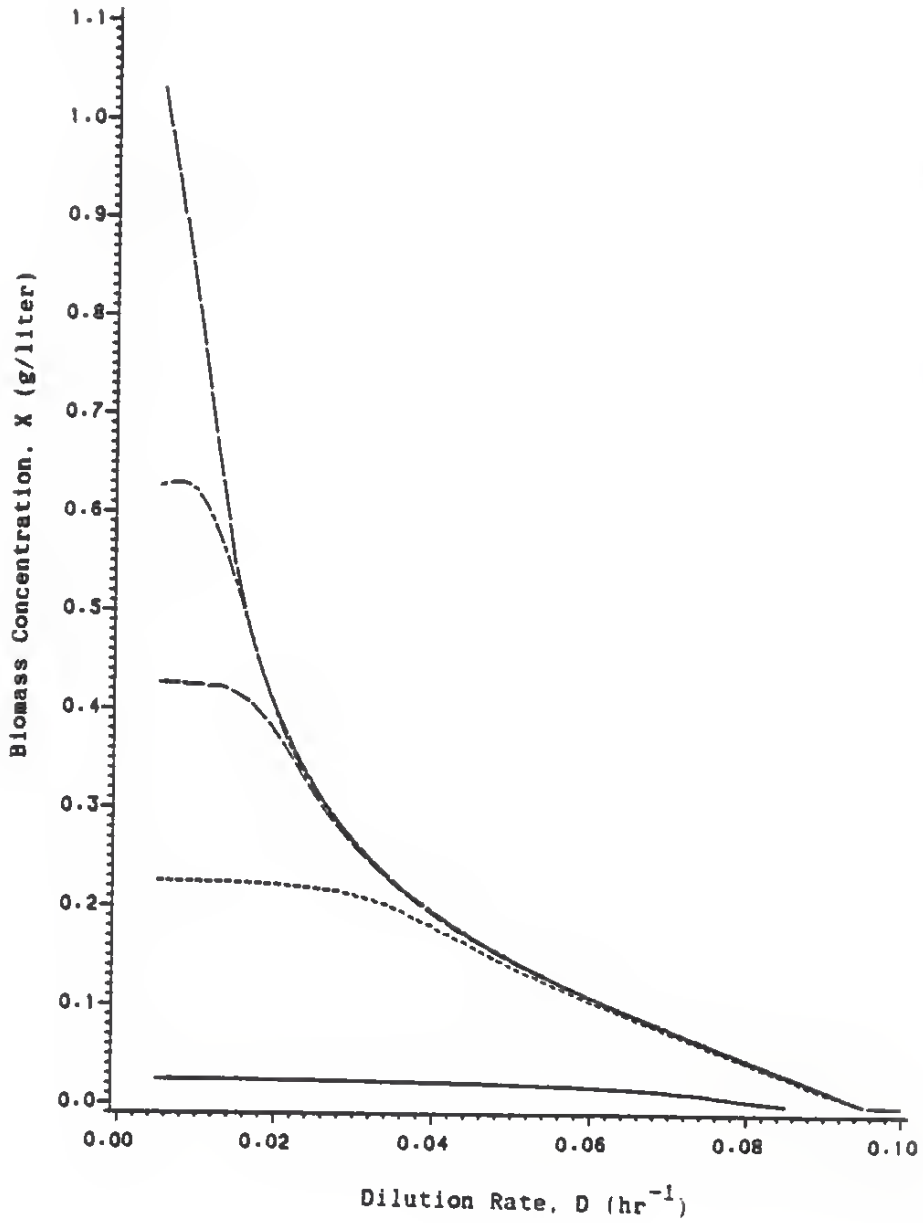

Figure 3-11. Model 4 predictions of the variation in biomass concentration with dilution rate with influent total carbon concentration as parameter. Values of $[C_{TOT}]_{in}$ in mmol/liter are ——— 1, - - - - - 9, — — — 17, - — - — 25, and —— — 41.

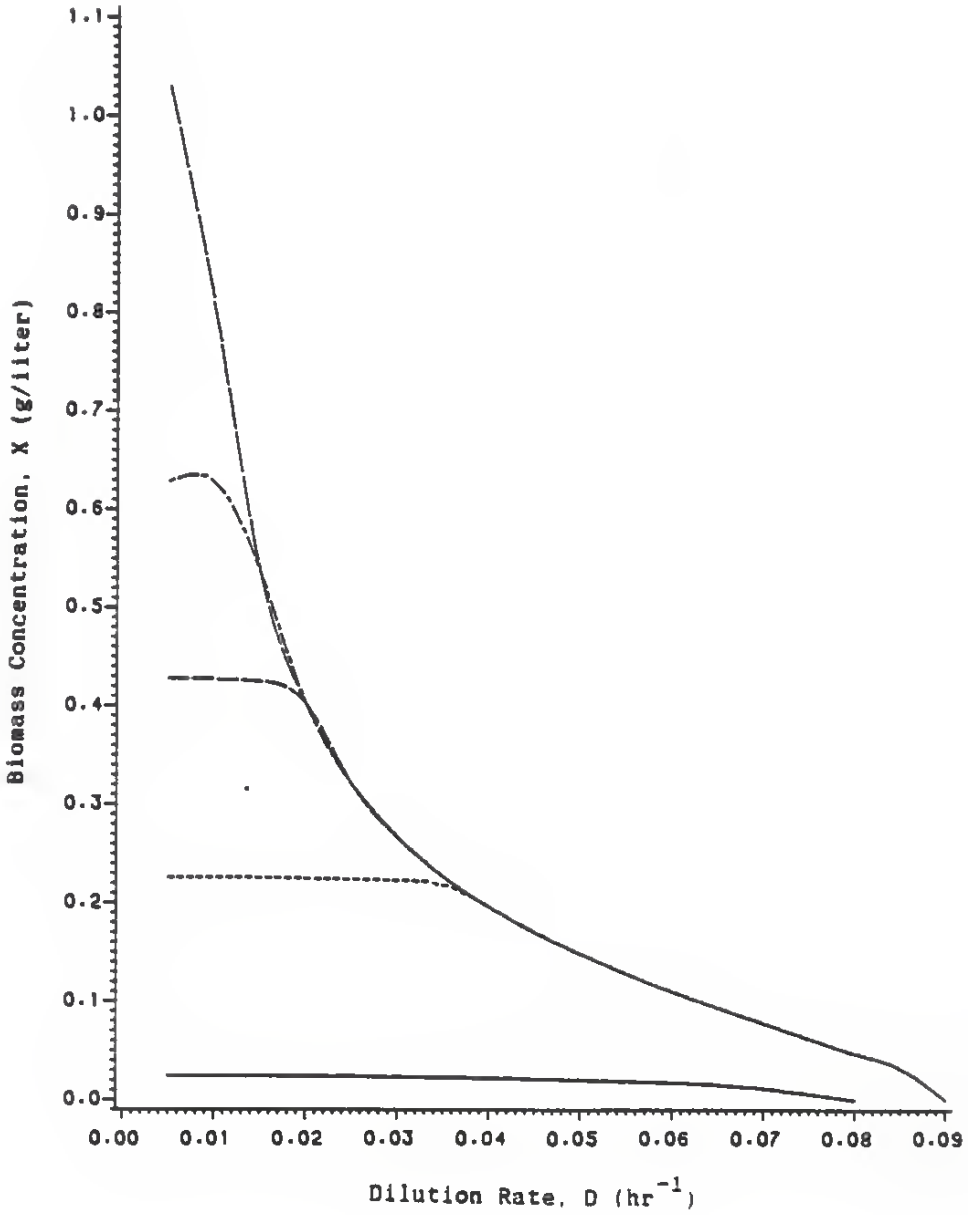

Figure 3-12. Model 5 predictions of the variation in biomass concentration with dilution rate with influent total carbon concentration as parameter. Symbols are as defined in Figure 3-11.

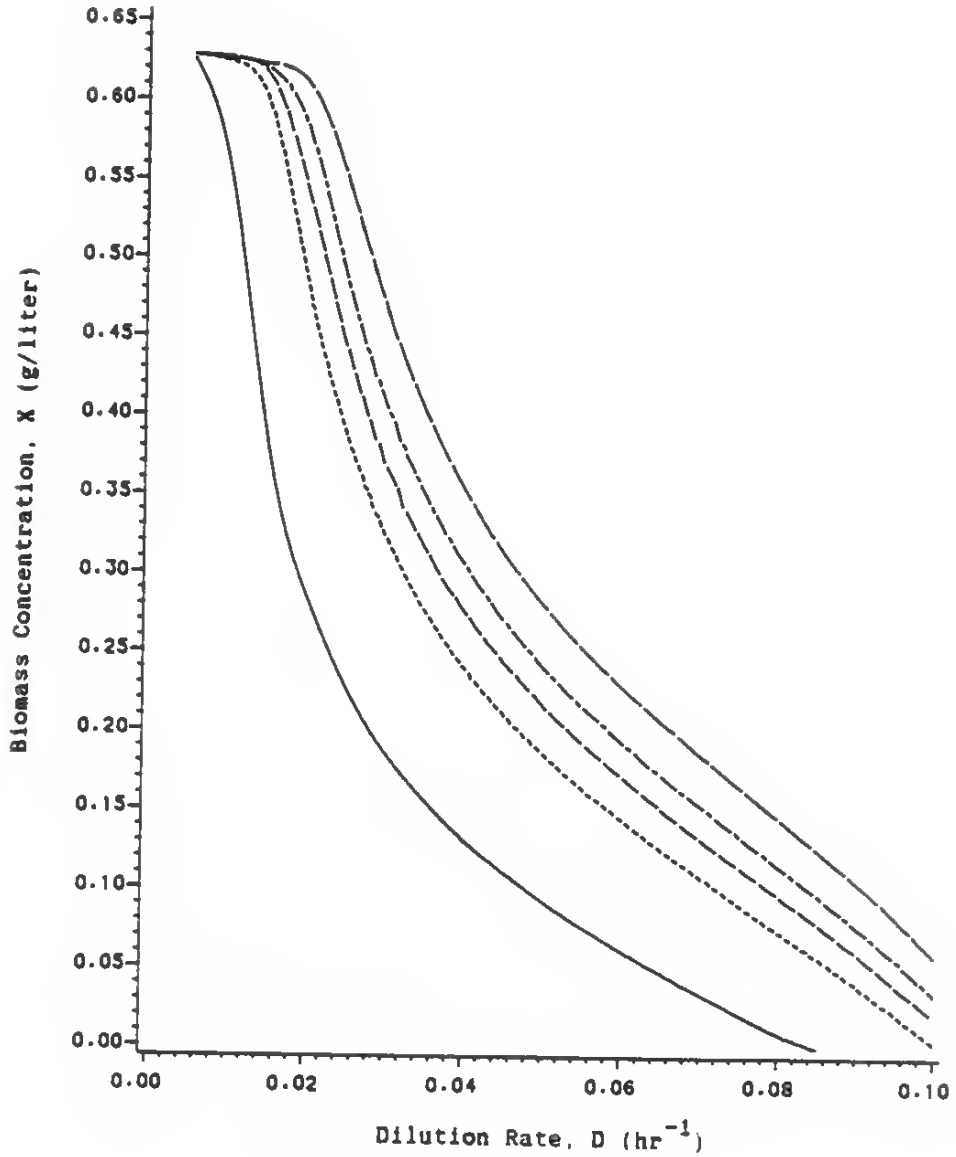

Figure 3-13. Model 4 predictions of the variation in biomass concentration with dilution rate with incident light intensity from each side as parameter. The total dissolved carbon in influent liquid is 25 mmol/liter. Values of I_o in W/m^2 are ——— 15, - - - - 35, — — — 45, - — - — 55, and ——— 75.

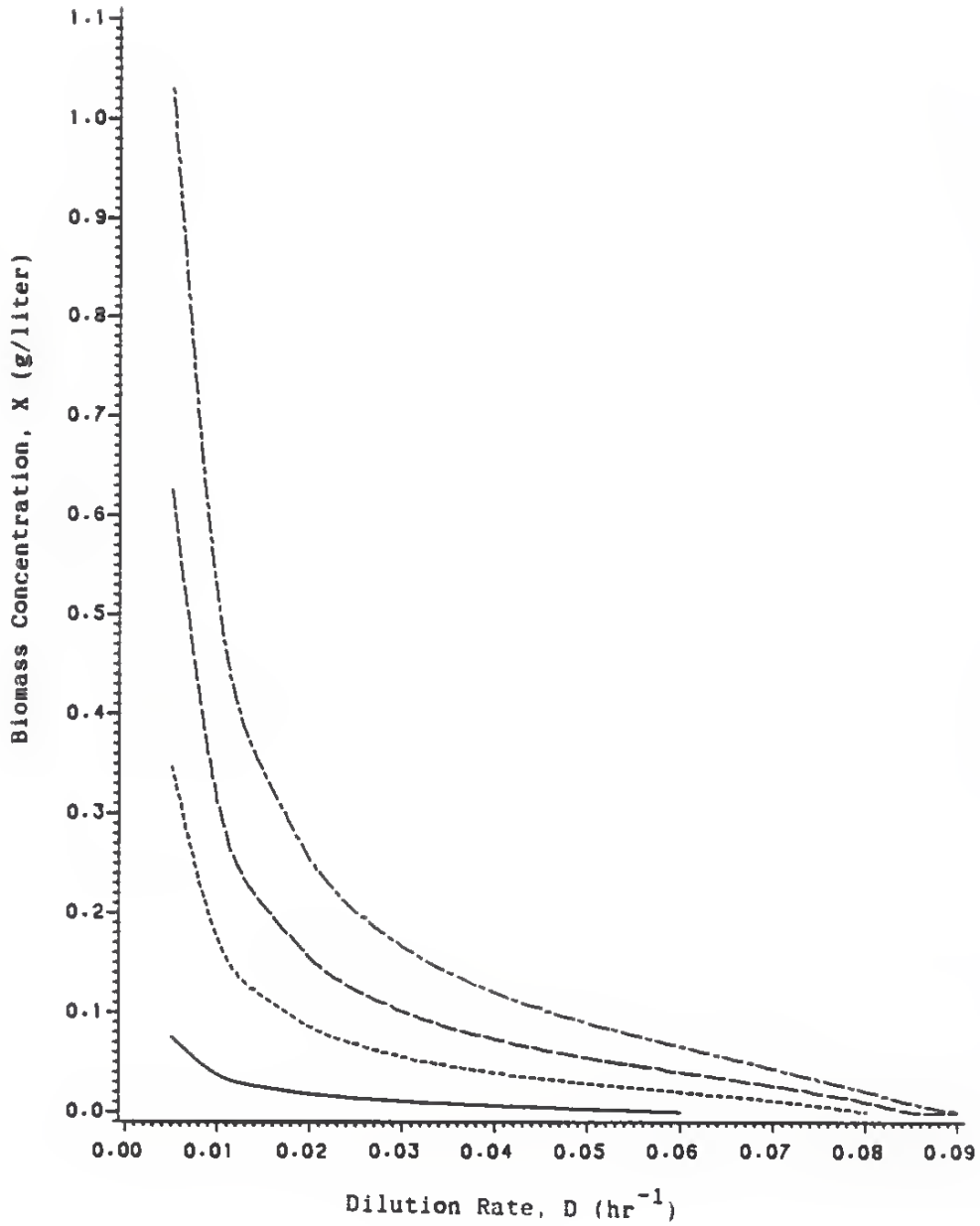

Figure 3-14. Model 4 predictions of the variation in biomass concentration with dilution rate with mass-transfer coefficient as parameter. Values of k_La in hr^{-1} are ——— 1.77, - - - - - 8.87, — — — 17.7, and — - — - 35.5.

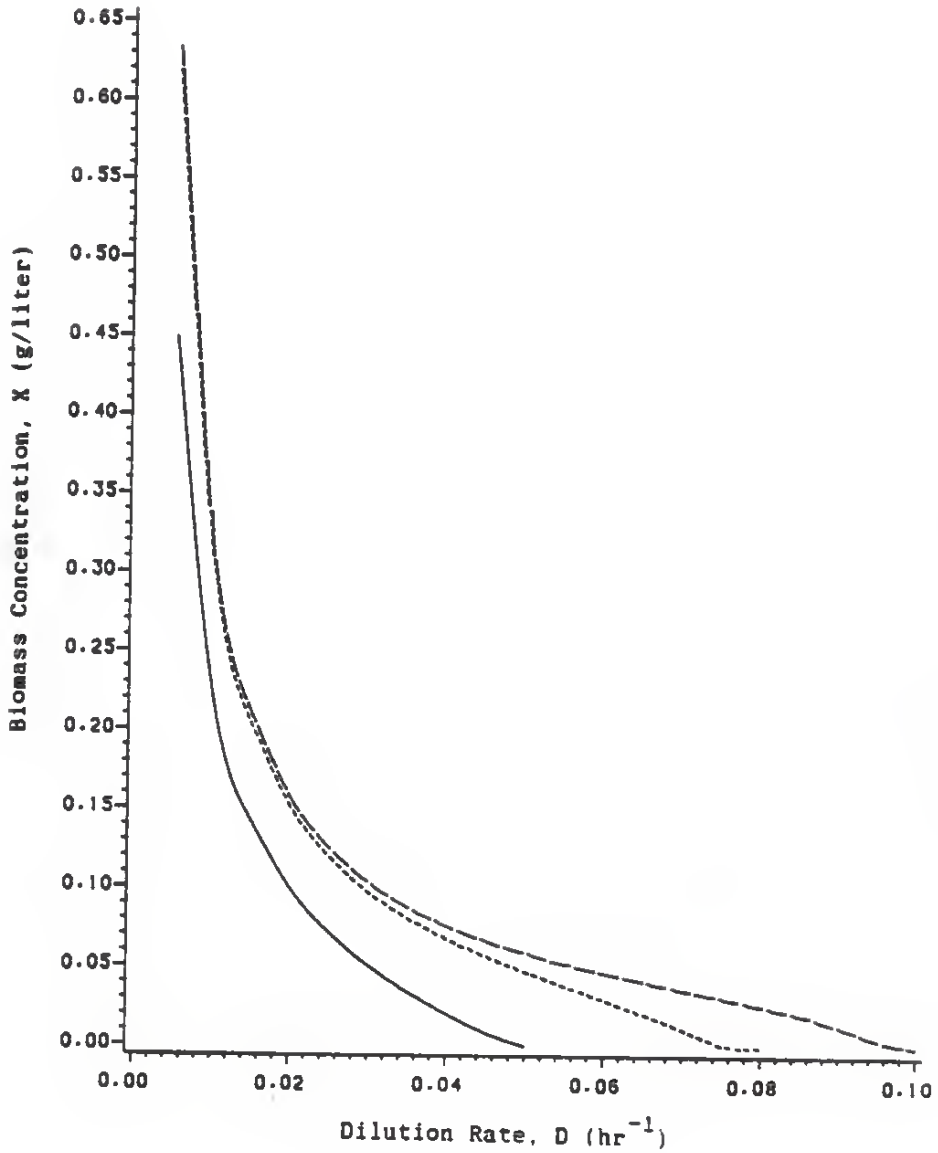

Figure 3-15. Model 4 predictions of the variation in biomass concentration with dilution rate with incident light intensity from each side as parameter. The mass-transfer coefficient is 17.7 hr^{-1}. Values of I_o in W/m^2 are ——— 5, - - - - - 15, and — — — 75.

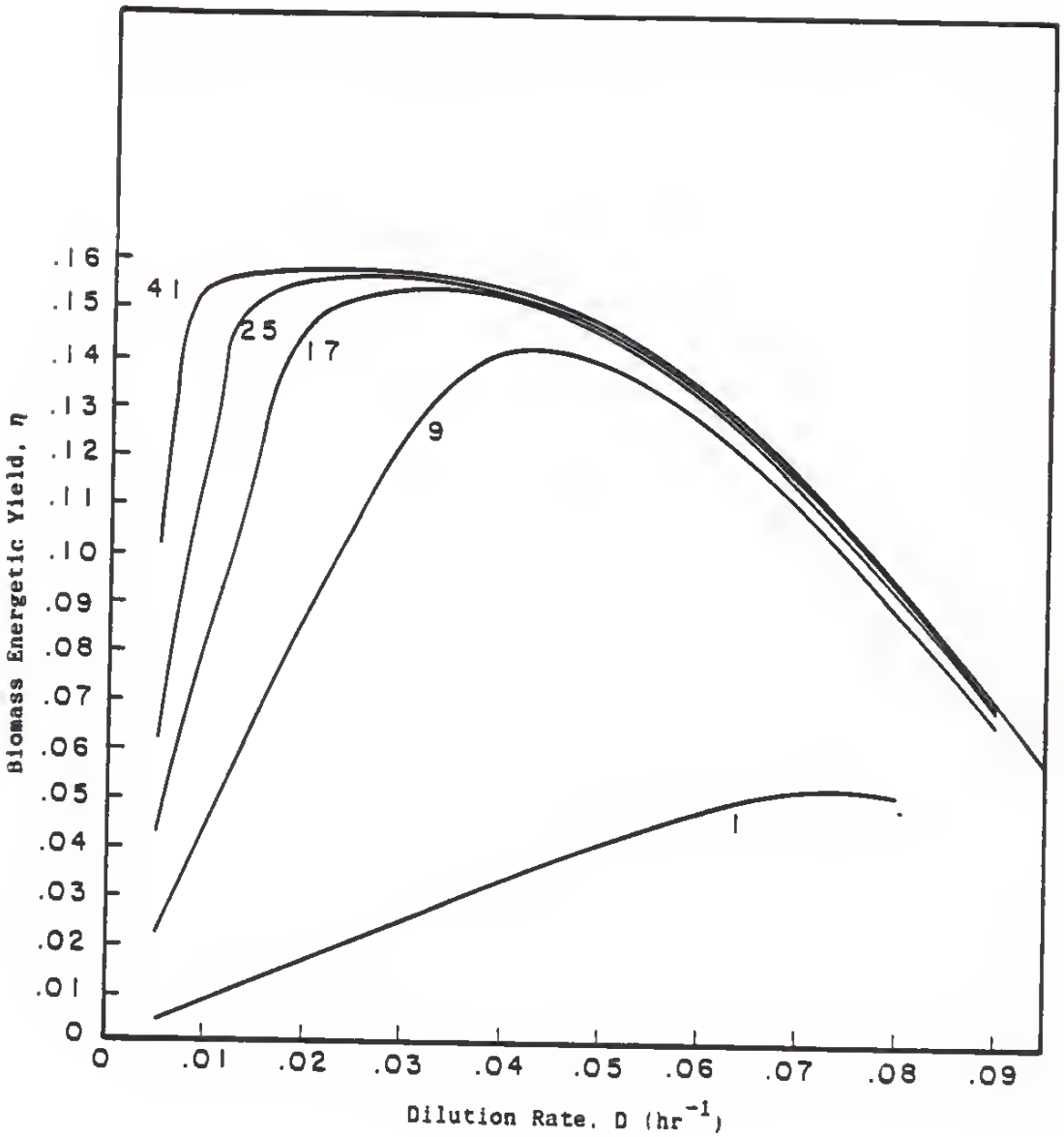

Figure 3-16. Model 4 predictions of the variation in biomass energetic yield with dilution rate with influent total carbon concentration as parameter. Values of $[C_{TOT}]_{in}$ in mmol/liter are listed with each curve.

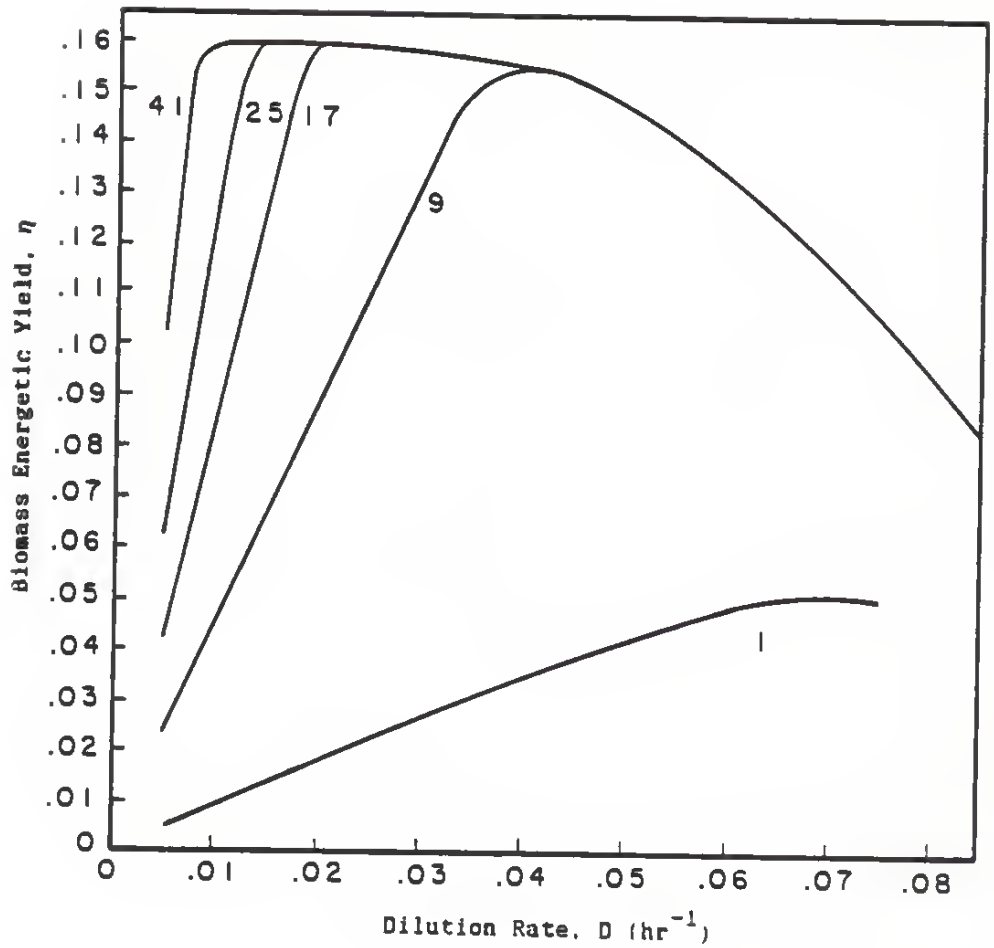

Figure 3-17. Model 5 predictions of the variation in biomass energetic yield with dilution rate with influent total carbon concentration as parameter. Values of $[C_{TOT}]_{in}$ in mmol/liter are listed with each curve.

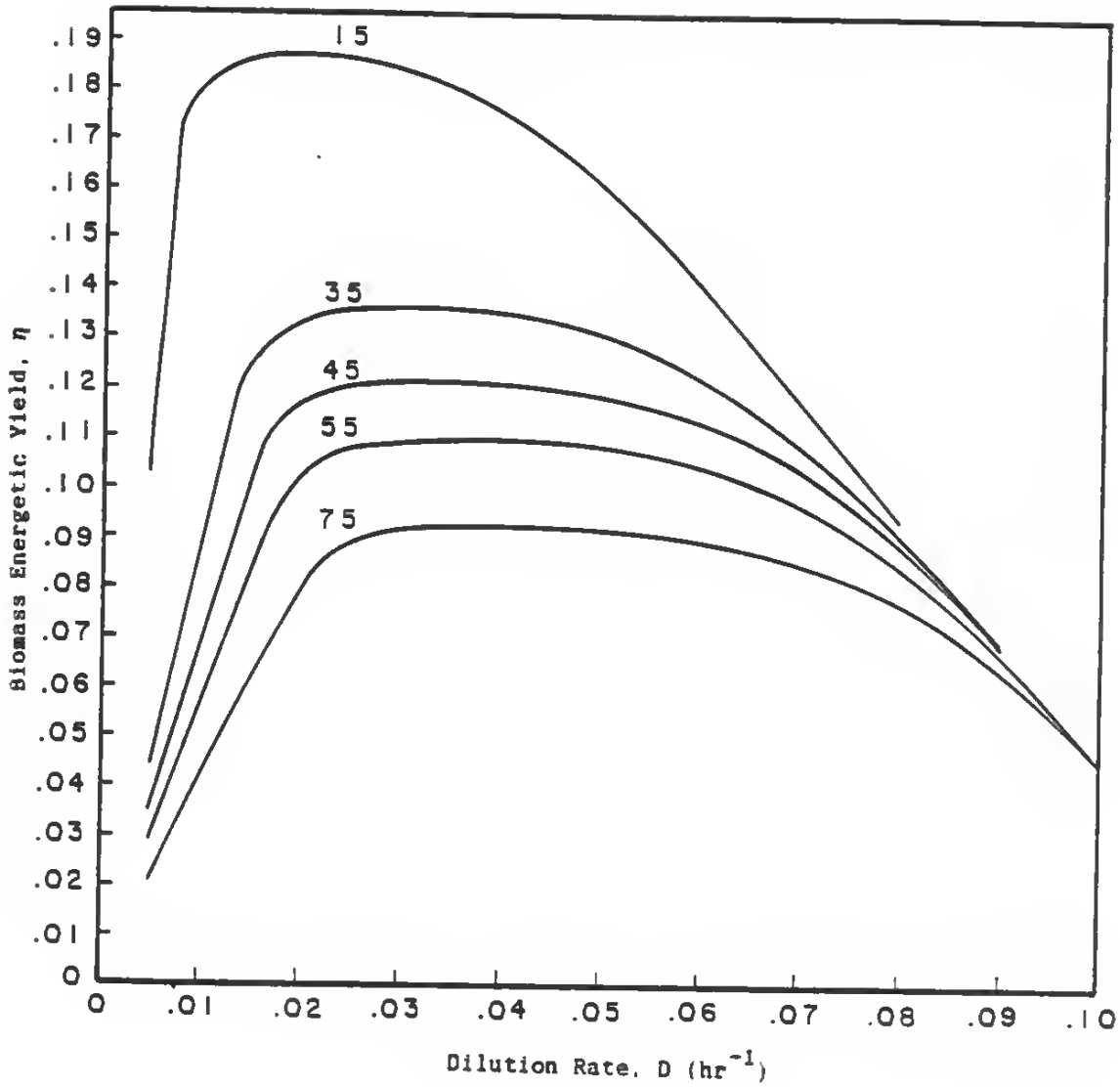

Figure 3-18. Model 4 predictions of the variation in biomass energetic yield with dilution rate with incident light intensity from each side as parameter. The total dissolved carbon concentration in influent liquid is 25 mmol/liter. Values of I_o in W/m^2 are listed with each curve.

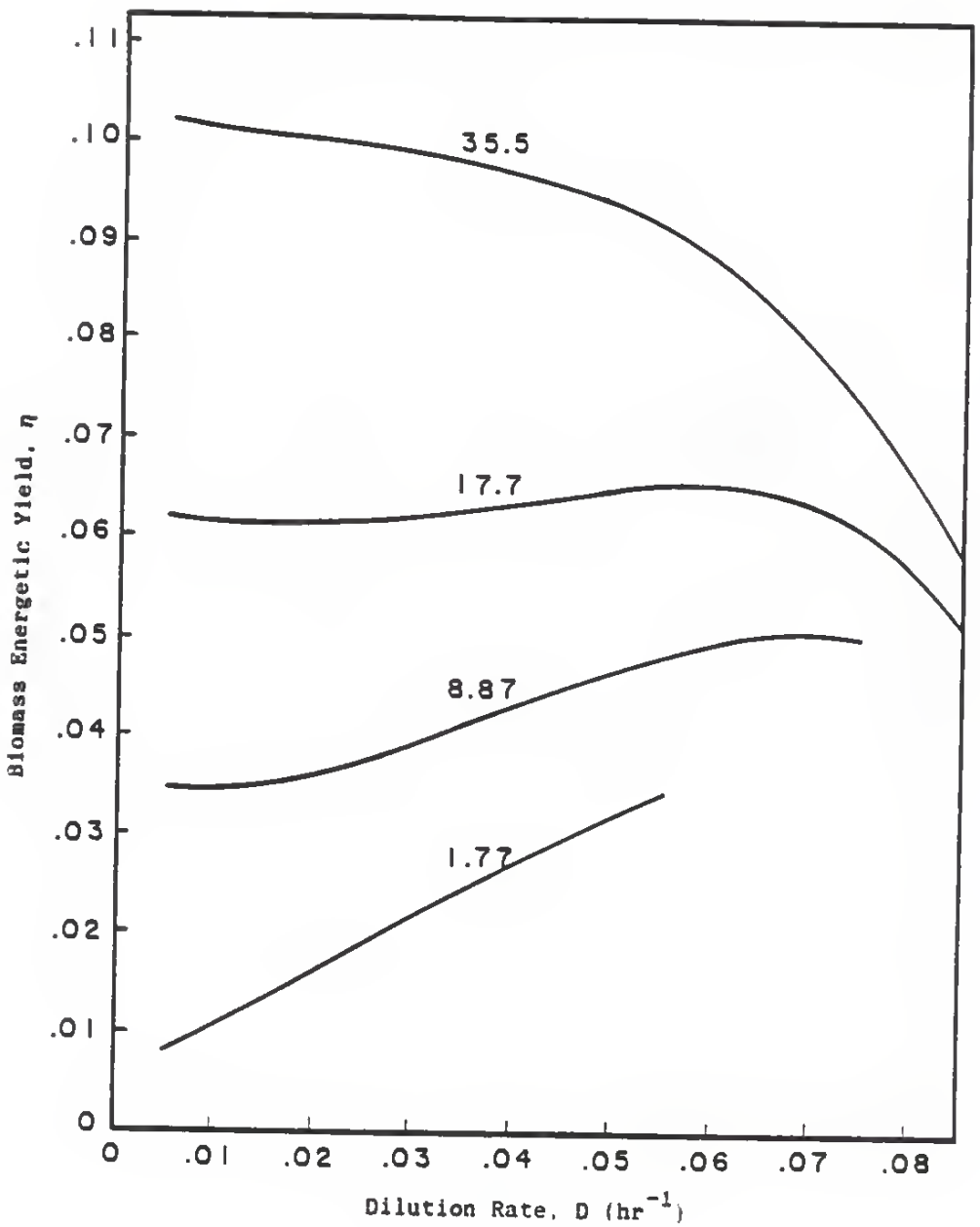

Figure 3-19. Model 4 predictions of the variation in biomass energetic yield with dilution rate with mass-transfer coefficient as parameter. Values of $k_L a$ in hr^{-1} are listed with each curve.

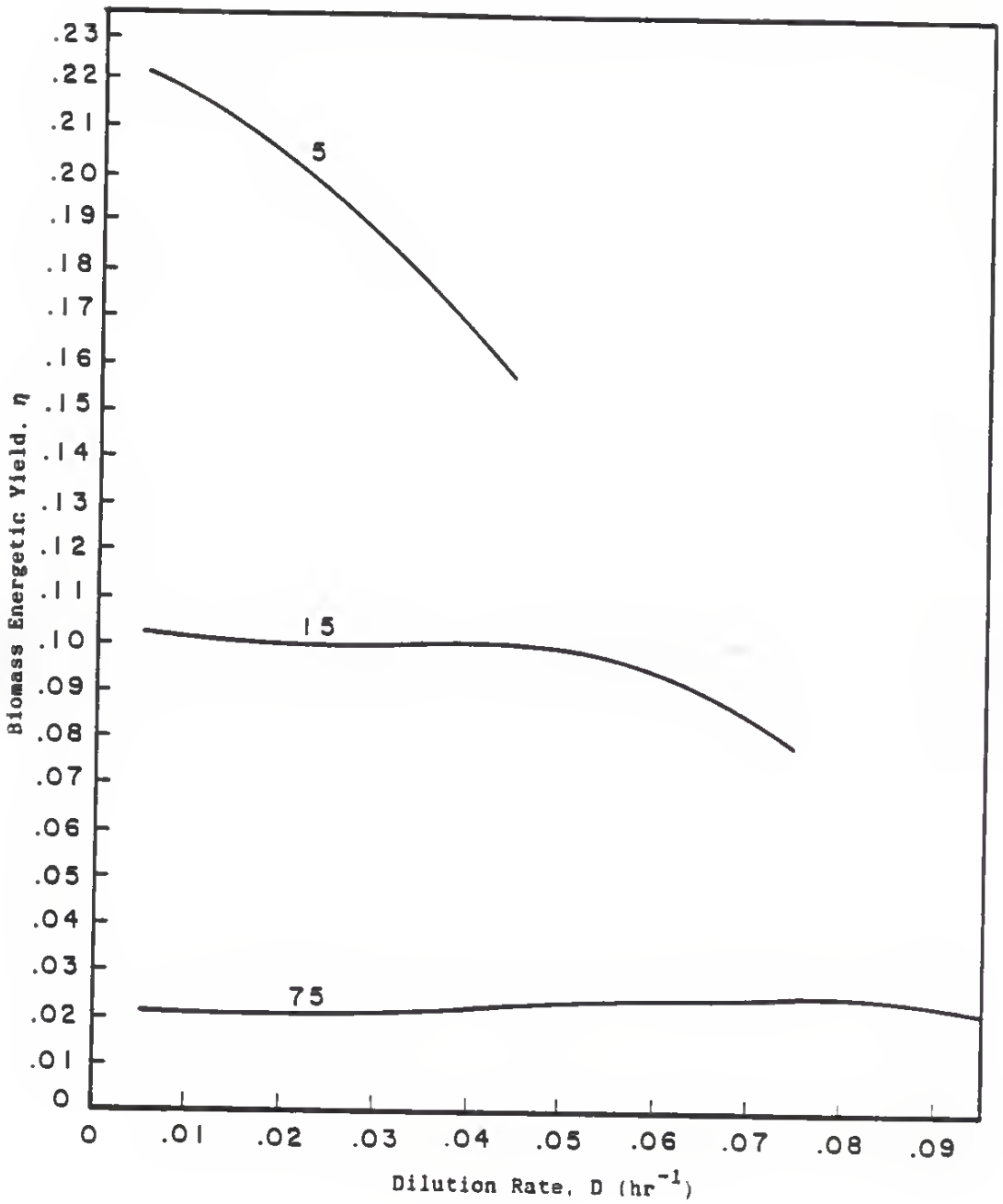

Figure 3-20. Model 4 predictions of the variation in biomass energetic yield with dilution rate with incident light intensity from each side as parameter. The mass-transfer coefficent is 17.7 hr^{-1}. Values of I_o in W/m^2 are listed with each curve.

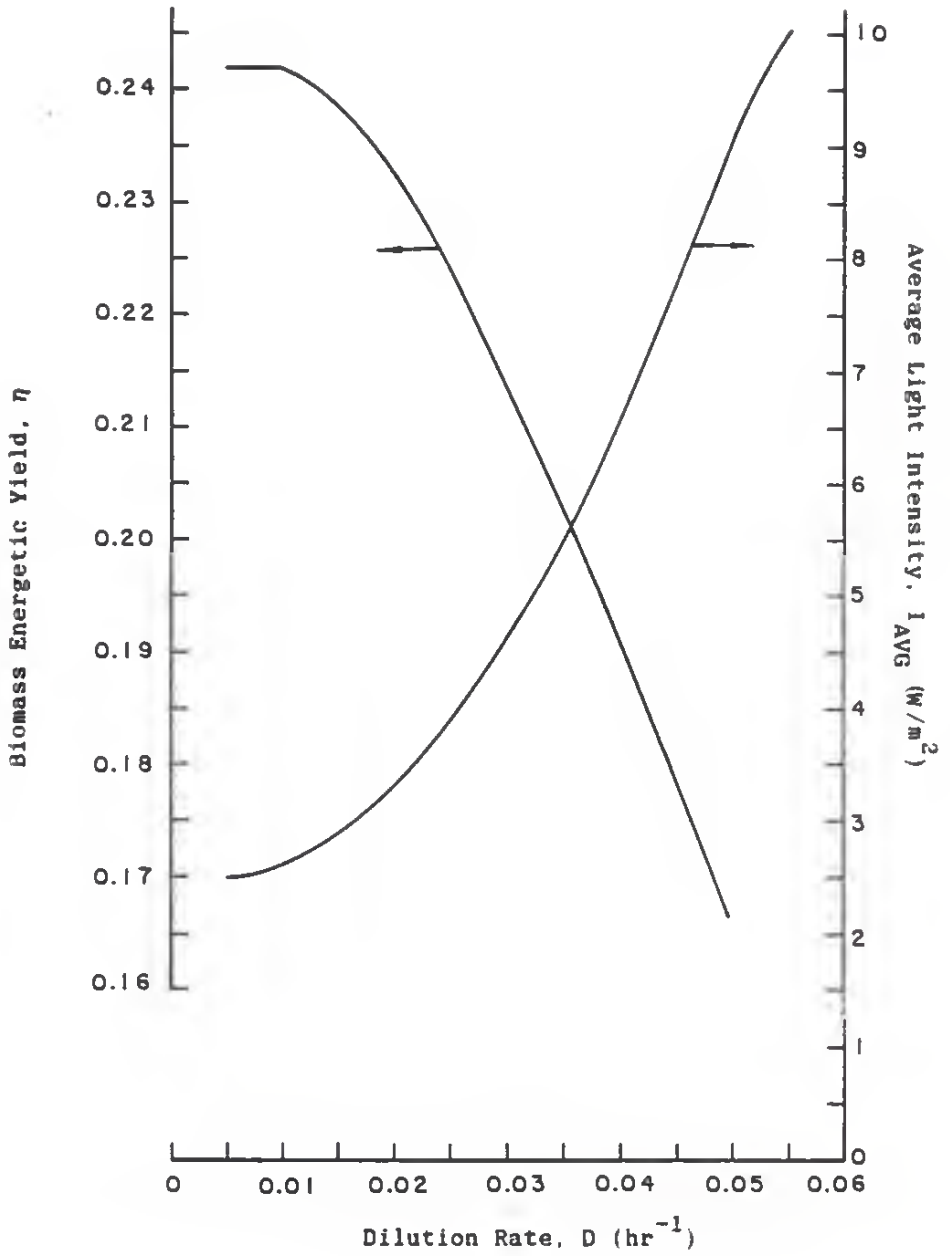

Figure 3-21. Variation in biomass energetic yield and average light intensity with dilution rate for Model 5. The mass-transfer coefficient is 17.7 hr^{-1} and the incident light intensity from each side is 5 W/m^2.

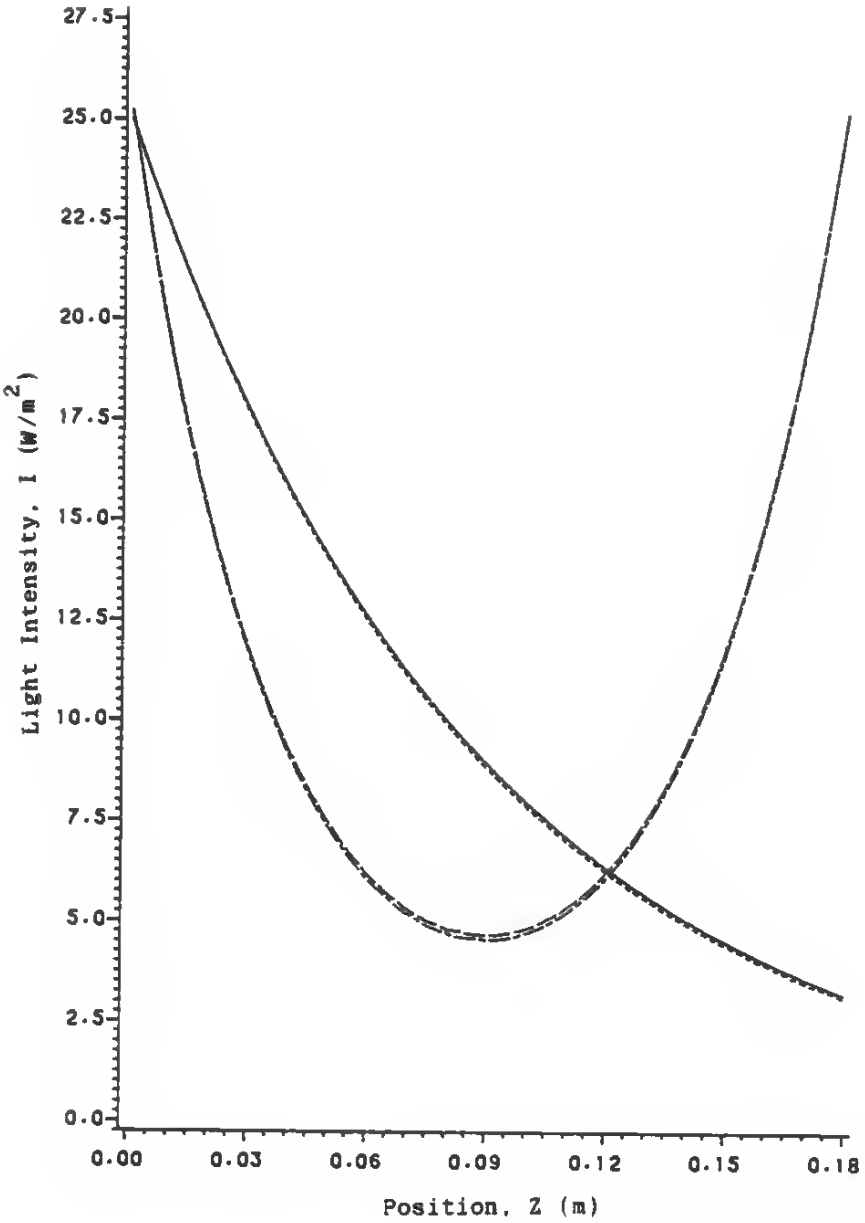

Figure 3-22. Variation of light intensity with position for each model. Incident light intensity from each side is 25 W/m^2, total dissolved carbon in influent liquid is 25 mmol/liter and the dilution rate is 0.05 hr^{-1}. Symbols for each model are ——— 2, - - - - 3, — — 4, and -—-—5.

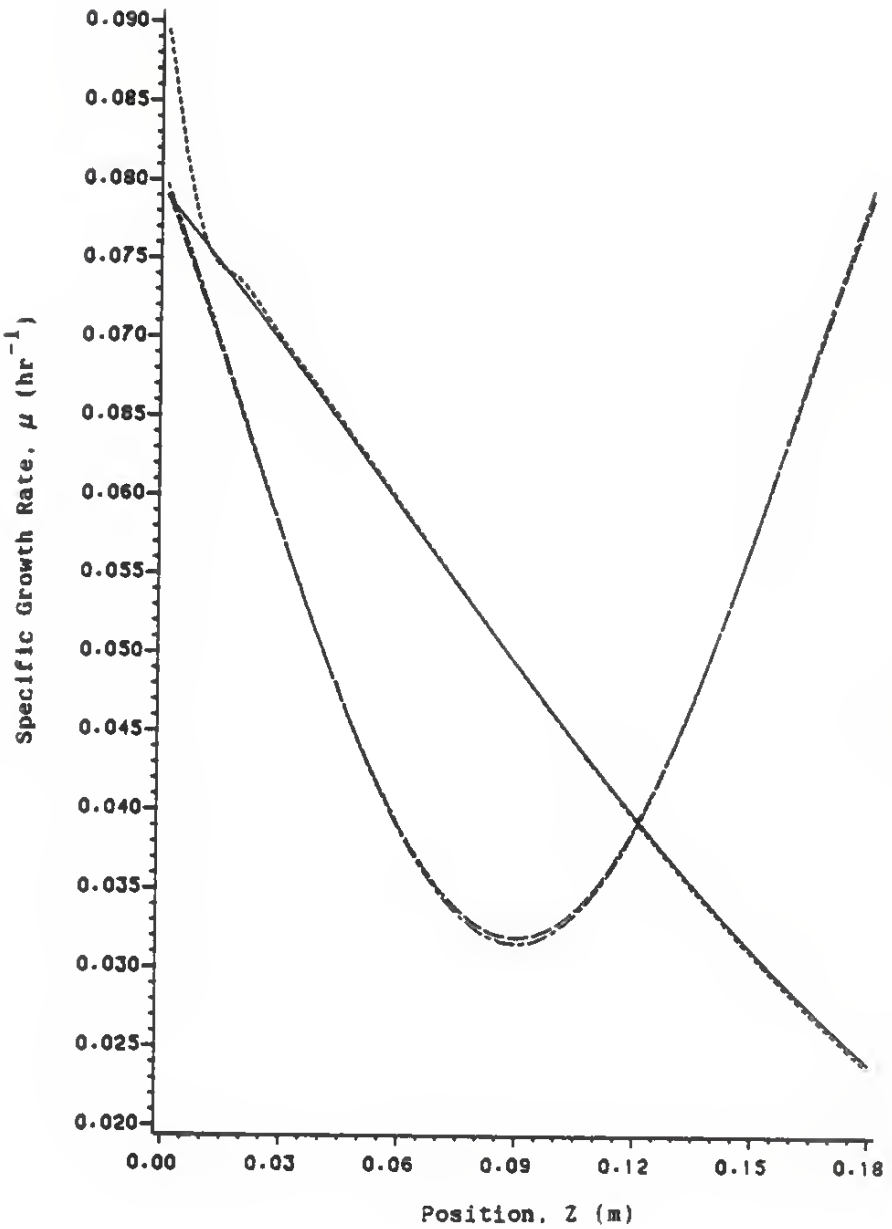

Figure 3-23. Variation of specific growth rate with position for each model. Incident light intensity from each side is 25 W/m^2, total dissolved carbon in influent liquid is 25 mmol/liter and the dilution rate is 0.05 hr^{-1}. Symbols are as defined in Figure 3-22.

APPENDIX

Table A-1: Fraction of tank that is carbon-limited at each dilution rate for model 3. I_0 = 25 W/m^2 and $[C_{TOT}]_{in}$ is in mmol/liter.

D	Fraction of Tank that is Carbon-Limited				
(hr^{-1})	$[C_{TOT}]_{in}$ = 1	$[C_{TOT}]_{in}$ = 5	$[C_{TOT}]_{in}$ = 9	$[C_{TOT}]_{in}$ = 13	$[C_{TOT}]_{in}$ = 17
.01	1.00	.727	.293	.126	0.00246
.02	1.00	.460	.00483	0	0
.03	1.00	.205	0	0	0
.04	1.00	0	0	0	0
.05	1.00	0	0	0	0
.06	1.00	0	0	0	0
.07	.873	0	0	0	0
.08	--	-	-	-	-

Table A-2. Fraction of tank that is carbon-limited at each dilution rate for model 3. $[C_{TOT}]$ = 25 mmol/liter and I_o is in W/m^2.

D	Fraction of Tank That is Carbon-Limited				
(hr^{-1})	I_o = 25	I_o = 35	I_o = 45	I_o = 55	I_o = 75
.01	0	.000753	.0193	.0388	.0773
.02	0	0	.0224	.0410	.0640
.03	0	0	.0324	.0600	.0941
.04	0	0	.0434	.0805	.126
.05	0	0	.0566	.104	.161
.06	0	0	.0747	.135	.204
.07	0	0	.104	.182	.266
.08	0	0	.173	.278	.378
.09	-	-	-	---	---

Table A-3. Fraction of tank that is carbon-limited at each dilution rate for model 3. I_0 = 25 W/m^2 and k_La is in hr^{-1}.

D	Fraction of Tank that is Carbon-Limited			
(hr^{-1})	k_La = 1.77	k_La = 8.87	k_La = 17.7	k_La = 35.5
.01	1.00	.457	.142	0
.02	1.00	.804	.284	.000867
.03	1.00	.979	.389	.0115
.04	1.00	1.00	.432	.0163
.05	1.00	1.00	.407	.00597
.06	--	1.00	.323	0
.07	--	1.00	.199	0
.08	--	--	--	-

Table A-4. Fraction of tank that is carbon-limited at each dilution rate for model 3. $k_L a$ = 17.7 hr^{-1} and I_o is in W/m^2.

D	Fraction of Tank that is Carbon-Limited		
(hr^{-1})	I_o = 10	I_o = 20	I_o = 75
.01	0	.0955	.310
.02	0	.193	.612
.03	0	.252	.849
.04	0	.238	1.00
.05	0	.134	1.00
.08	-	0	1.00
.07	-	0	1.00
.08	-	-	1.00
.09	-	-	--

Table A-5: Fraction of tank that is carbon-limited at each dilution rate for model 5. I_0 = 25 W/m^2 and $[C_{TOT}]_{in}$ is in mmol/liter.

D	Fraction of Tank that is Carbon-Limited				
(hr^{-1})	$[C_{TOT}]_{in}$ = 1	$[C_{TOT}]_{in}$ = 9	$[C_{TOT}]_{in}$ = 17	$[C_{TOT}]_{in}$ = 25	$[C_{TOT}]_{in}$ = 41
.01	1.00	1.00	.324	.139	0
.02	1.00	.585	.00486	0	0
.03	1.00	.327	0	0	0
.04	1.00	0	0	0	0
.05	1.00	0	0	0	0
.06	1.00	0	0	0	0
.07	1.00	0	0	0	0
.08	--	-	-	-	-

Table A-6. Fraction of tank that is carbon-limited at each dilution rate for model 5. $[C_{TOT}]_{in}$ = 25 mmol/liter and I_o is in W/m^2.

D	Fraction of Tank That is Carbon-Limited				
(hr^{-1})	I_o = 15	I_o = 35	i_o = 45	I_o = 55	I_o = 75
.01	0	.199	.239	.268	.312
.02	0	.00151	.0386	.0777	.155
.03	0	0	.0362	.0647	.101
.04	0	0	.0451	.0822	.128
.05	0	0	.0562	.103	.159
.06	0	0	.0712	.128	.196
.07	0	0	.0971	.165	.245
.08	0	0	.165	.245	.334
.09	-	-	-	---	---

Table A-7. Fraction of tank that is carbon-limited at each dilution rate for model 5. I_0 = 15 W/m^2 and k_La is in hr^{-1}.

D	Fraction of Tank that is Carbon-Limited			
(hr^{-1})	k_La = 1.77	k_La = 8.87	k_La = 17.7	k_La = 35.5
.01	1.00	1.00	.534	.209
.02	1.00	1.00	1.00	.419
.03	1.00	1.00	1.00	.620
.04	1.00	1.00	1.00	.851
.05	1.00	1.00	1.00	1.00
.06	--	1.00	1.00	1.00
.07	--	1.00	1.00	1.00
.08	--	--	1.00	1.00
.09	--	--	--	--

Table A-8. Fraction of tank that is carbon-limited at each dilution rate for model 5. $k_L a = 17.7\ hr^{-1}$ and I_o is in W/m^2.

D	Fraction of Tank that is Carbon-Limited		
(hr^{-1})	$I_o = 5$	$I_o = 15$	$I_o = 75$
.01	0	.386	.839
.02	0	.828	1.00
.03	0	1.00	1.00
.04	0	1.00	1.00
.05	0	1.00	1.00
.06	-	1.00	1.00
.07	-	1.00	1.00
.08	-	1.00	1.00
.09	-	-	--

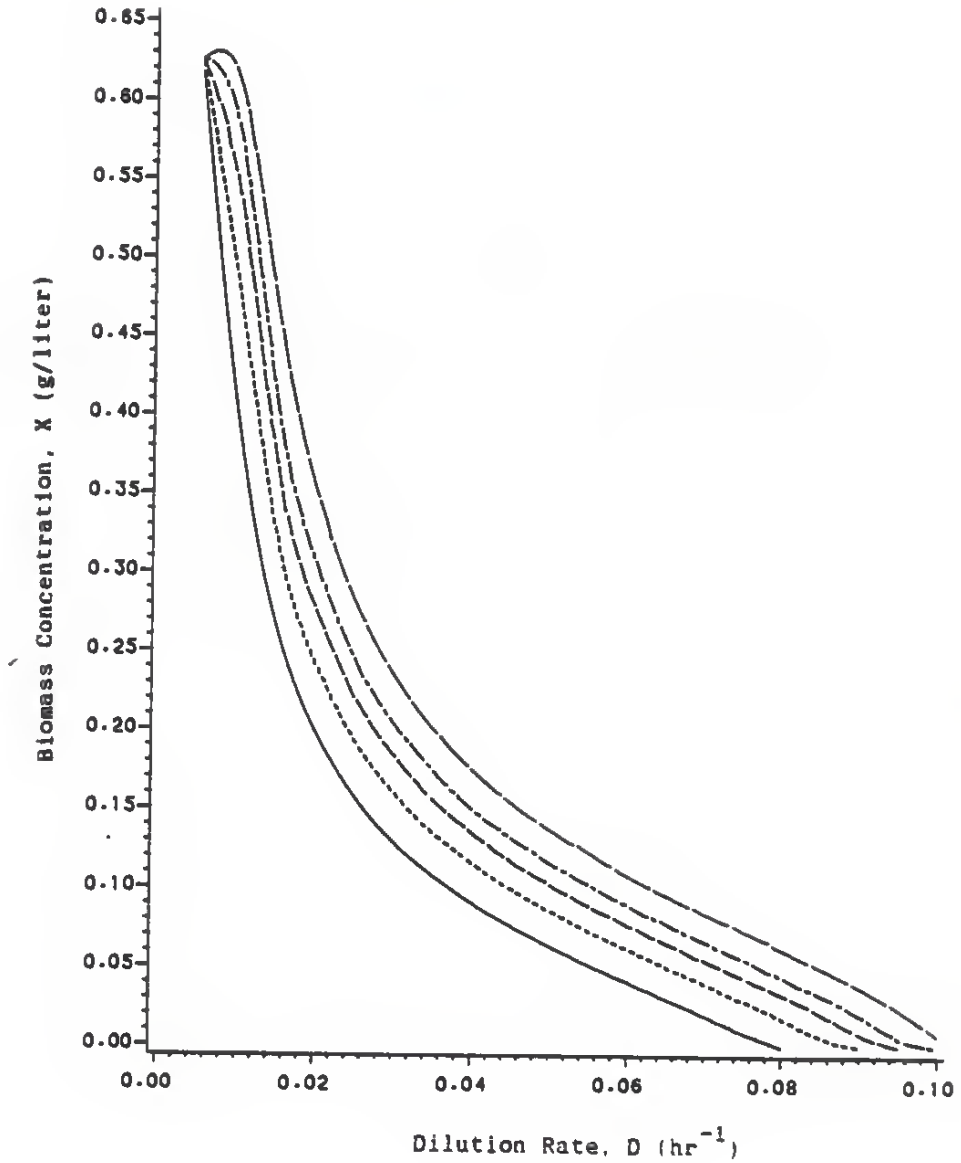

Figure A-1. Model 2 predictions of the variation in biomass concentration with dilution rate with incident light intensity as parameter. The total dissolved carbon in the influent is 25 mmol/liter. Values of I_o in W/m^2 are ——— 25, ------ 35, — — — 45, - — - — 55, and — — — 75.

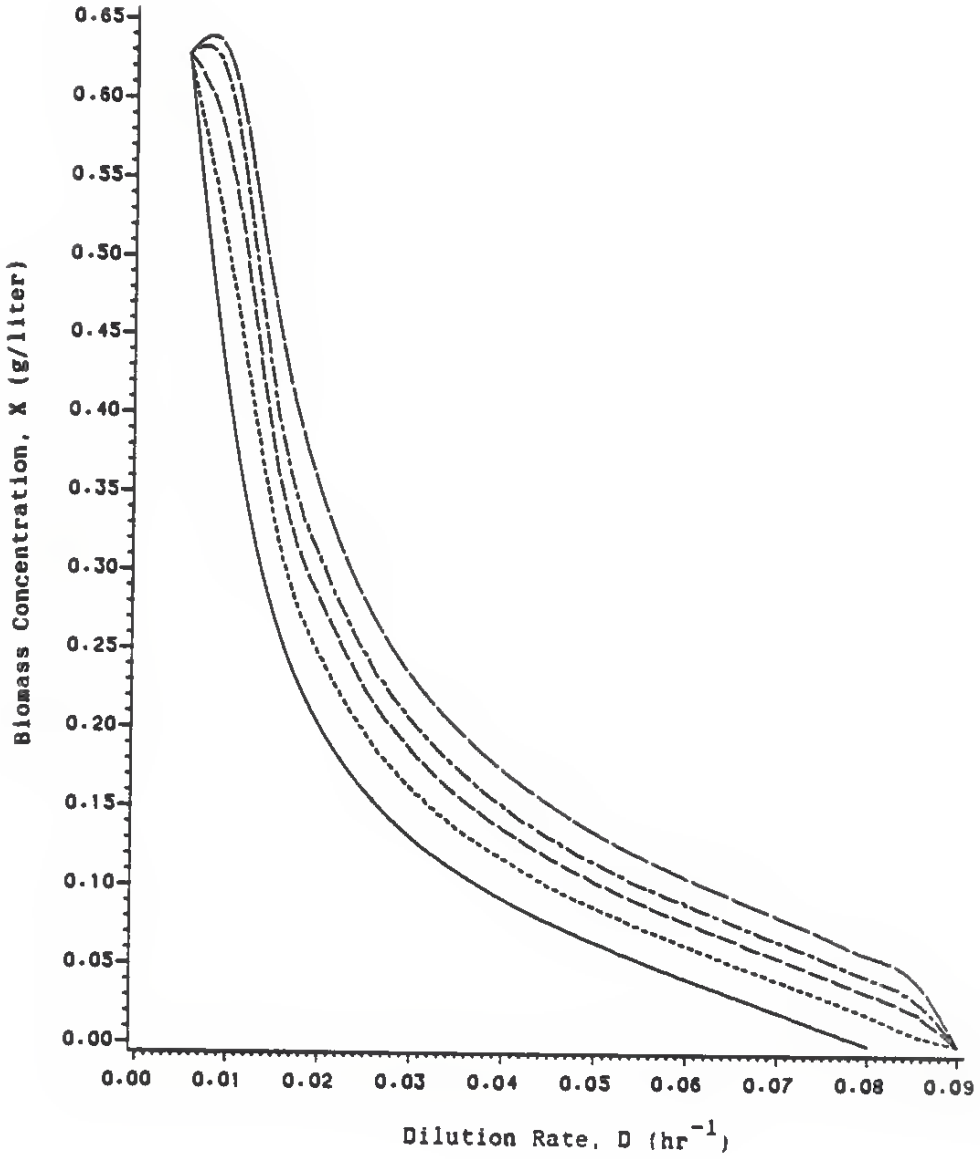

Figure A-2. Model 3 predictions of the variation in biomass concentration with dilution rate with incident light intensity as parameter. The total dissolved carbon in the influent is 25 mmol/liter. Symbols are as defined in Figure A-1.

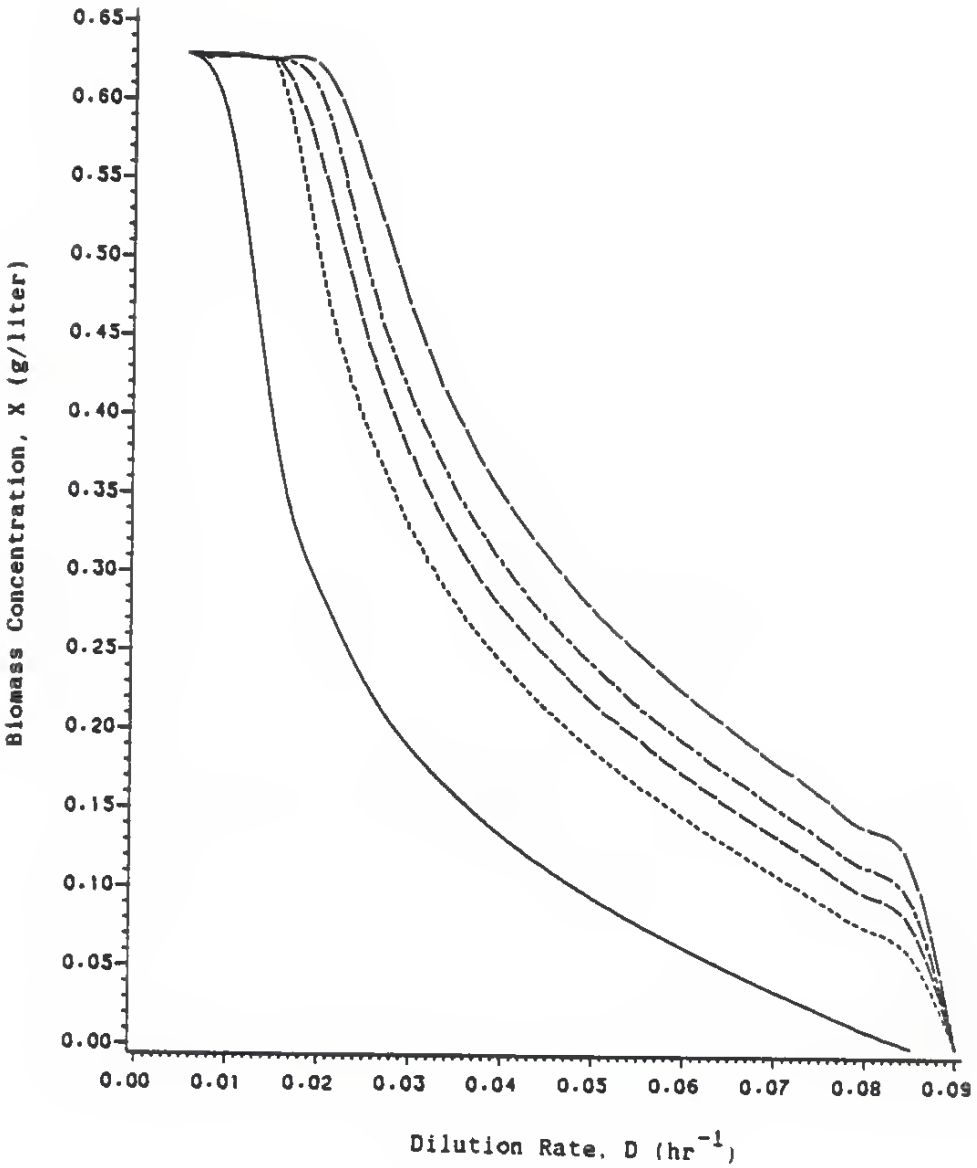

Figure A-3. Model 5 predictions of the variation in biomass concentration with dilution rate with incident light intensity from each side as parameter. The total dissolved carbon in the influent is 25 mmol/liter. Symbols are as defined in Figure 3-13.

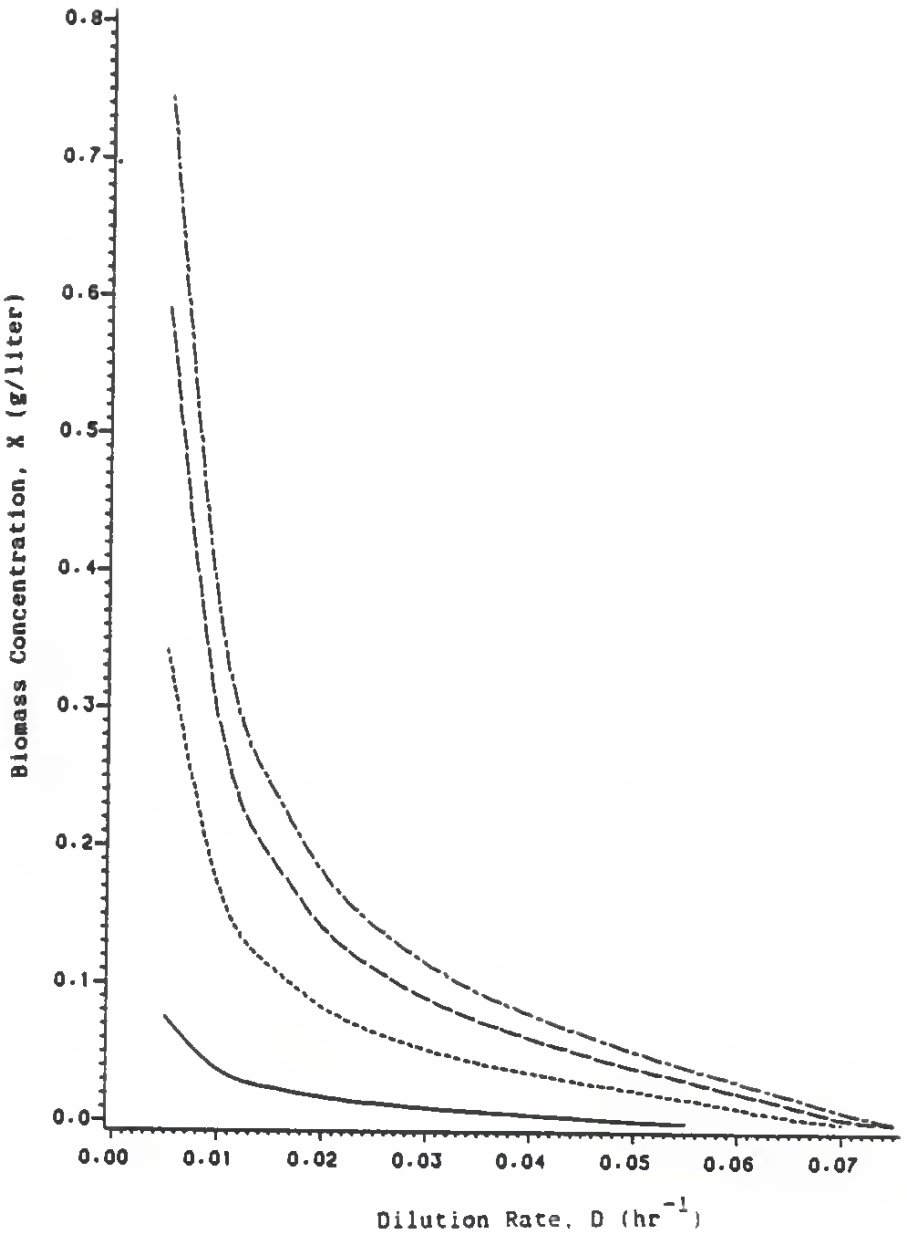

Figure A-4. Model 2 predictions of the variation in biomass concentration with dilution rate with mass-transfer coefficient as parameter. Symbols are as defined in Figure 3-14.

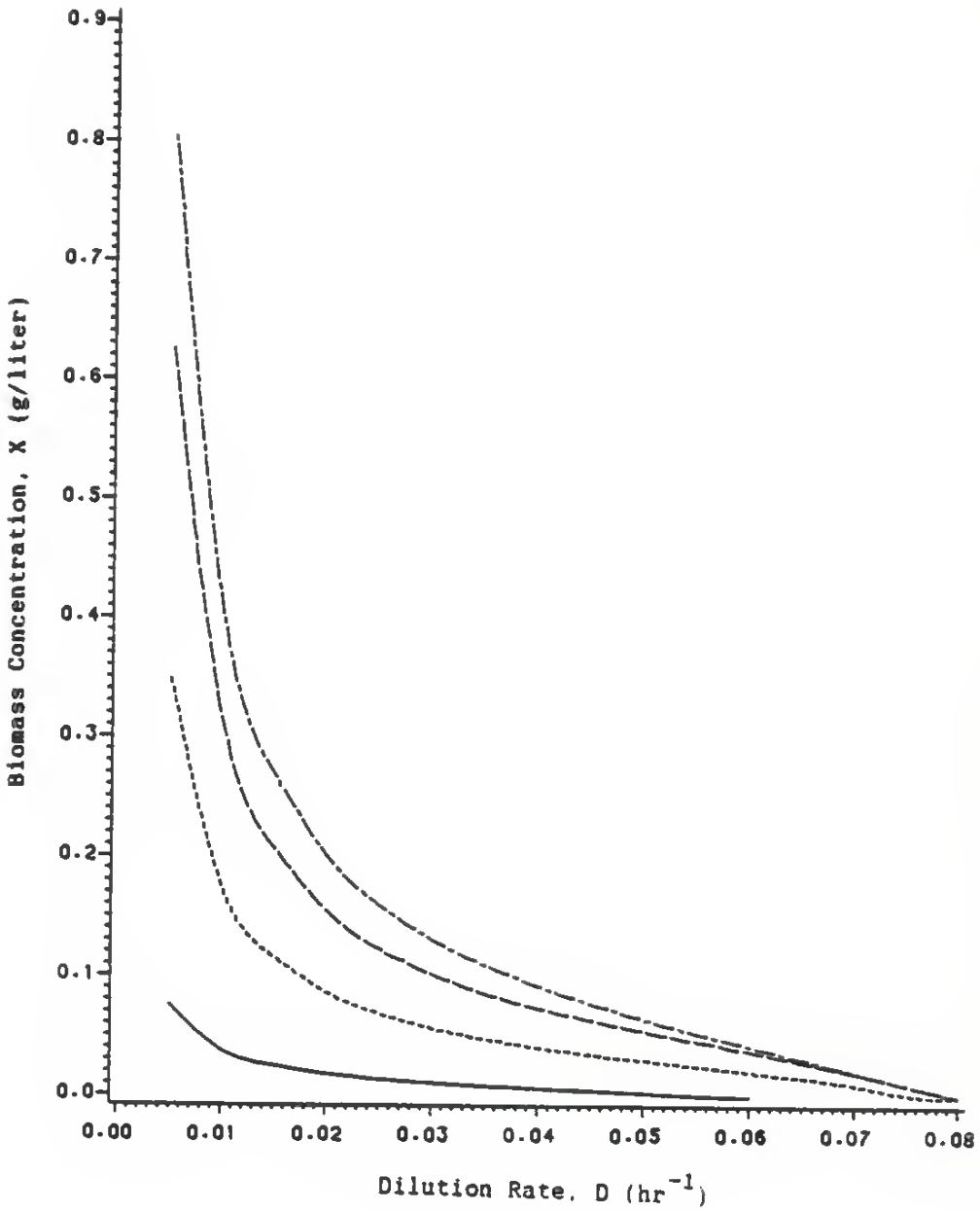

Figure A-5. Model 3 predictions of the variation in biomass concentration with dilution rate with mass-transfer coefficient as parameter. Symbols are as defined in Figure 3-14.

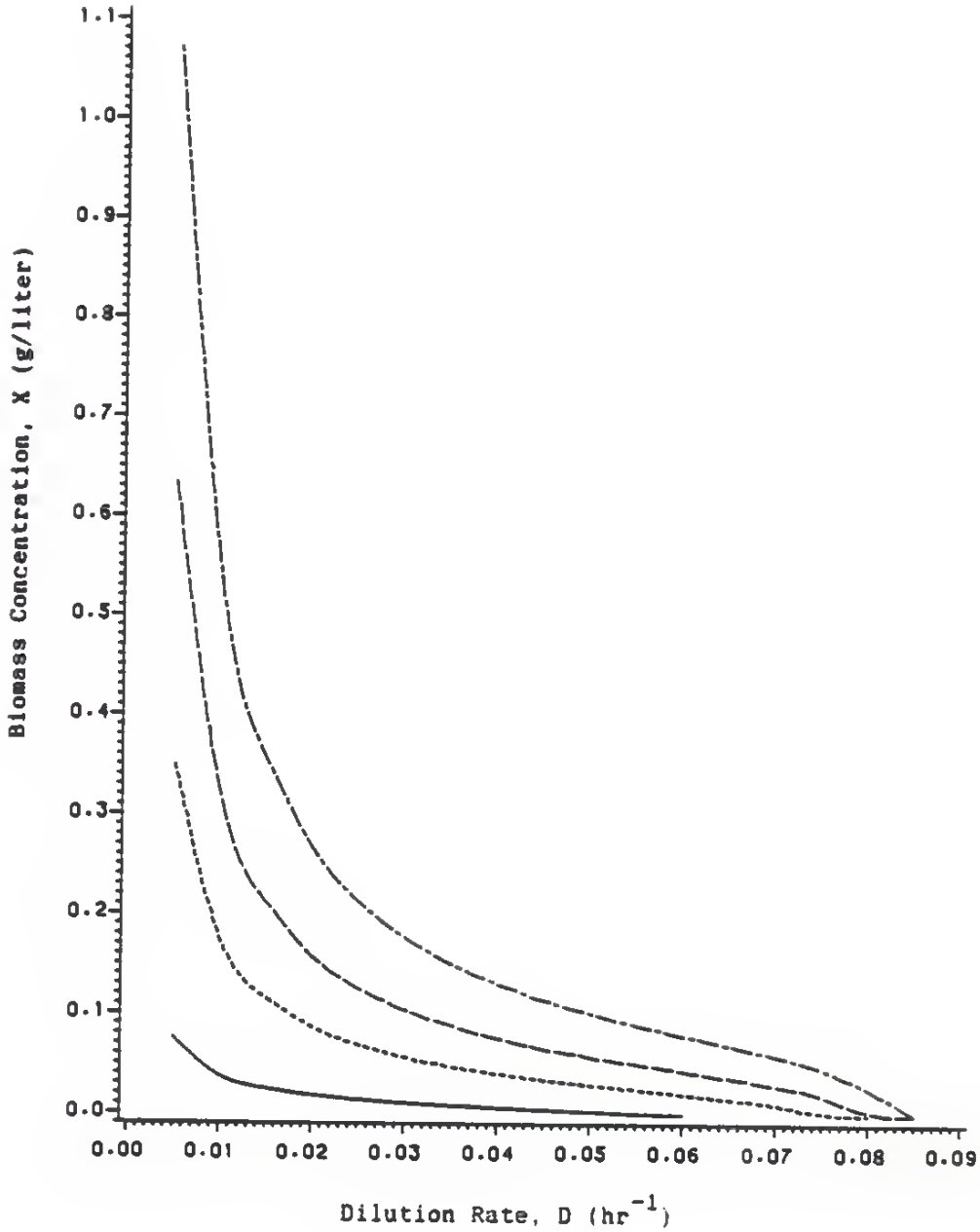

Figure A-6. Model 5 predictions of the variation in biomass concentration with dilution rate with mass-transfer coefficient as parameter. Symbols are as defined in Figure 3-14.

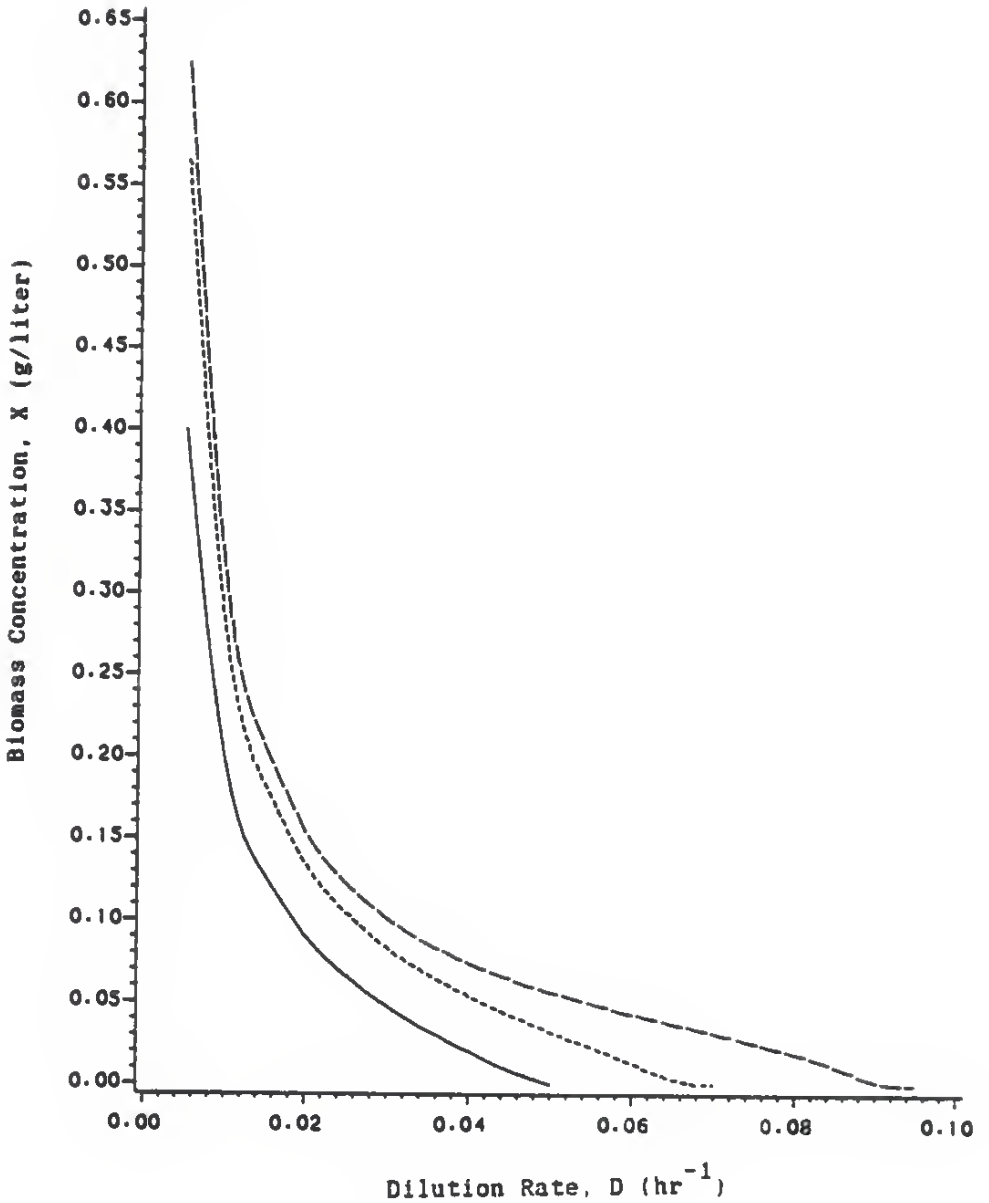

Figure A-7. Model 2 predictions of the variation in biomass concentration with dilution rate with incident light intensity as parameter. The mass-transfer coefficient is 17.7 hr^{-1}. Values of I_o in W/m^2 are ——— 10, - - - - 20, and — — — 75.

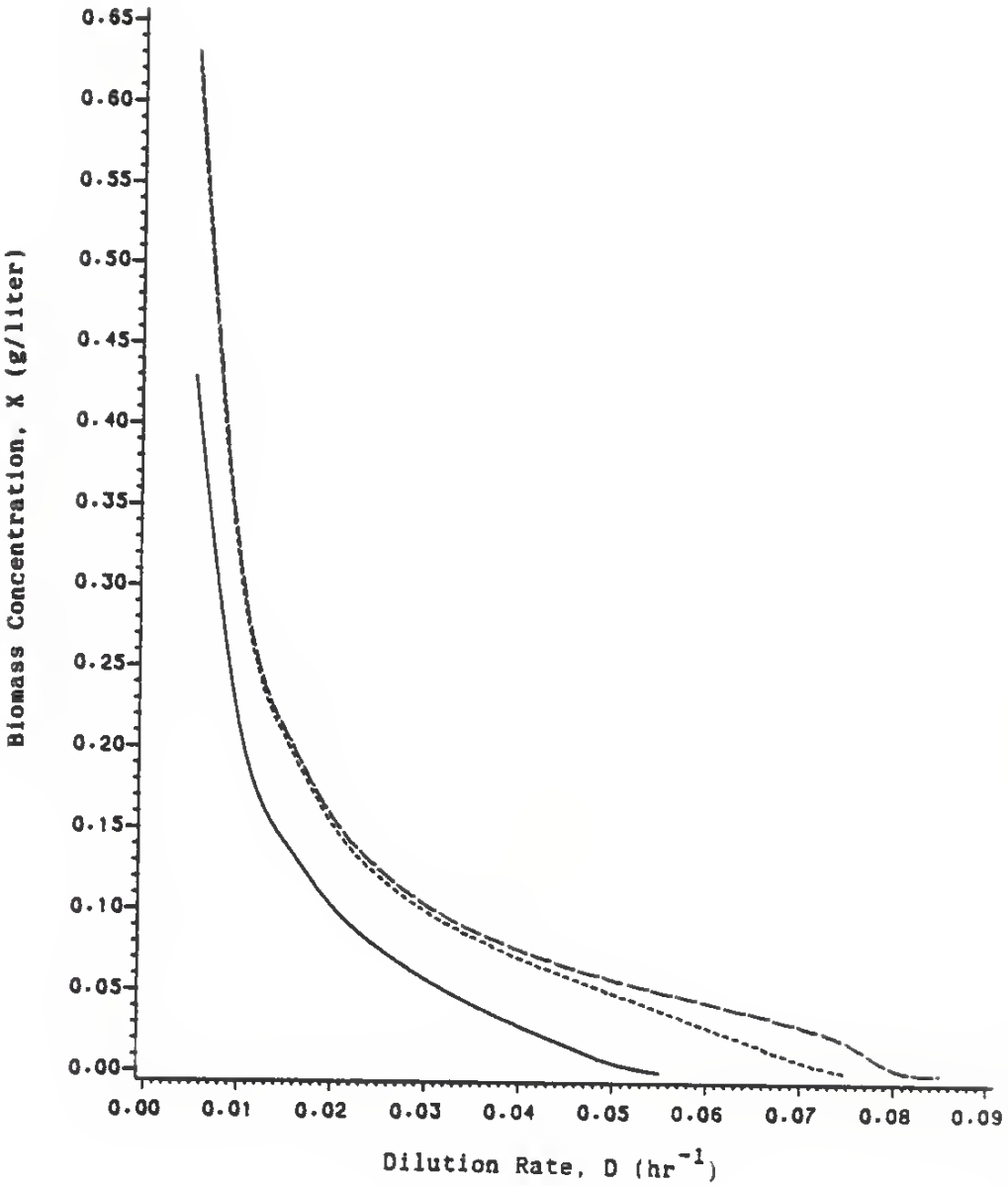

Figure A-8. Model 3 predictions of the variation in biomass concentration with dilution rate with incident light intensity as parameter. The mass-transfer coefficient is 17.7 hr^{-1}. Symbols are as defined in Figure A-7.

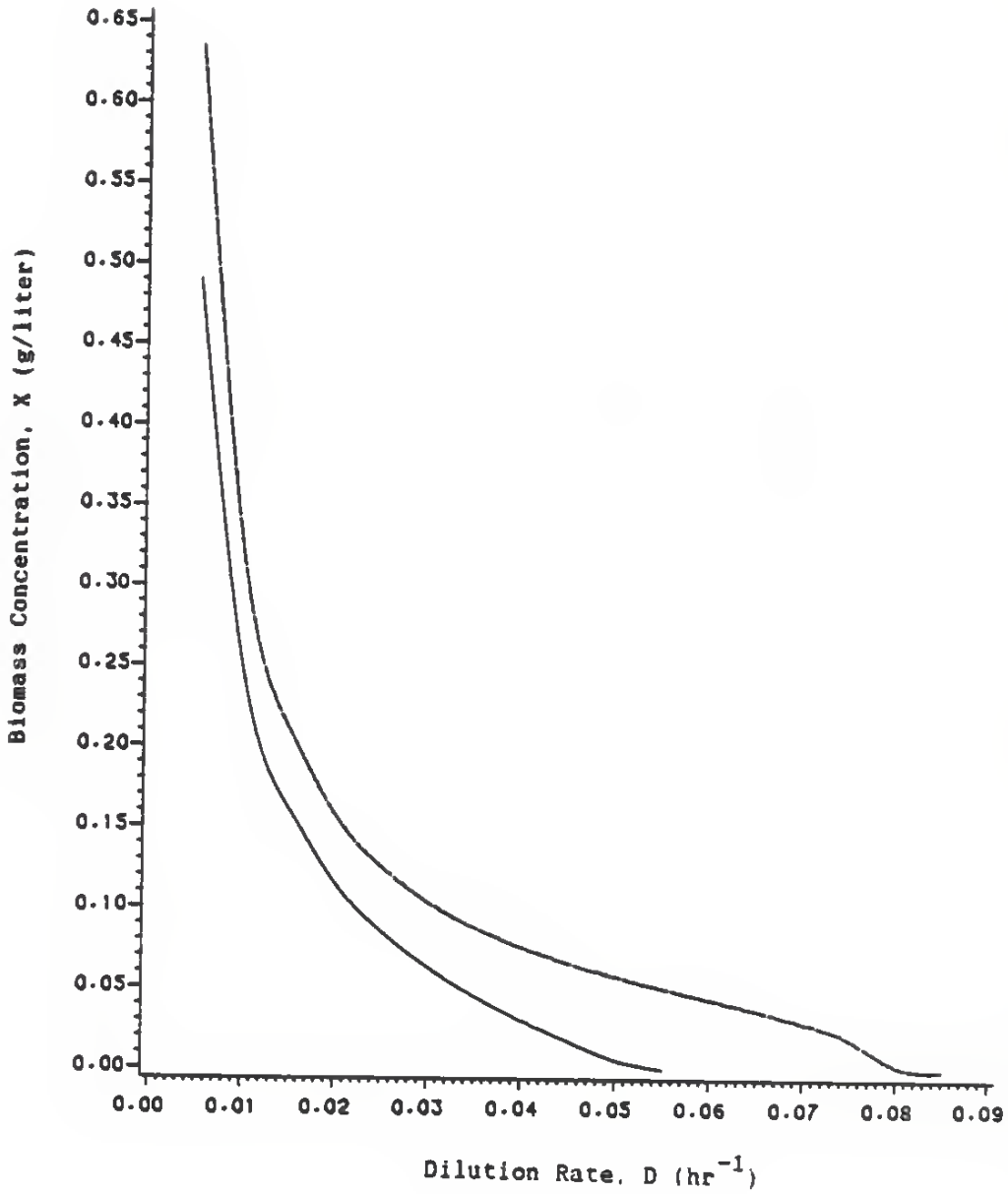

Figure A-9. Model 5 predictions of the variation in biomass concentration with dilution rate with incident light intensity from each side as parameter. The mass-transfer coefficient is 17.7 hr^{-1}. Values of I_o in W/m^2 are ——— 5, - - - - - - 15, — — — 75.

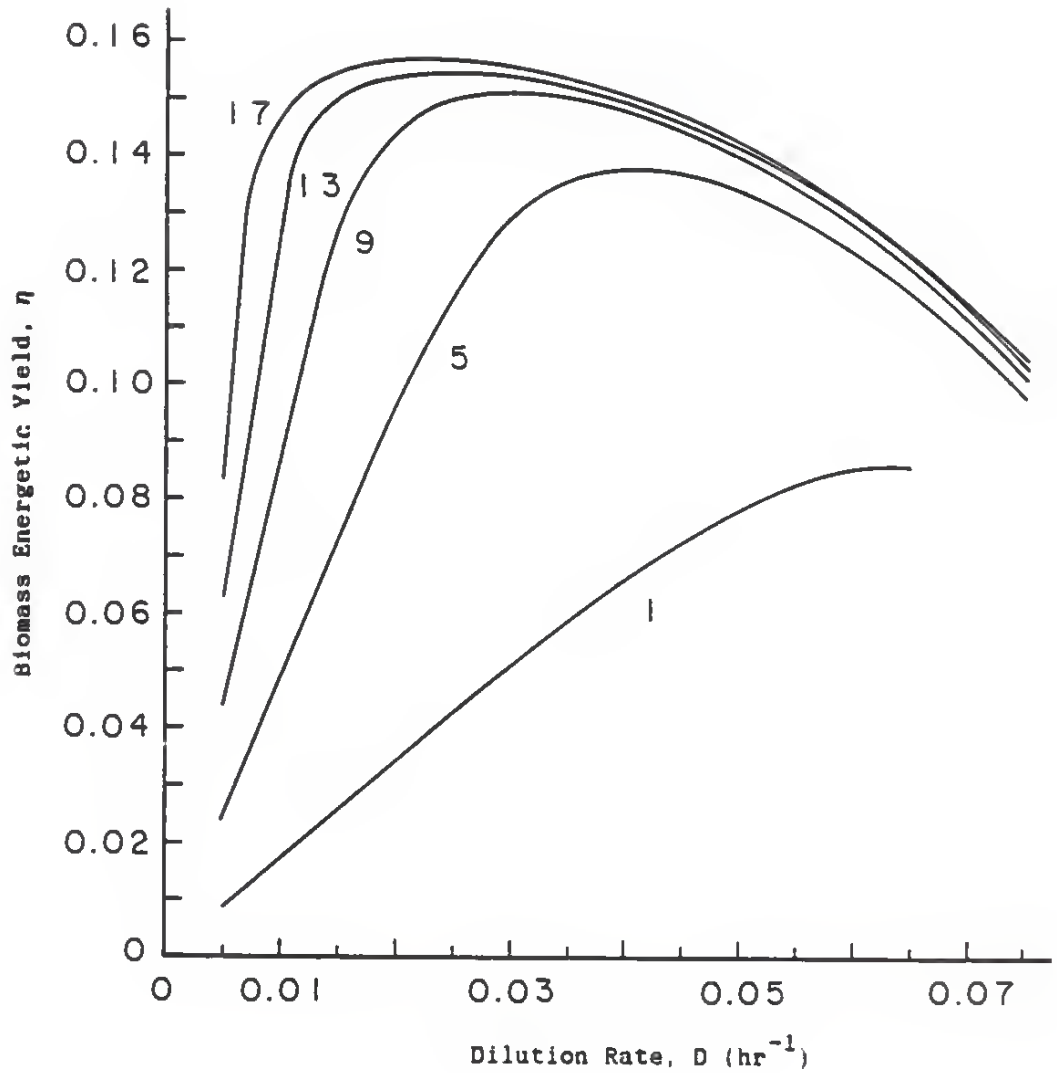

Figure A-10. Model 2 predictions of the variation in biomass energetic yield with dilution rate with influent total carbon concentration as parameter. Values of $[C_{TOT}]_{in}$ in mmol/liter are listed with each curve.

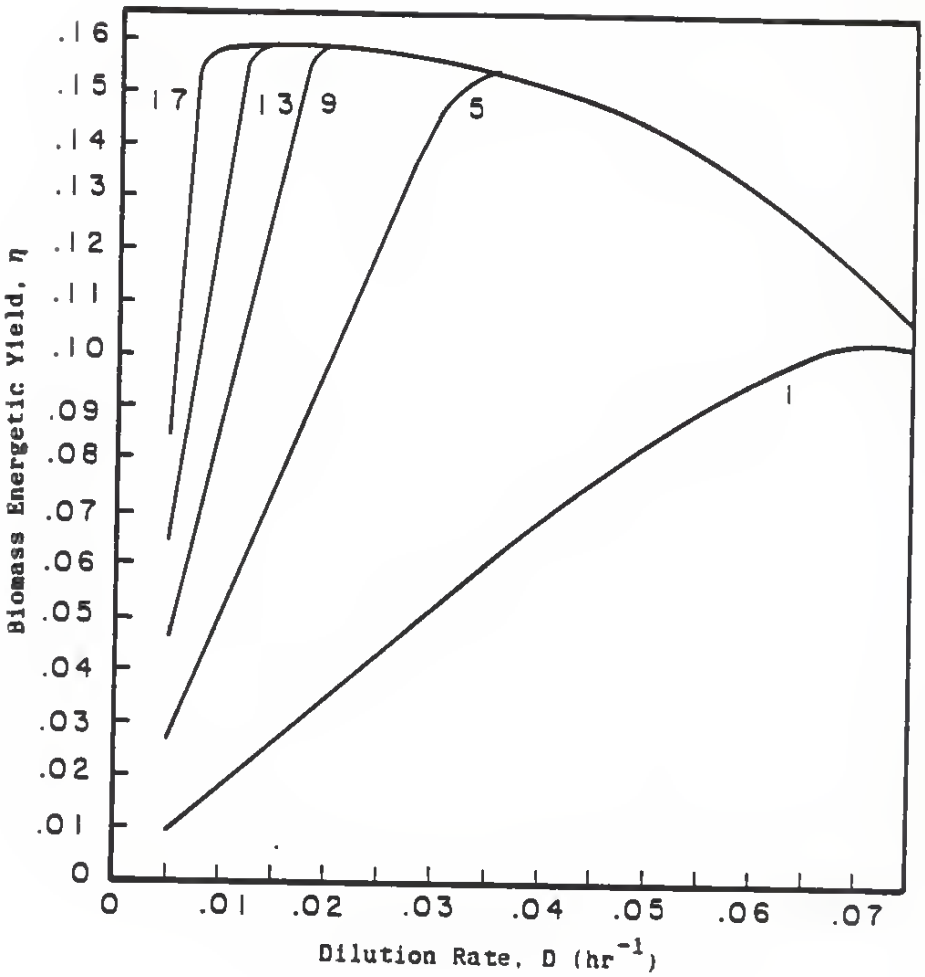

Figure A-11. Model 3 predictions of the variation in biomass energetic yield with dilution rate with influent total carbon concentration as parameter. Values of $[C_{TOT}]_{in}$ in mmol/liter are listed with each curve.

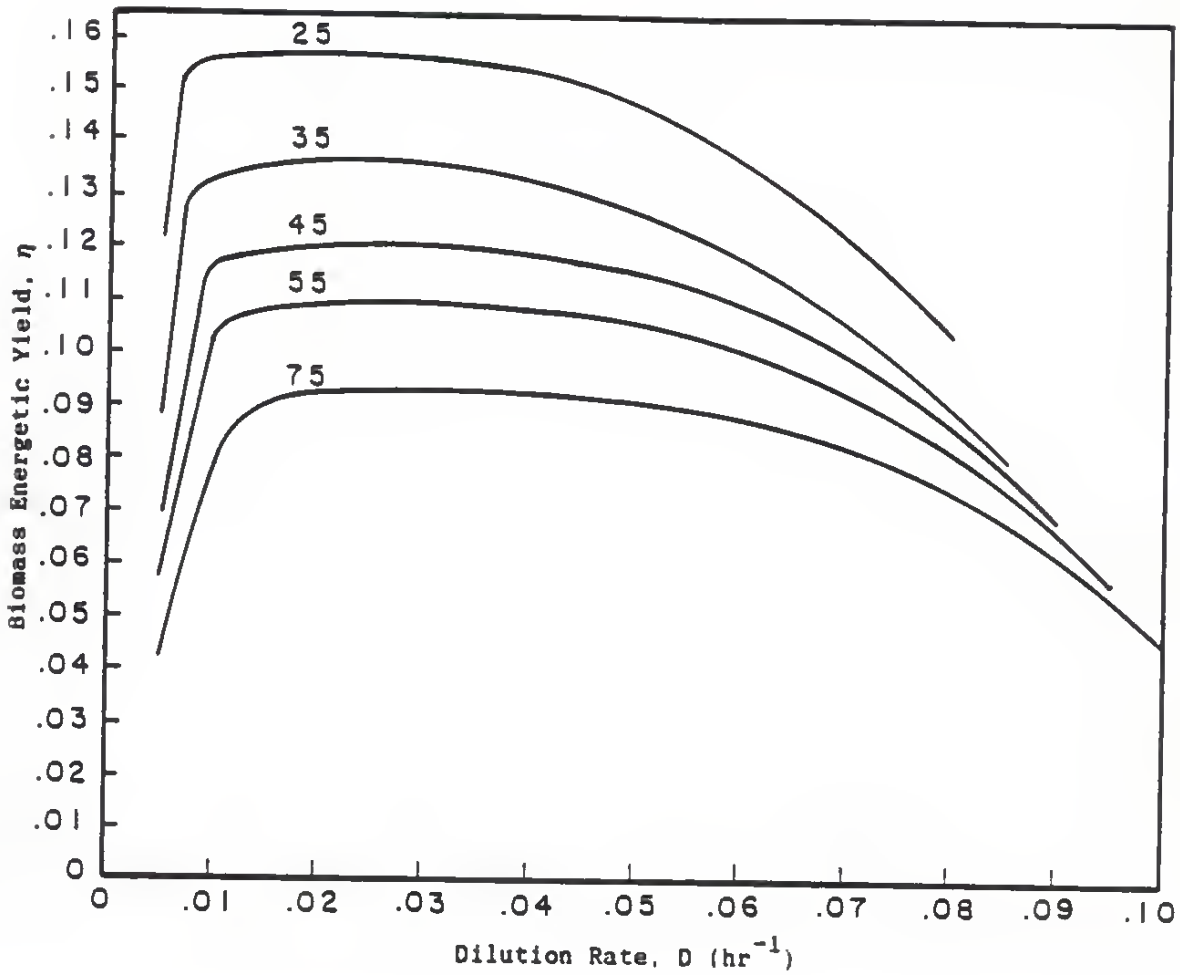

Figure A-12. Model 2 predictions of the variation in biomass energetic yield with dilution rate with incident light intensity as parameter. The total dissolved carbon concentration in liquid feed is 25 mmol/liter. Values of I_o in W/m^2 are listed with each curve.

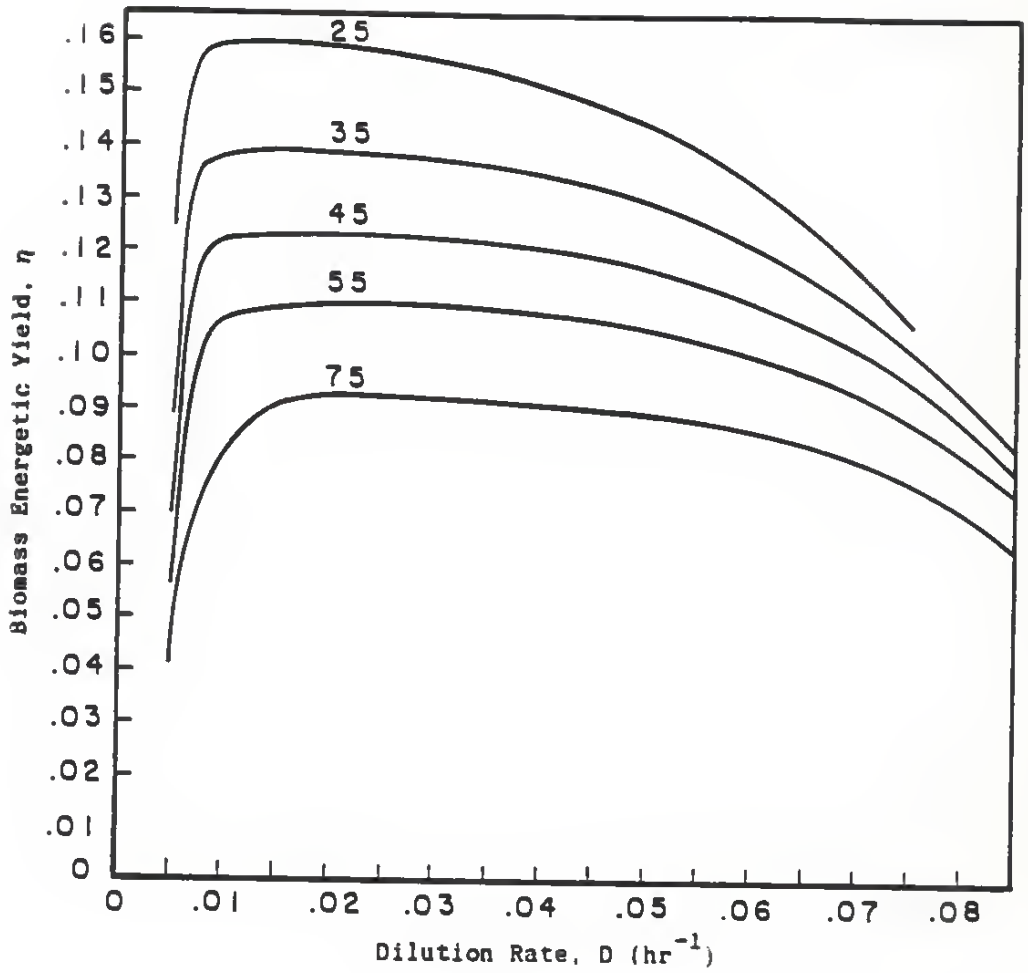

Figure A-13. Model 3 predictions of the variation in biomass energetic yield with dilution rate with incident light intensity as parameter. The total dissolved carbon concentration in liquid feed is 25 mmol/liter. Values of I_o in W/m^2 are listed with each curve.

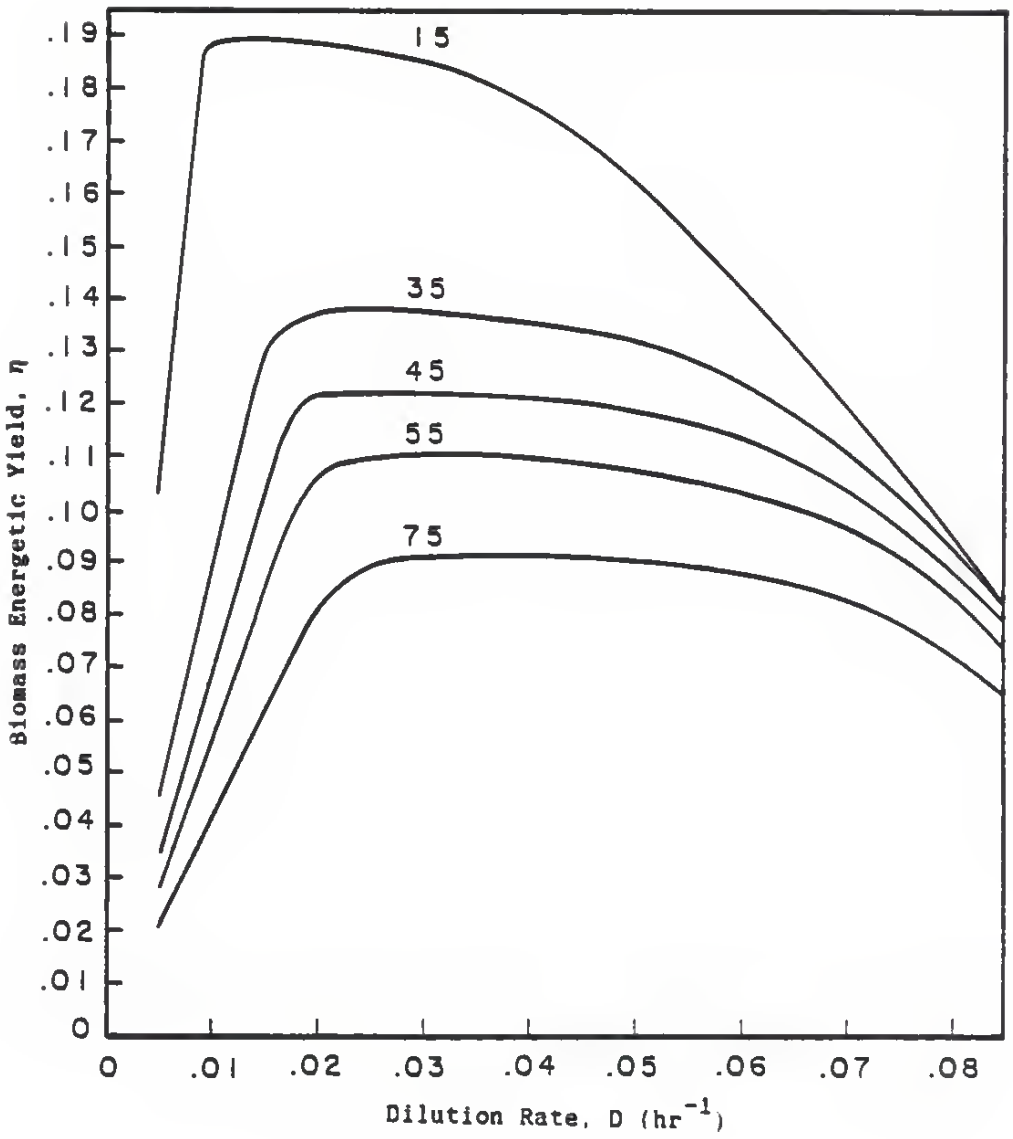

Figure A-14. Model 5 predictions of the variation in biomass energetic yield with dilution rate with incident light intensity from each side as parameter. The total dissolved carbon concentration in liquid feed is 25 mmol/liter. Values of I_o in W/m^2 are listed with each curve.

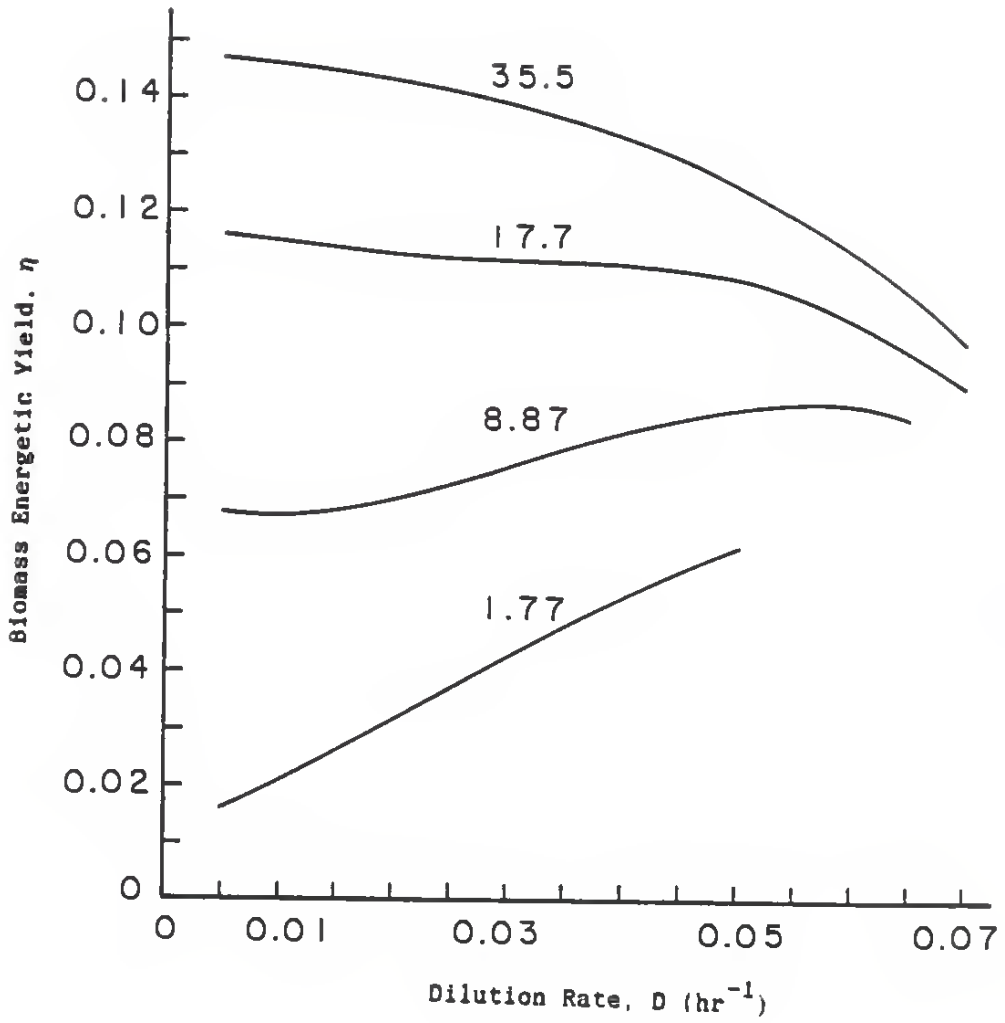

Figure A-15. Model 2 predictions of the variation in biomass energetic yield with dilution rate with mass-transfer coefficient as parameter. Values of $k_L a$ in hr^{-1} are listed with each curve.

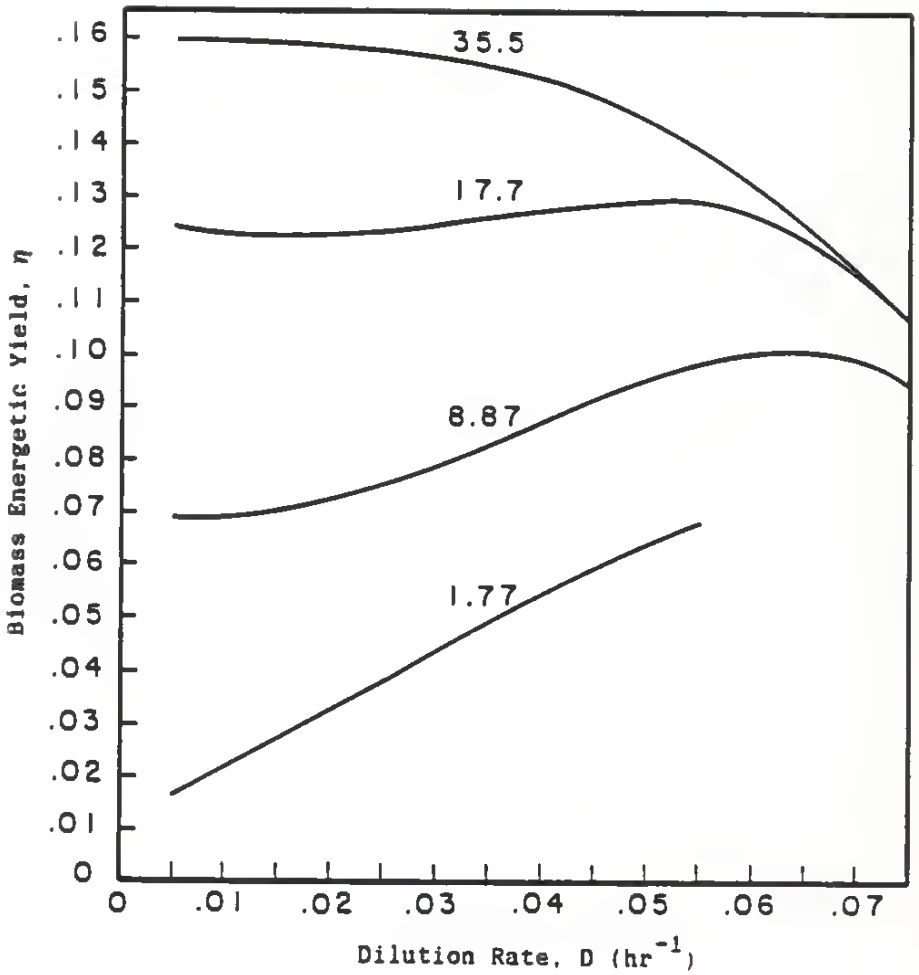

Figure A-16. Model 3 predictions of the variation in biomass energetic yield with dilution rate with mass-transfer coefficient as parameter. Values of $k_L a$ in hr^{-1} are listed with each curve.

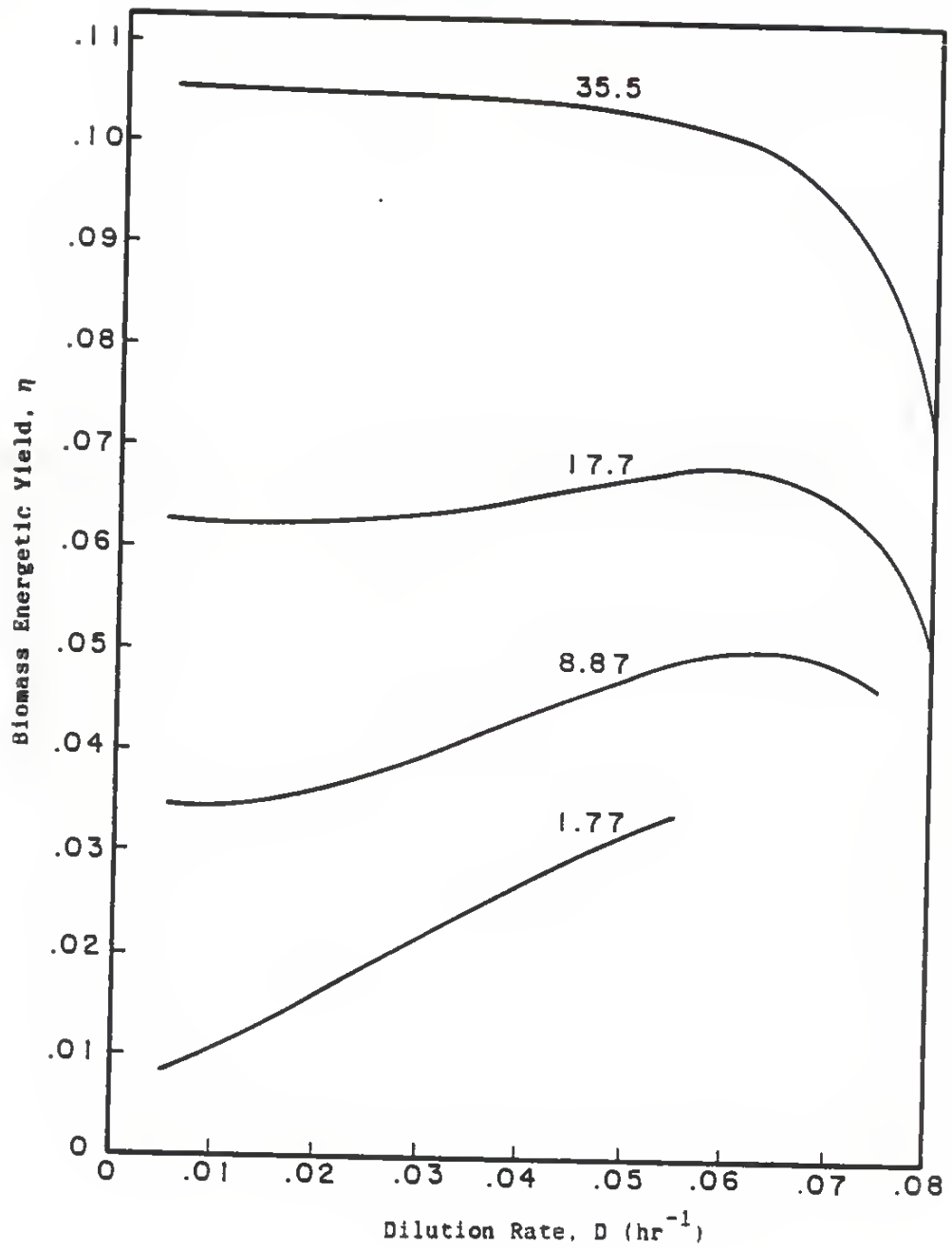

Figure A-17. Model 5 predictions of the variation in biomass energetic yield with dilution rate with mass-transfer coefficient as parameter. Values of $k_L a$ in hr^{-1} are listed with each curve.

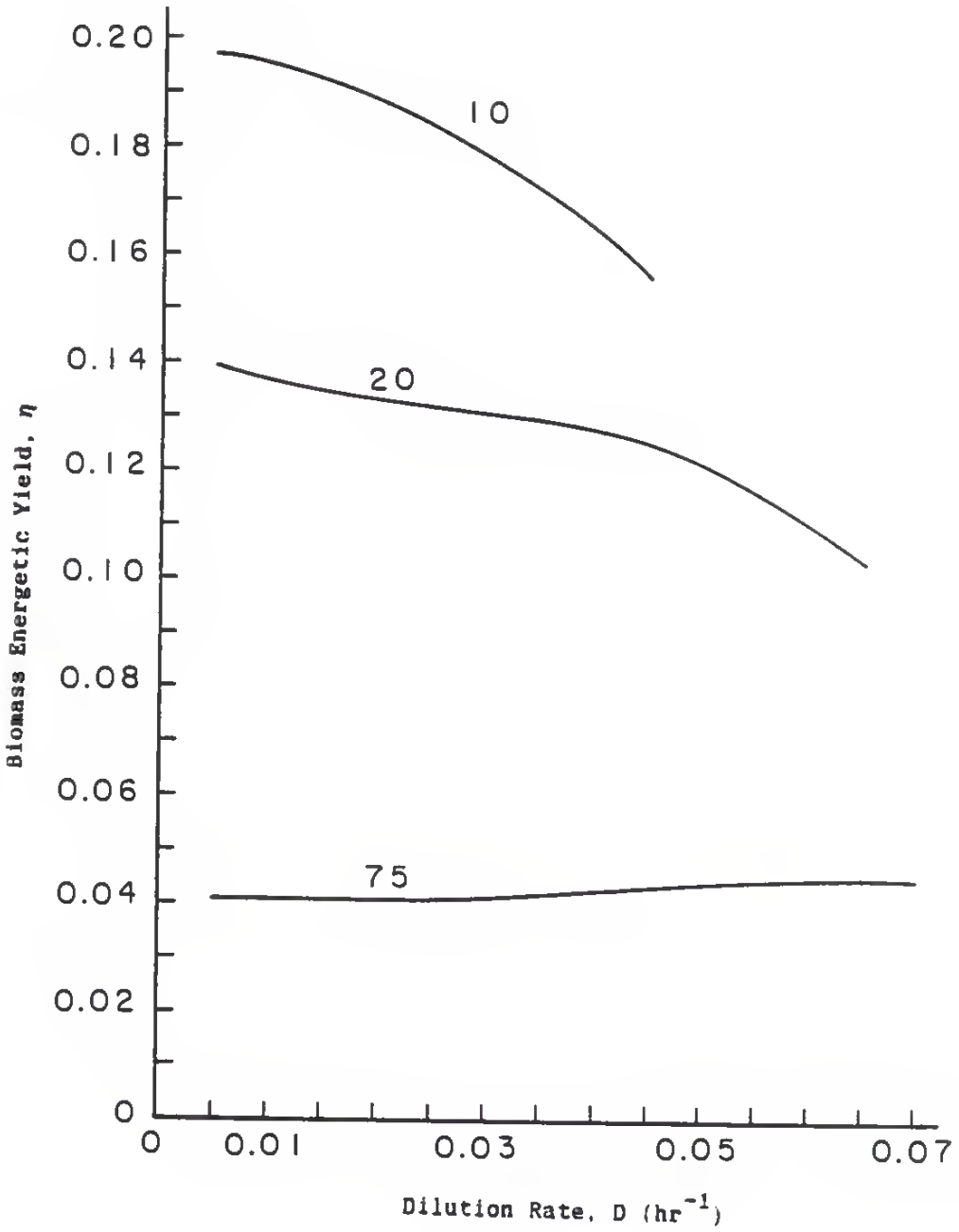

Figure A-18. Model 2 predictions of the variation in biomass energetic yield with dilution rate with incident light intensity as parameter. Mass-transfer coefficient is 17.7 hr^{-1}. Values of I_o in W/m^2 are listed with each curve.

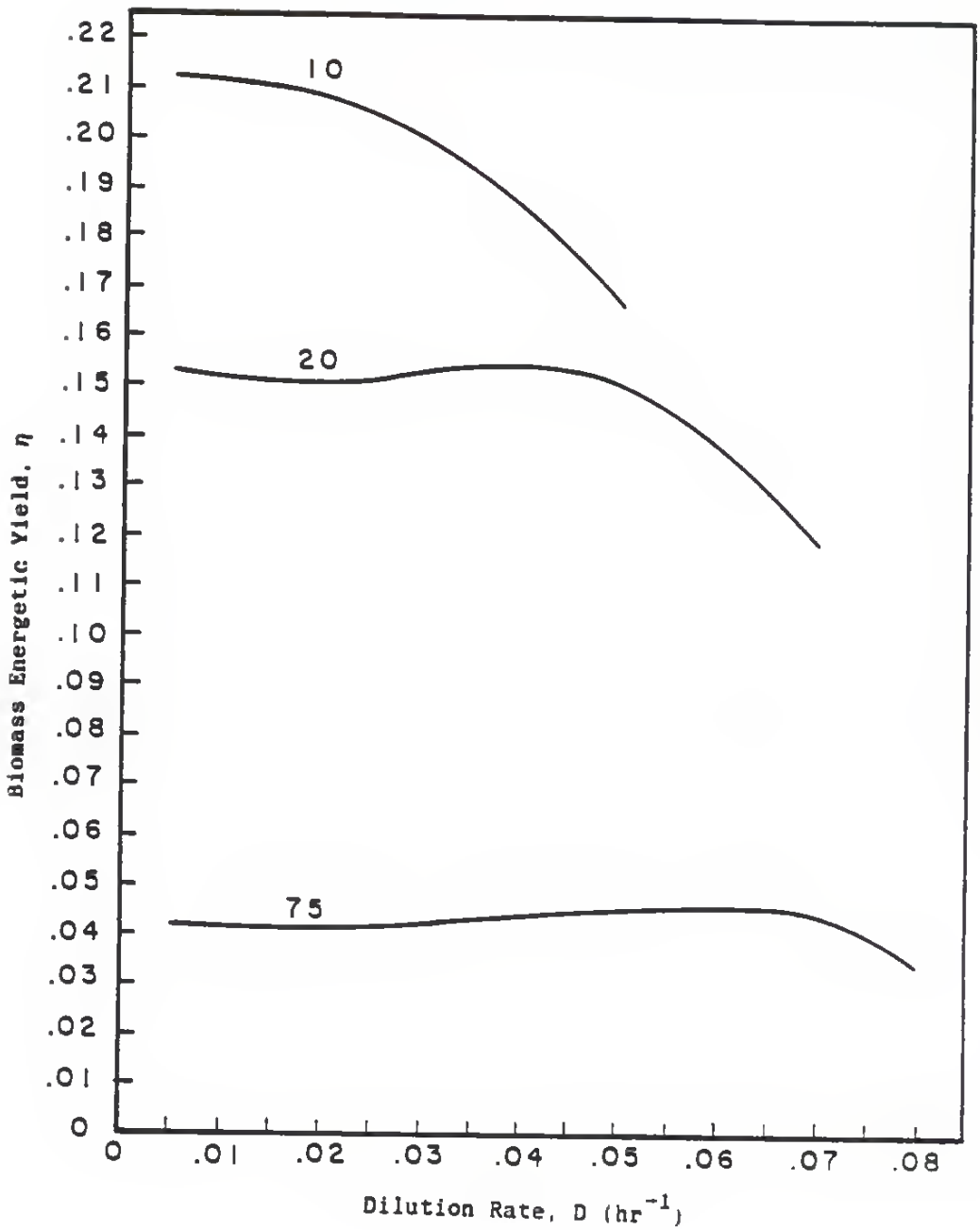

Figure A-19. Model 3 predictions of the variation in biomass energetic yield with dilution rate with incident light intensity as parameter. Mass-transfer coefficient is 17.7 hr^{-1}. Values of I_o in W/m^2 are listed with each curve.

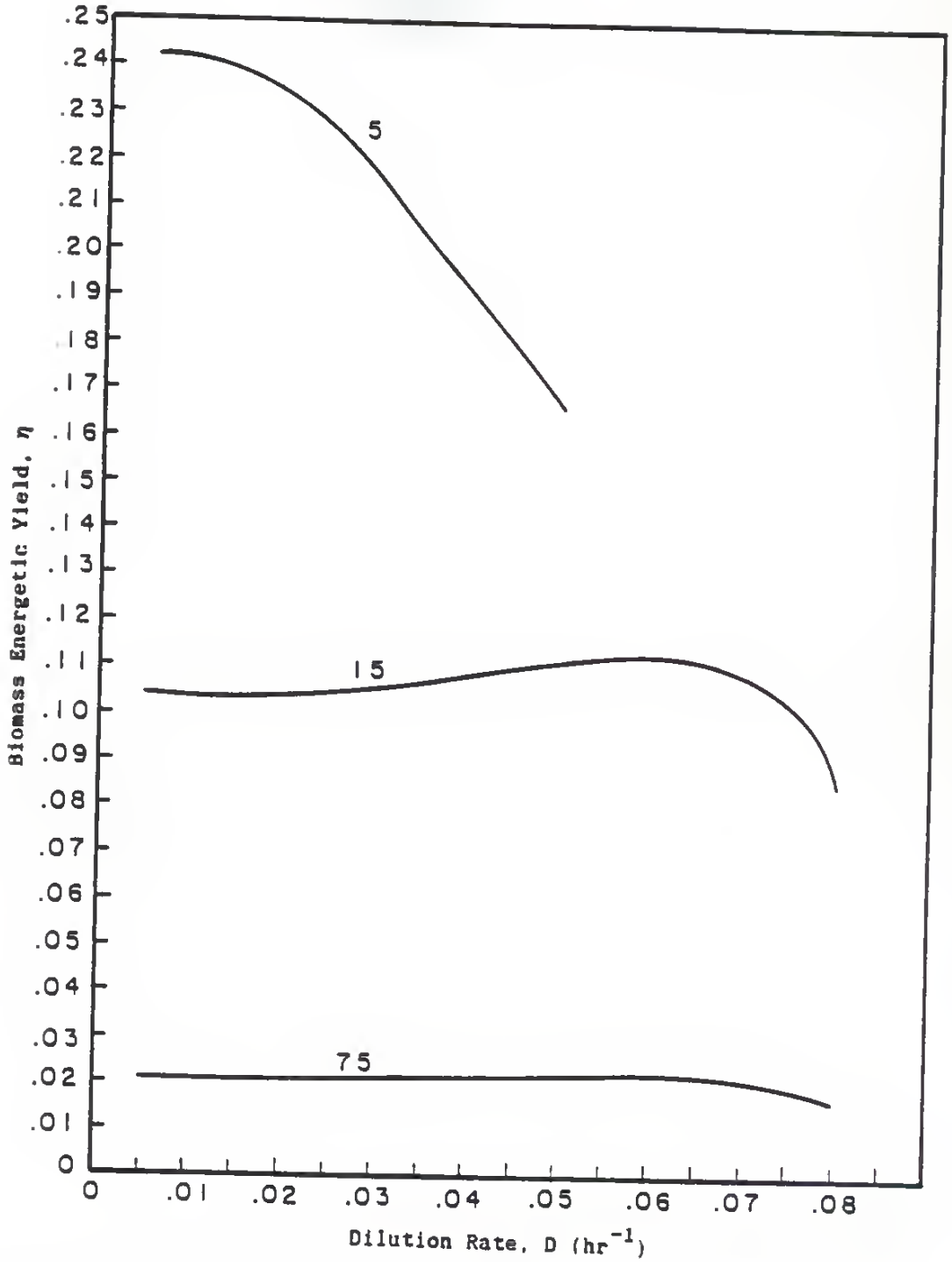

Figure A-20. Model 5 predictions of the variation in biomass energetic yield with dilution rate with incident light intensity from each side as parameter. Mass-transfer coefficient is 17.7 hr^{-1}. Values of I_o in W/m^2 are listed with each curve.

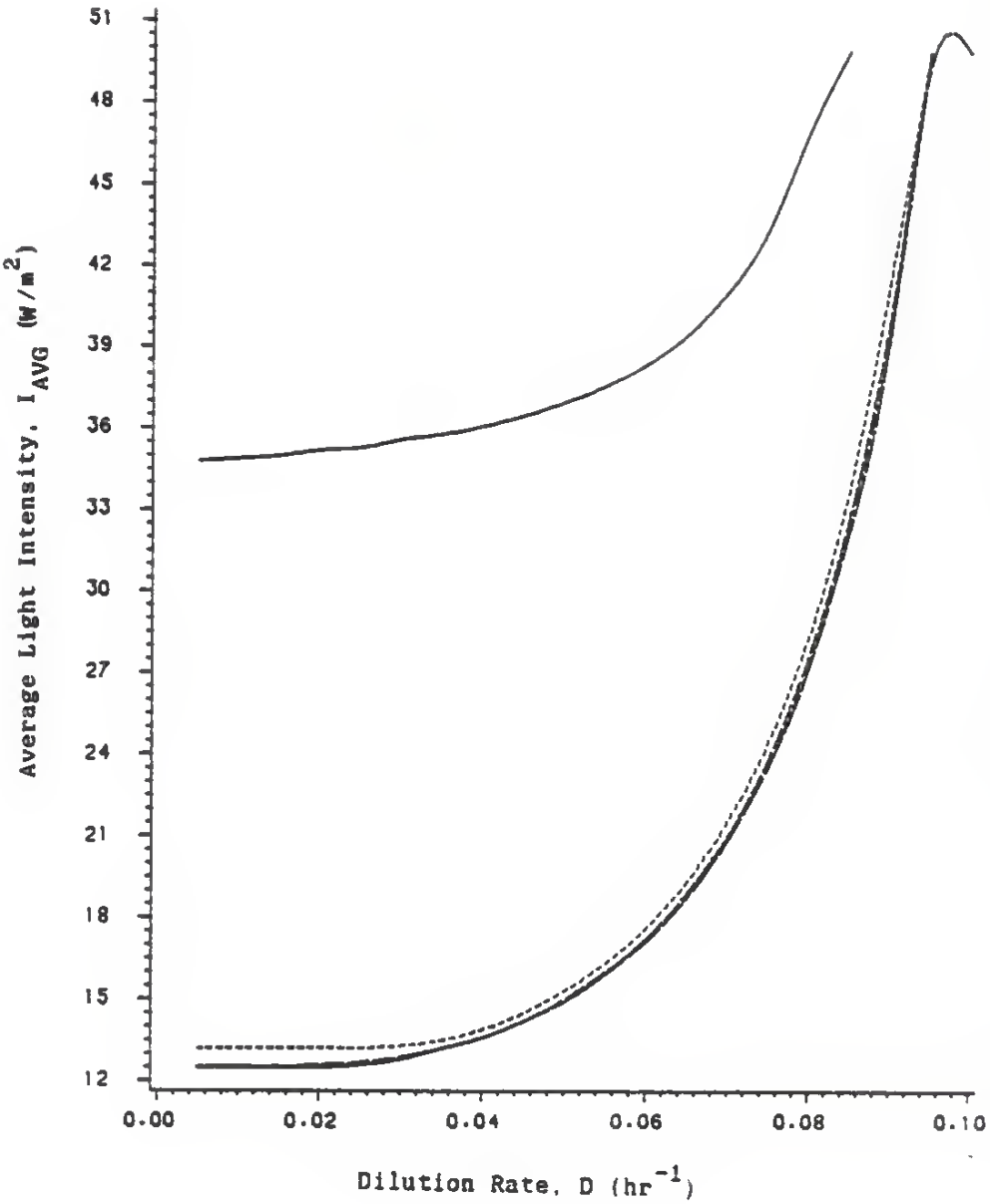

Figure A-21. Model 4 predictions of variation in average light intensity with dilution rate with influent total carbon concentration as parameter. Values of $[C_{TOT}]_{in}$ in mmol/liter are ——— 1, - - - - 9, — — — 17, — · — · — 25, and ——— — 41.

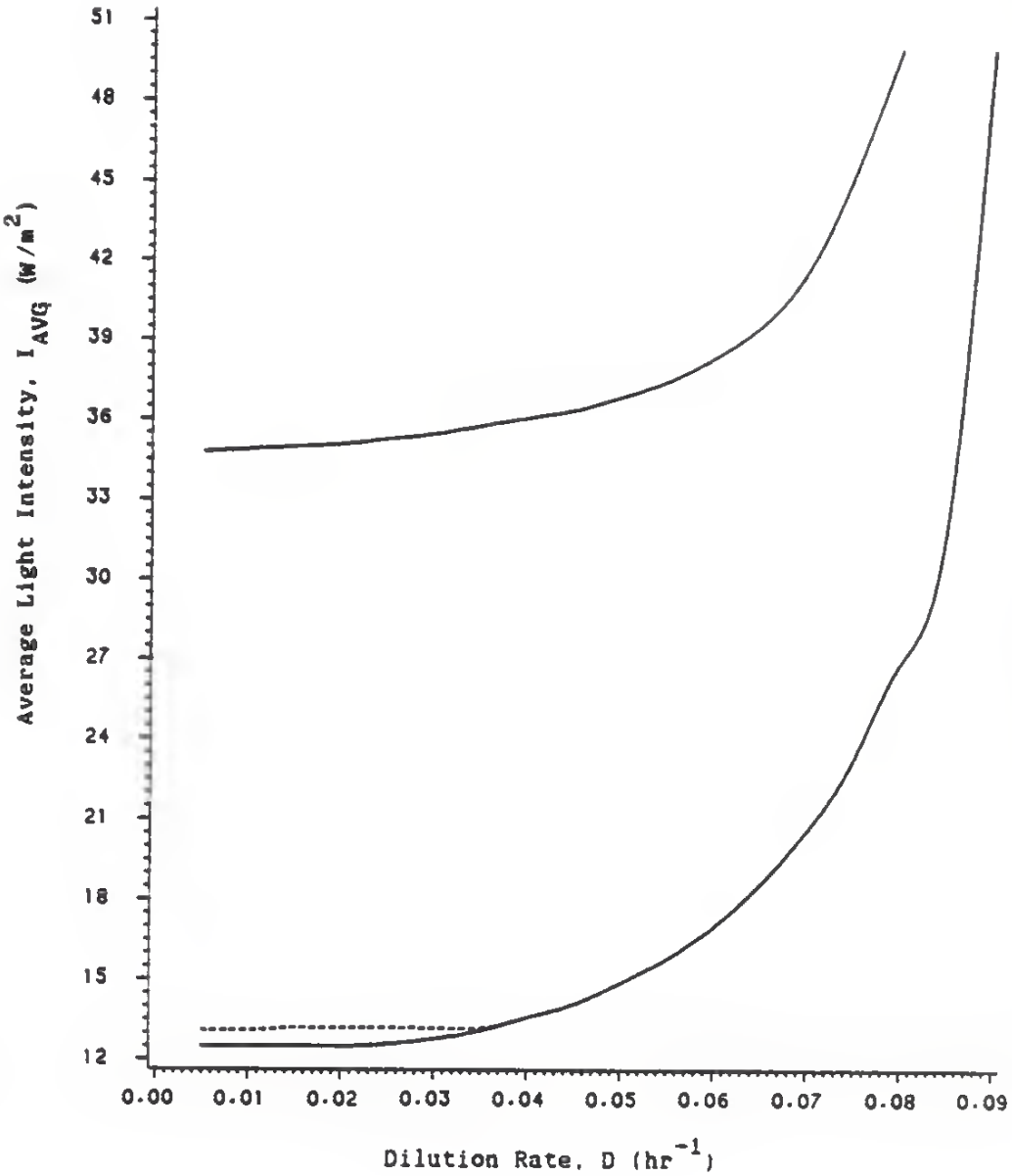

Figure A-22. Model 5 predictions of variation in average light intensity with dilution rate with influent total carbon concentration as parameter. Symbols are as defined in Figure A-21.

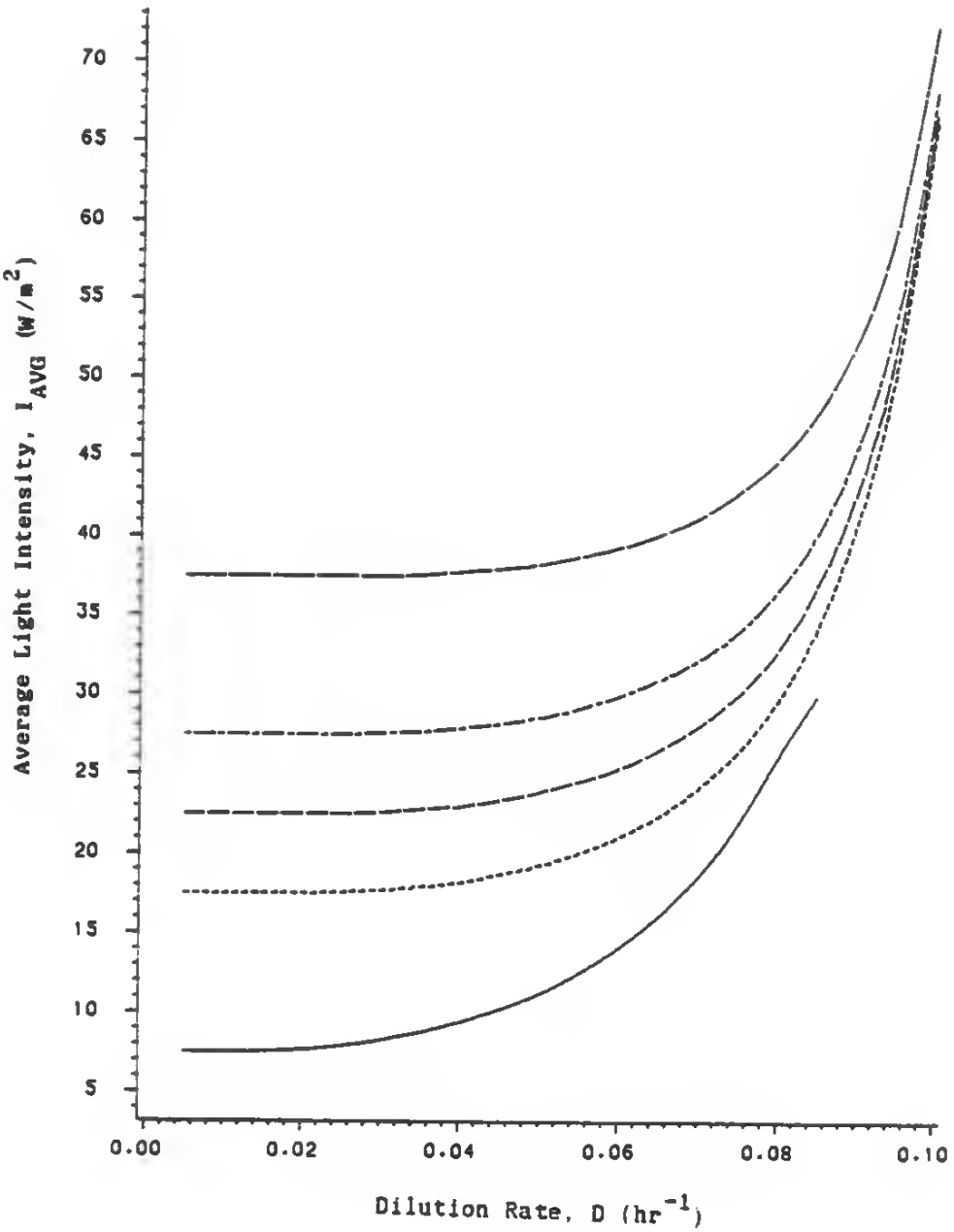

Figure A-23. Model 4 predictions of variation in average light intensity with dilution rate with incident light intensity from each side as parameter. The total dissolved carbon in the liquid feed is 25 mmol/liter. Values of I_o in W/m^2 are ——— 15, - - - - - 35, — — — 45, - — - — 55, and ——— 75.

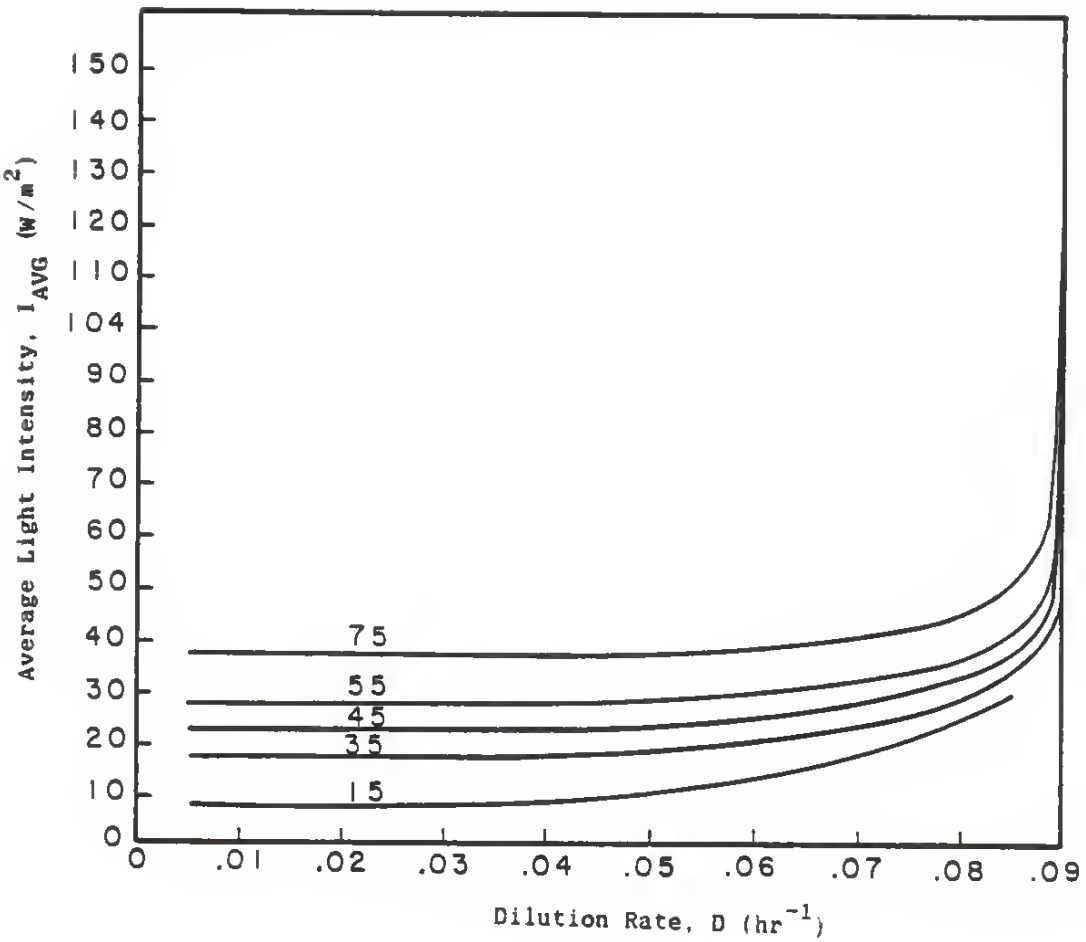

Figure A-24. Model 5 predictions of variation in average light intensity with dilution rate with incident light intensity from each side as parameter. The total dissolved carbon in the liquid feed is 25 mmol/liter. Symbols are as defined in Figure A-23.

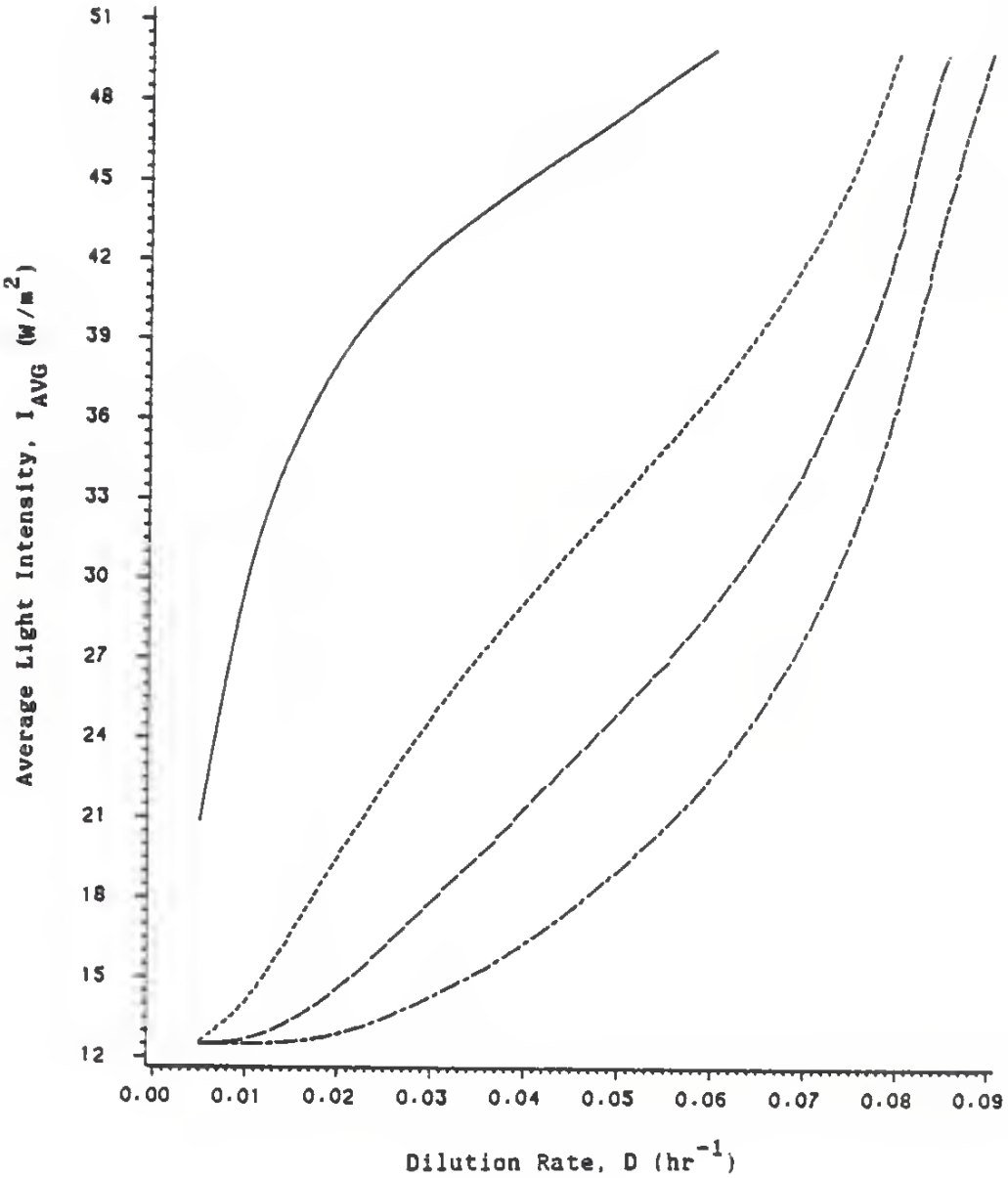

Figure A-25. Model 4 predictions of variation in average light intensity with dilution rate with mass-transfer coefficient as parameter. Values of $k_L a$ in hr^{-1} are ——— 1.77, - - - - - 8.87, — — — 17.7, - — - — 35.5.

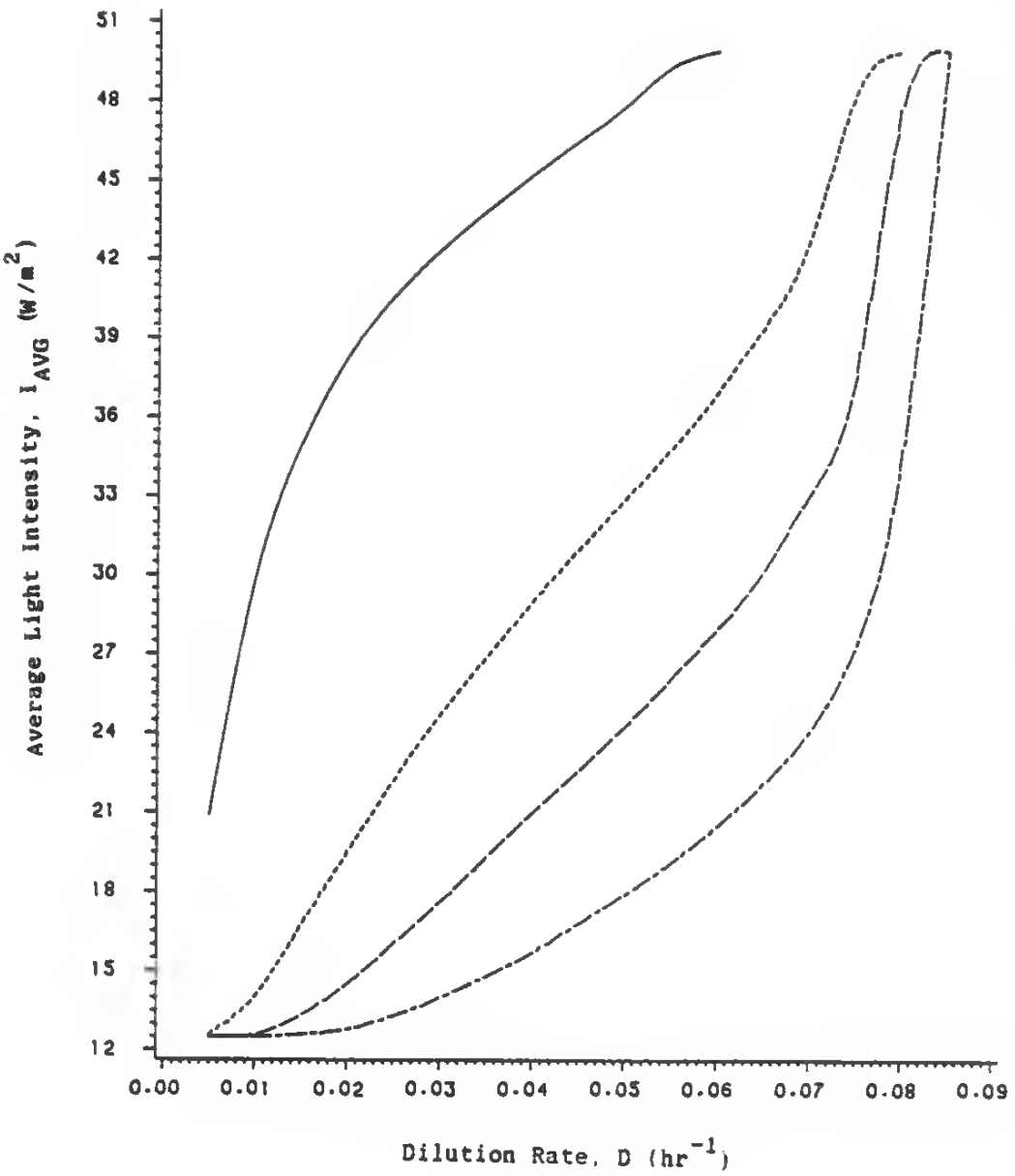

Figure A-26. Model 5 predictions of variation in average light intensity with dilution rate with mass-transfer coefficient as parameter. Symbols are as defined in Figure A-25.

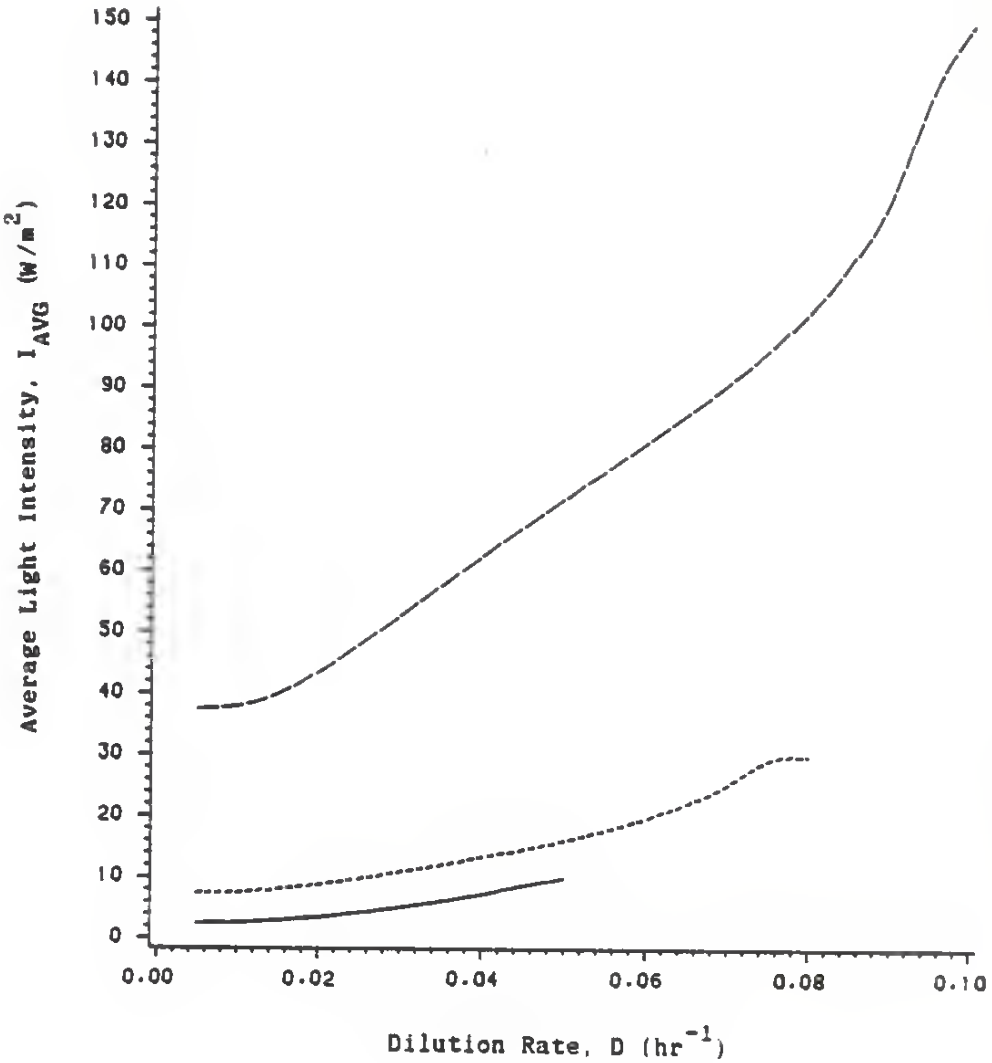

Figure A-27. Model 4 predictions of variation in average light intensity with dilution rate with incident light intensity from each side as parameter. The mass-transfer coefficient is 17.7 hr^{-1}. Values of I_o in W/m^2 are ——— 5, - - - - - 15, — — — 75.

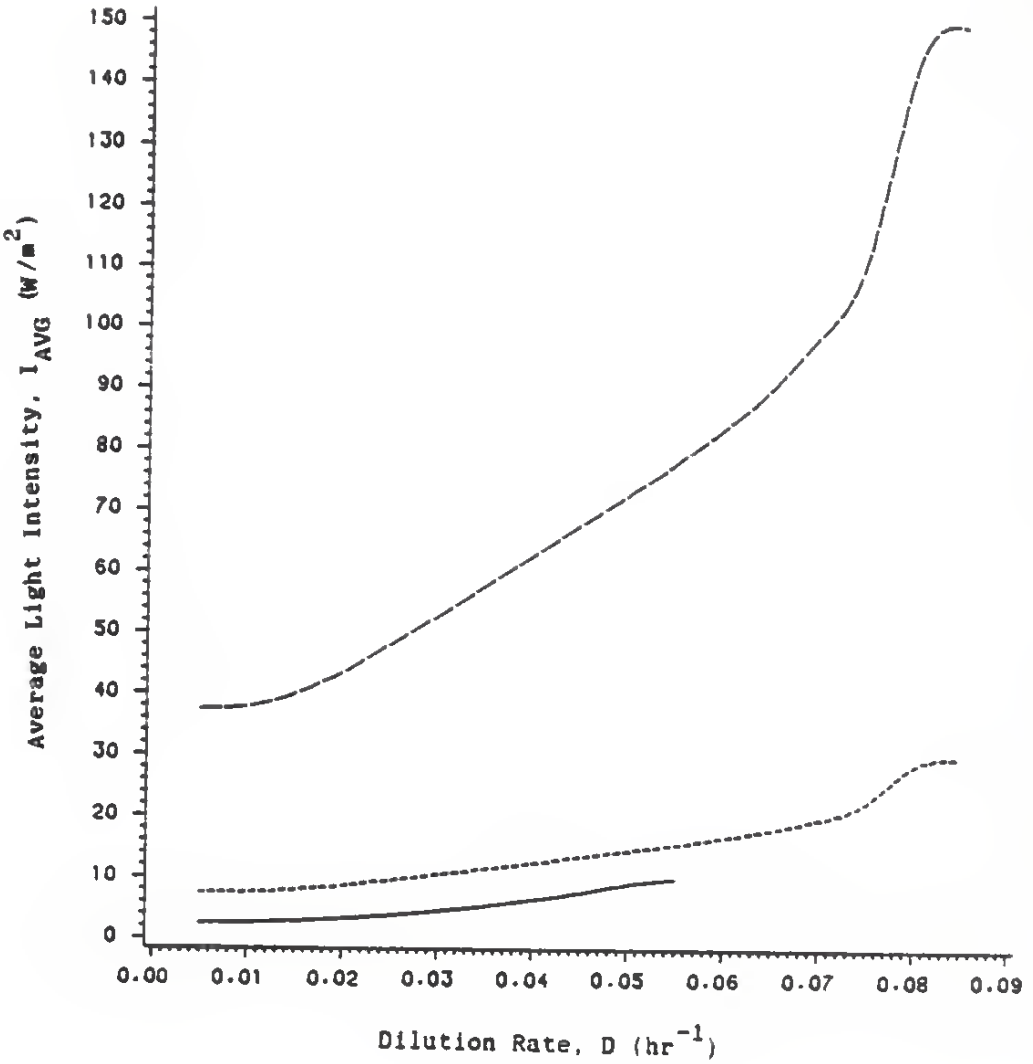

Figure A-28. Model 5 predictions of variation in average light intensity with dilution rate with incident light intensity from each side as parameter. The mass-transfer coefficient is 17.7 hr^{-1}. Symbols are as defined in Figure A-27.

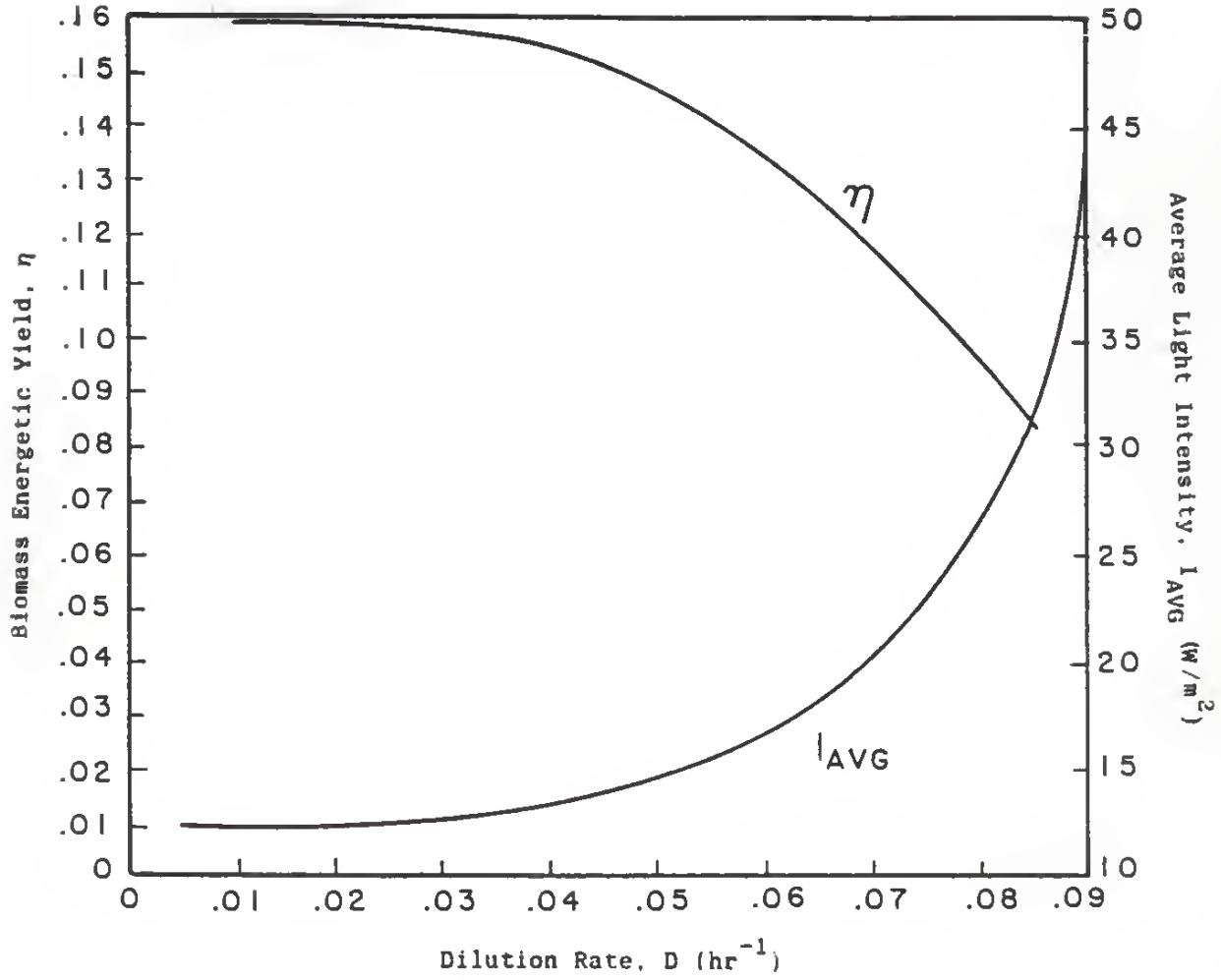

Figure A-29. Variation in biomass energetic yield and average light intensity with dilution rate for Model 5. The total dissolved carbon concentration in the influent is 41 mmol/liter and the incident light intensity from each side is 25 W/m^2.

Suggestions for Future Work

The Monod model assumes that growth occurs under all conditions. In an actual culture a state of zero growth can occur while the organisms maintain life. A possibility for future work is to include a maintenance coefficient in the kinetic model for bicarbonate consumption.

Another possibility involves experimentally determining the temperature dependence of μ_{maxC} and the pH dependence of K_S and K_I for S. platensis. Expressions for each parameter could be incorporated into the computer simulation program. The program can then be used to explore the effects of temperature and pH on both inorganic carbon chemistry and algal growth kinetics.

Two other possibilities for experimental work will also be mentioned. First, data for simultaneous light and bicarbonate limited growth of S platensis could be collected. This data could then be compared to each model to determine which is more appropriate. Finally, growth data could be obtained under carbon-limited, air-fed conditions. This data could be used to test the simulation prediction that the rate of conversion of $CO_{2(aq)}$ to HCO_3^- can limit the rate of carbon assimilation.

MATHEMATICAL MODELING AND SIMULATION OF PHOTOSYNTHETIC GROWTH IN CONTINUOUS CULTURE UNDER BICARBONATE AND LIGHT LIMITED CONDITIONS

by

CRAIG E. CURLESS

B. S., Kansas State University, 1985

AN ABSTRACT OF A MASTER'S THESIS

submitted in partial fulfillment of the

requirements for the degree

MASTER OF SCIENCE

College of Engineering
Department of Chemical Engineering

KANSAS STATE UNIVERSITY
Manhattan, Kansas

1986

Abstract

The literature relevent to modeling carbon and light limited aquatic photosynthetic growth is reviewed. Studies that address which carbon species is assimilated by algae are discussed. It is the general concensus that all aquatic, photosynthetic organisms can assimilate dissolved CO_2 under certain circumstances. However, nearly all also have the ability to consume bicarbonate. Research on the modeling of carbon-limited photosynthetic growth is surveyed. Models commonly used are of the Monod form and are based on carbon dioxide, bicarbonate or total dissolved inorganic carbon, as the limiting nutrient. Finally, studies which include the effects of both light and nutrients on photosynthetic growth are reviewed. Models suggested were of two types: two Monod models based on light and nutrient, respectively, which are multiplied together to give a product model, and a two part Monod model which assumes that either light limits growth or the nutrient does.

A mathematical model describing carbon-limited algal growth in a chemostat is presented. The model takes the kinetics of organic carbon chemistry into account. The algae are assumed to use bicarbonate as the only carbon source. Consequently, the model is valid for algae that consume only bicarbonate or in situations where the total aqueous inorganic carbon pool is at equilibrium. A computer program calculates the composition of the exiting stream for given reactor conditions and input streams (gas and/or liquid) using the model. Computer simulations were made using the growth parameters of Scenedesmus obliquus and Spirulina platensis, respectively. Simulation predictions matched the experimental results reasonably well. It was also found that, in general, inorganic carbon concentrations are close to their equilibrium values in the chemostat if the

carbon is fed in the liquid stream. However, for gas-fed chemostats, the model predicts that a state of nonequilibrium between aqueous CO_2 and HCO_3^- will exist.

Kinetic models of aqueous photosynthetic growth under simultaneous light/bicarbonate limitations are developed. Two types of models are considered. The first is a product model in which two Monod-type models based on local light intensity and bicarbonate concentration, respectively, are multiplied together. The second is a threshold model where either light or bicarbonate limits growth at each position in the tank. The degree of self-shading is taken into account using Beer's Law and a rectangular reactor geometry is considered. Cases considered include light introduced from one side and light introduced from two, opposing sides. For the case of light incident from two sides, model predictions for Spirulina platensis match experimental data well for both light-limited and carbon-limited growth conditions. A series of simulations for the simultaneous light and bicarbonate limited growth of S. platensis are also presented. The product-type of model predicts a more gradual transition from carbon to light limitation than does the threshold model. Also, the threshold model predicts washout at lower dilution rates under carbon-limited conditions.